Corso di dottorato di ricerca in:

"Scienze Biomediche e Biotecnologiche"

in convenzione con Centro di Riferimento Oncologico di Aviano, IRCCS

Ciclo 35°

Titolo della tesi

"MOLECULAR DISSECTION OF THE MALIGNANT EVOLUTION OF RETROPERITONEAL WELL DIFFERENTIATED/ DEDIFFERENTIATED LIPOSARCOMA"

Dottorando

Valenti Beatrice

Supervisore

Dott.ssa Maestro Roberta

Anno 2023

ABSTRACT

Well differentiated liposarcoma (WDLS) is a rare form of low-grade malignancy that mostly occurs in the retroperitoneum. WDLS may evolve into a more aggressive form, dedifferentiated liposarcoma (DDLS), that loses adipocytic characteristics and, in a fraction of cases, undergoes heterologous differentiation acquiring phenotypic features of other mesenchymal tissues. A differentiation toward muscle lineage is the most common form of heterologous DDLS differentiation. In particular, DDLS undergoing rhabdomyoblastic differentiation are characterized by the *de novo* expression of myogenin. These tumors show a particularly aggressive clinical behavior with a high propensity to metastasis and a significantly reduced overall survival.

This study aims to dissect the molecular mechanism underlying the malignant evolution to retroperitoneal WDLS to DDLS and in particular the evolution toward rhabdomyosarcomatous DDLS.

A series of 18 WDLS and 42 DDLS, 9 of which DDLS with rhabdomyoblastic differentiation, were molecularly profiled by RNA-sequencing and targeted DNA sequencing. The analysis of the transcriptome confirmed the retention of adipocytic features in WDLS and indicated an enrichment for cell proliferation signatures in DDLS, in line with their more aggressive features. Interestingly, while the mutation load of WDLS and DDLS was similar, these tumors differ in number of structural alterations. Both tumors showed amplification of genes located in chromosome 12q13-15, notoriously amplified in WDLS and DDLS, but additional copy number gains were observed in DDLS. This supports the notion that structural alterations are likely to play a major role in the malignant evolution of WDLS to DDLS.

Focusing on DDLS tumors, we found that DDLS undergoing rhabdomyoblastic differentiation are characterized by a profound transcriptional reprogramming with the activation of a large set of genes involved in different phases of skeletal muscle development. Moreover, this differentiation drift was associated with reduced immune cell infiltration, as evidenced by both transcriptome and *in situ* analyses, suggesting that the activation of "immune evasion" mechanisms may contribute to the particularly malignant phenotype of this sarcoma subtype.

INDEX

INDEX

1. INTRODUCTION

1.1. Soft tissue tumor

The word sarcoma comes from Greek and it is a fusion between the words sarcos (flesh) and oma (tumor). The term refers to a group of rare and aggressive tumors of mesenchymal nature characterized by remarkable morphological and molecular heterogeneity (*1, 2*). Sarcomas account for <1% of all adult malignancies, whereas they account for approximately 20% of non-hematologic malignancies in children (*3-5*). Sarcomas can affect bones or soft tissues (STS) of various anatomic sites, including head and neck, extremities, retroperitoneum, and mediastinum (*1, 6-8*). STS are a heterogeneous group of tumors with over 70 subtypes included in the most recent WHO classification of Soft Tissue and Bone Tumors (Fig.1) (*9*). These subtypes are classified according to the mesenchymal tissue they most closely resemble and specific molecular features.

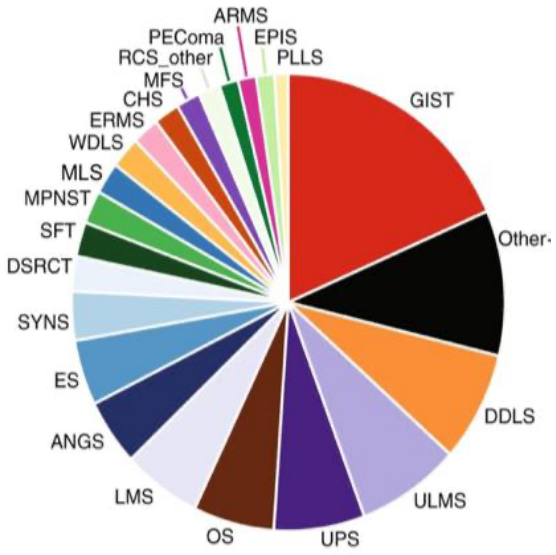

Fig.1 STS subtypes distribution in a representative mono-institutional cohort**.** Adapted from (*3*): ANGS, angiosarcoma; DSRCT, desmoplastic small round cell tumour; MPNST, malignant peripheral nerve sheath tumour; ULMS, uterine leiomyosarcoma; PLLS, pleomorphic liposarcoma; UPS, undifferentiated pleomorphic sarcoma; LMS, leiomyosarcoma; SYNS, synovial sarcoma; PEComa, perivascular epithelioid cell tumour; OS, osteosarcoma; EPIS, epithelioid sarcoma; SFT, solitary fibrous tumour; WDLS and DDLS, well differentiated and dedifferentiated liposarcoma; MLS, myxoid liposarcoma; CHS, chondrosarcoma; RCS_other, round cell sarcoma; MFS, myxofibrosarcoma; ES, Ewing sarcoma; ERMS and ARMS, embryonal and Alveolar rhabdomyosarcoma; GIST, gastrointestinal stromal tumour.

Conventionally, STS are distinguished into simple karyotype STS, hallmarked by recurrent and pathognomonic gene mutations (e.g. Gastrointestinal stromal tumors i.e. GIST) or chromosome rearrangements (e.g Ewing sarcoma, Myxoid liposarcoma, Extraskeletal myxoid chondrosarcoma, Synovial sarcoma) (*2, 10-12*), and complex karyotype STS, showing numerous and non-recurrent structural and numerical

aberrations (e.g. Leiomyosarcoma, Pleomorphic sarcoma, Malignant peripheral nerve sheath tumor, Dedifferentiated liposarcoma (*1, 2, 10, 13, 14*).

1.2. Liposarcoma

As highlighted in Figure 1, the most common STS types include GIST, Undifferentiated pleomorphic sarcomas, Leiomyosarcomas, and Liposarcomas (LPS) (*15*). LPS represent approximately 15% of all STS (*16-18*). Around half of LPS occur in the retroperitoneum and about a quarter in the limbs (*19, 20*).

LPS are "adipocytic malignant tumors" i.e., tumor displaying some degree of adipocytic differentiation. According to the most recent WHO classification, LPS are distinguished into five subtypes: myxoid liposarcoma, pleomorphic liposarcoma, myxoid pleomorphic liposarcoma, well differentiated and dedifferentiated liposarcoma. These last two types of LPS are the focus of this thesis and will be discussed in detail further on (*9, 21*). As far as the other LPS subtypes are concerned, myxoid liposarcoma accounts about 1/3 of LPS and 5% of all STS in adults (*9*). This tumor is histologically characterized by lipoblasts surrounded by a myxoid (gelatinous) stroma and arborizing blood vessels (Fig.2) (*7, 22, 23*). Myxoid liposarcoma most commonly develop in the extremities and it is exceedingly rare in retroperitoneum (*24*).

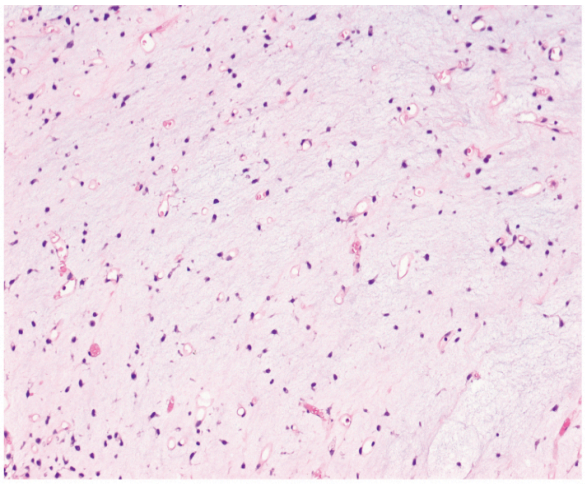

Fig.2 Histology of myxoid liposarcoma. From (*24*)

The molecular hallmark (pathognomonic alteration) of this simple-karyotype STS is a reciprocal translocation involving the chromosome 12 with either chromosome 16 or 22,

namely t(12;16)(q13;p11) and (12;22)(q13;q12). In the first case, the gene mapping on chromosome 12, *DDIT3* (DNA damage inducible transcript 3) is fused in-frame with the *FUS* RNA binding protein (*25*). In the second case, a less frequent fusion, *DDIT3* fuses with *EWSR1* (EWS RNA Binding Protein 1). *DDIT3,* previously known as *CHOP*, is a DNA-binding transcription factor that belongs to the CCAAT/enhancer (*C/EBPA*) family of basic-leucin zipper (bZIP) transcription factors. *DDIT3* is usually expressed at low levels but it is induced following cellular stresses (e.g. endoplasmic reticulum stress, starvation, DNA damage, and hypoxia), conditions under which, by antagonizing C/EBP-mediated transcription, *DDIT3* promotes cell cycle arrest and inhibition of terminal cell differentiation, in particular adipocytic differentiation (*9, 26, 27*). *FUS* and *EWSR1* are members of a highly conserved and widely expressed family of proteins known as the FET family. These versatile proteins bind RNA and are involved in the control of RNA transcription and processing. In addition, with their N-terminus, they are implicated in the generation of several fusion oncoproteins involved in various types of STS (*28*).

Pleomorphic liposarcoma mainly arises in the extremities, but may also occur in the abdomen, trunk or chest wall and retroperitoneum (*29*). This tumor is histologically characterized by cellular atypia, large lipoblasts with hyperchromatic and irregular nuclei, and multivacuolated cytoplasm (Fig.3) (*30*). From the molecular point of view, pleomorphic liposarcomas are complex karyotype STS characterized by multiple and non-recurrent chromosomal losses and gains (*31, 32*).

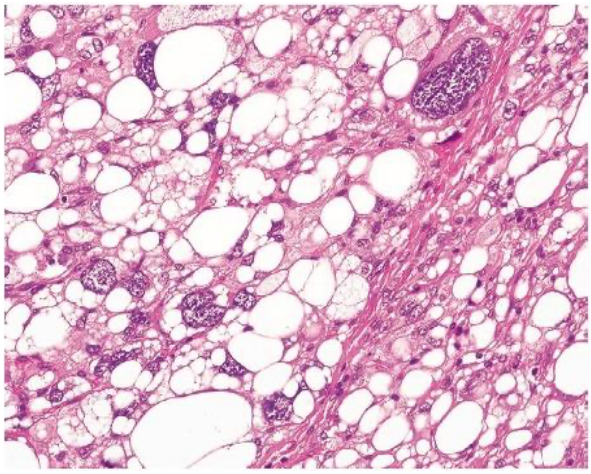

Fig.3 Histology of pleomorphic liposarcoma. From (*30*)

The WHO classification of STS has recently included the myxoid pleomorphic liposarcoma in the list of liposarcoma subtypes (*9*). This type of STS is commonly detected in children and young adults affected by the Li-Fraumeni syndrome, typically associated with heterozygous *TP53* germline mutations (*33, 34*). The most common development site is the mediastinum, although occasionally it may involve also other sites. Histologically it shows intermediate features between pleomorphic liposarcomas and myxoid liposarcomas, hence the name. Nevertheless different from classical myxoid liposarcomas, the myxoid pleomorphic liposarcoma lacks the pathognomonic translocations of DDIT3 (Fig.4) (*9*).

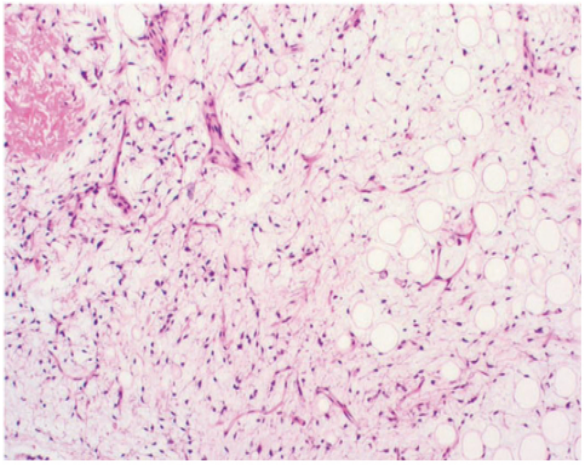

Fig.4 A myxoid pleomorphic liposarcoma. From (*35*)

1.3. Well differentiated and Dedifferentiated liposarcoma

Well Differentiated Liposarcomas (WDLS) are low-grade adipocytic malignant tumors that, when arising in the extremities, are also defined Atypical Lipomatous Tumors (*24*). Although WDLS are characterized by an indolent course, they show a tendency to recur, with recurrence rates ranging between 30 to 50%, depending on the site (*9, 36, 37*). WDLS account for about 30-40% of all LPS and represent the second most frequent category of LPS after dedifferentiated liposarcoma (*30, 38, 39*). WDLS show commonly arise in the limbs and retroperitoneum, more rarely in other sites (spermatic cord, mediastinum, trunk, head and neck) (*9*). Macroscopically, WDLS are

well circumscribed masses comprised of lobulated yellowish fatty masses (*30*). Based on histological characteristics, WDLS are classified into 3 main subtypes by the WHO classification (*9*): the most common is the sclerosing type, which commonly occurs in the retroperitoneal and pretesticular regions and consists of scattered atypical stromal cells within a prominent collagenous stroma (*37, 39*); adipocytic or lipoma-like type is characterized by the presence of the proliferation of mature adipocytic cells of variable sizes with focal nuclear atypia and atypical stromal cells (Fig.5) (*30, 37, 39*); the inflammatory type is the rarest tumor type and occurs only in the retroperitoneum. This subtype is characterized by the presence of a prominent inflammatory infiltrate and a very low level of adipocytic component (*9, 37, 39*).

WDLS can progress to a more malignant form, the Dedifferentiated Liposarcoma (DDLS). Indeed, the term "dedifferentiated liposarcoma" was coined by Evans in 1979 to indicate the morphologic progression of a WDLS to a high-grade non lipogenic sarcoma (*40*), although DDLS may also develop as *de novo* tumor, in the absence of evidence of a pre-existing WDLS component (*9*). Macroscopically, a DDLS appears as a multinodular mass with a yellow cut surface and firm tan-gray areas (*30, 37, 41*). DDLS show a high propensity to local recurrence, particularly in the retroperitoneum where they invariably recur within 10-20 years from diagnosis. Paradoxically, a DDLS may recur as a pure WDLS. On one hand this fact further stresses the common origin of the two neoplasms; on the other hand, it indicates the reversibility of the phenomenon of dedifferentiation (*24*). The metastatic rate is 15-20% but mortality is most commonly related to uncontrolled local recurrence than distal spreading. The 5-year overall survival rate is about 30% and decreases over time (*9*).

The evolution of WDLS into DDLS is most commonly observed in the retroperitoneum, most likely due to the delayed diagnosis of tumors developing in this anatomical location (*9, 37*).

The transition from WDLS to DDLS is generally abrupt, but in few cases WDLS and DDLS areas may be intermingled (Fig.5) (*9, 30*). The persistence of elements with adipocytic features is fundamental in the differential diagnosis of DDLS with other STS (*9, 37*).

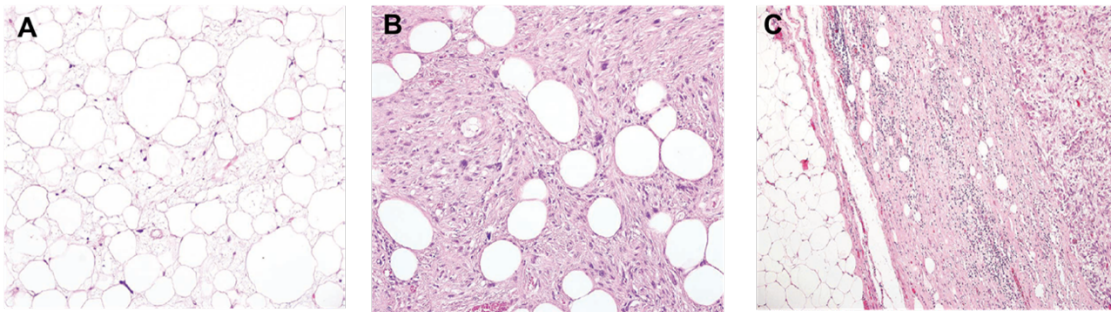

Fig.5 Histology of WDLS and DDLS **(**A) Histology of adipocytic or lipoma-like variant of WDLS, (B) Gradual transition from WDLS to higher grade areas (C) DDLS showing an abrupt transition from WDLS to non-lipogenic sarcoma. Adapted from (*30*).

As WDLS, DDLS commonly arise in the retroperitoneum and limbs, and less frequently in other sites (*9*). Currently, tumor location is the most important prognostic factor: due to the depth and wideness of the retroperitoneum, tumors developing in this anatomical region tend to reach a very large size (up to over 20 cm in diameter) before causing any symptom. Moreover, these symptoms are often nonspecific resulting in a misdiagnosis and making surgical resection very challenging (*36, 42*). Thus, retroperitoneal STS feature in general a worst outcome compared to tumors that develop in other regions.

1.3.1. Molecular genetics of WDLS and DDLS

WDLS and DDLS are genetically characterized by the amplification of the chromosome region 12q13-15. This amplicon typically includes *MDM2*, *HMGA2* and, but not always, *CDK4* genes (Fig.6) (*43*).

The amplicon consists of up to hundreds of extra-copies of these genes that are commonly organized in extrachromosomal rings or giant rods (*9, 45, 46*). Whilst WDLS show a relatively simple karyotype, DDLS are complex karyotype tumors in which, besides the pathognomonic 12q amplification, multiple numerical and structural alterations are present (Fig.6) (*10, 47*).

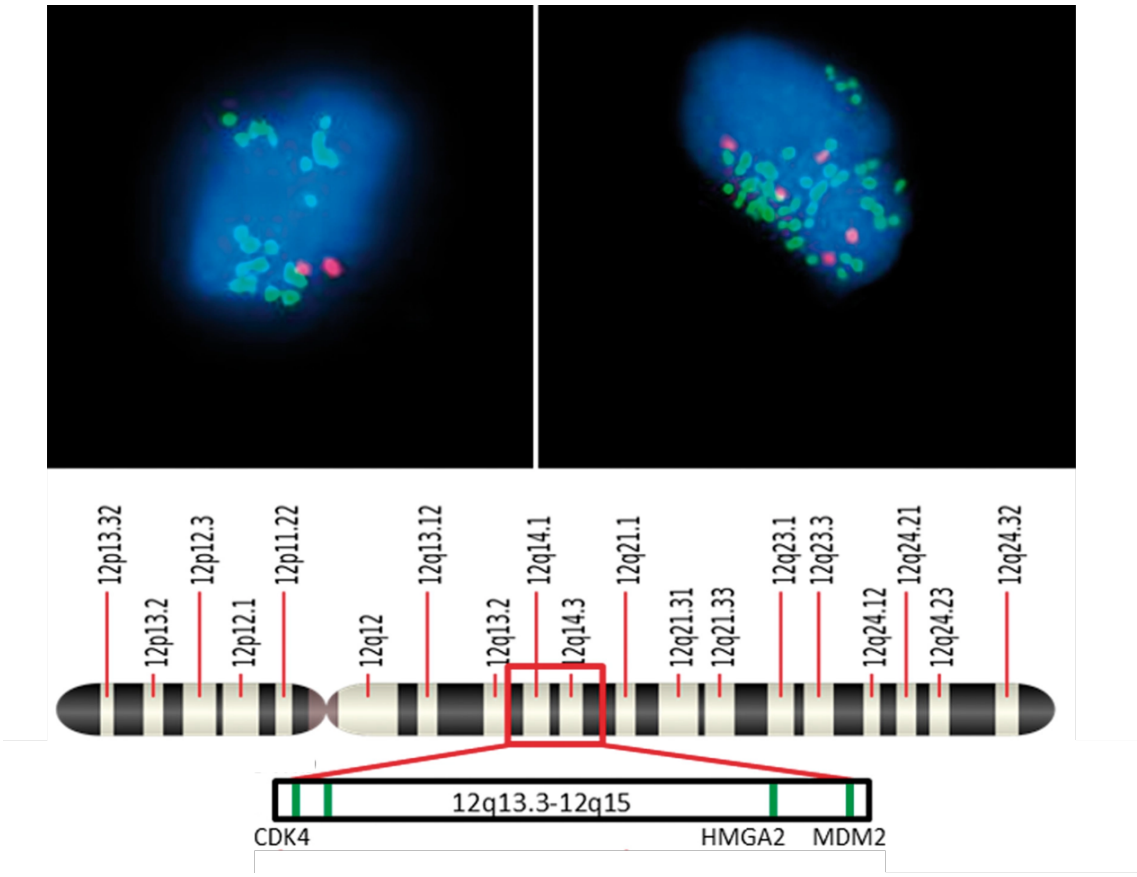

Fig.6 Upper panel: FISH analysis indicating the amplification of MDM2 (green) in a WDLS (left) and the recurrence as DDLS of the same case (right). The red signal marks the 12q centromeric marker (CEN12). Lower panel: cartoon showing the 12q13-15 amplicon involving MDM2, HMGA2 and CDK4. Adapted from (*44*).

1.3.2. MDM2, HMGA2 and CDK4

The *MDM2* gene, located on 12q15, encodes for a E3 ubiquitin ligase. The main and best characterized target of MDM2 is the tumor suppressor p53 (*48*). p53 is the most commonly mutated tumor in cancer (*49*). In fact, in many tumors the p53 tumor suppressive activity is hampered due to the presence of loss of function mutations of the *TP53* gene. p53 is a transcription factor that was defined "guardian of the genome" (*50*) due to its involvement in numerous pathways related to DNA damage and repair but also cell cycle regulation, apoptosis, premature senescence, autophagy, and other forms of cell death. However, more and more physiological (e.g. metabolism, protein translation, differentiation) and pathological processes (invasion, metastasis, chemoresistance) were

being found to be controlled by p53, either as wild type or gain-of-function mutant forms (*51-54*).

p53 is typically post-transcriptionally regulated and the p53 protein is physiologically maintained at low levels through a constant proteasome-mediated degradation orchestrated by MDM2. The capacity of MDM2 to post-transcriptionally regulate p53 has therefore a significant impact on cellular homeostasis. MDM2 binds p53 primarily at the N-terminus although the C-terminal region seems also be involved in this interaction (*55-57*). Once it has been bound, MDM2 ubiquitinates p53 and promotes its proteasome-mediated degradation (Fig.7) (*58-60*). In the presence of a stress signal, p53 becomes phosphorylated and MDM2-mediated degradation is impeded. Interestingly, MDM2 is a transcriptional target of p53. This generated a feedback loop that ensures the restoration of physiological low levels of p53 once the "alarm" is over.

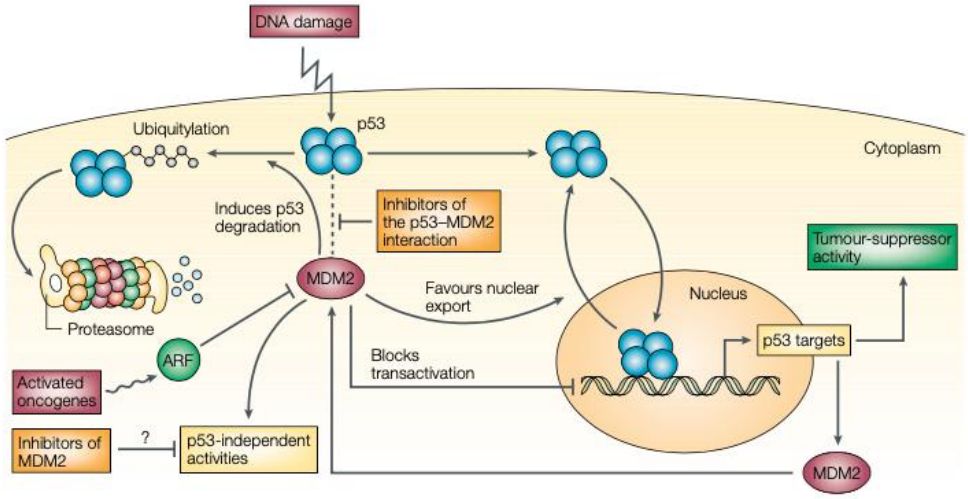

Fig.7 MDM2-p53 pathway. From (*58*).

Although in most tumors the inactivation of p53 tumor suppressive activities is achieved through *TP53* inactivation mutations, a subset of tumors, among which sarcomas and leukemias, retain *TP53* in a wild type status and rely on the overexpression of *MDM2* as a strategy for p53 inactivation (*61*). WDLS and DDLS represent paradigmatic examples of this phenomenon (*37, 62*) and the targeting of p53:MDM2 interaction represents a very promising therapeutic strategy for the reactivation of a p53 response in these tumors.

Indeed, several MDM2 inhibitors are currently in clinical trials for the treatment of MDM2 amplified/overexpressing sarcomas with very encouraging results, including Nutlins such as RG7112 (*63, 64*), and other small molecular inhibitors like SAR405838 (*65*) and HDM201 (*66, 67*).

Noteworthy, MDM2 exerts additional functions besides controlling p53. For instance, MDM2 contributes to the regulation of chromatin remodeling by both interacting with PRC2 (polycomb repressive complex 2) and by ubiquitinating the Histone Methyltransferase SUV39H1 (*68, 69*). Interestingly, it has been shown that MDM2 sustains adipogenic differentiation in a p53-independent manner and its ectopic expression promotes the conversion of myoblast cells into adipocytes, thus acting as a differentiation switch (*68, 70*). Additionally, MDM2 is known to regulate the protein turnover of PPARα and PPARγ, master regulators of lipid homeostasis (*71, 72*).

HMGA2, located on 12q14.3, encodes a protein belonging to the family of non-histone chromosomal high mobility group proteins. It functions as an architectural transcription factor that, through the interaction with other proteins of the enhanceosome, controls chromatin structure and favors gene transcription (*73*). The HMGA2 protein is highly expressed in embryonic cells whereas it is almost undetectable in adult tissues. In the mesenchyme, it has been demonstrated to play a key role in adipogenesis and stemness (*74, 75*). Elevated HMGA2 levels are detected in different tumor types (*76*). *HMGA2* overexpression exerts a pro-tumorigenic activity through direct or indirect induction of cell cycle genes and apoptosis inhibition (Fig.8). HMGA2 also influences the DNA repair machinery and promotes a drug resistance and an epithelial-to-mesenchymal transition (*77*).

The protein contains an AT-hook domain, a DNA binding region that recognizes AT-rich DNA regions, at the N-terminus (exon 1-3) whilst the C-terminus has essentially regulatory functions (*78, 79*). *HMGA2* overexpression in tumors is often associated with gene amplification or translocation leading to the loss of the regulatory C-terminus (exons 4 and 5) resulting in altered mRNA and increased HMGA2 protein levels and activity (*80-82*).

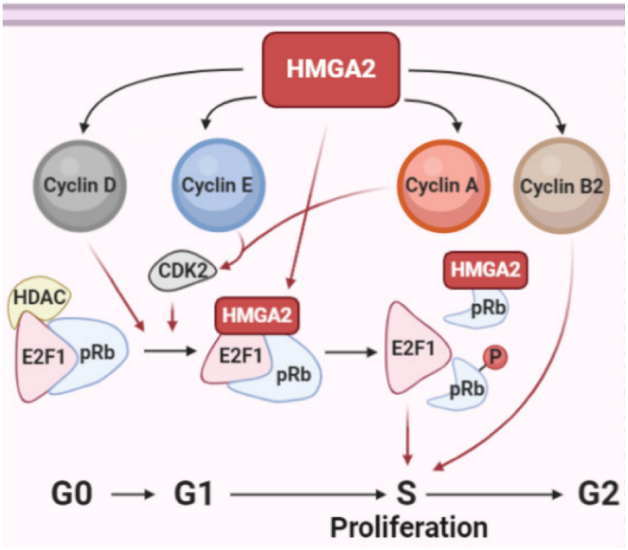

Fig.8 *HMGA2* promotes cell proliferation**.** HMGA2 promotes pRB phosphorylation and activates cyclins D1, E, and A. The phosphorylation of pRB results in the release of E2F1 which promotes the transcription of target genes that induce S phase entry. Moreover, HMGA2 is capable of displacing HDAC1 from pRB thereby activating E2F1. Adapted from (*77*).

CDK4 (12q14.1) is a cyclin-dependent kinase (CDK) that plays a central role in the control of the cell cycle. CDKs are a group of serine/threonine kinases that form active heterodimeric complexes when they are bound to cyclins that act as regulatory subunits (*83-85*). Analogously to its paralog *CDK6*, *CDK4* forms active complexes with type D cyclins (D1, D2 and D3). CDK4/CyclinD complexes are the trigger of the transition through the G1/S phase of the cell cycle (*85-87*). Specifically, CDK4/6-cyclin D acts by inactivating the tumor suppressor *RB1*. Physiologically, *RB1* binds and inhibits the E2F family of transcription factors, thus preventing E2F-mediated transcriptional activation of gene necessary for the G1/S phase transition (*88, 89*). By phosphorylating RB, the CDK4/6-Cyclin D complexes promote the dissociation of E2F from RB thus relieving E2F from RB-mediated inhibition and unleashing E2F-mediated transcription (*90, 91*). The kinase activity of cyclin D-CDK4/6 complexes, like other cyclin/CDK complexes of the cell cycle, is regulated by diverse members of the INK family of CDK inhibitors (p14/p19, p15, p16, p18, p21, p27, p57) (Fig.9) (*92*).

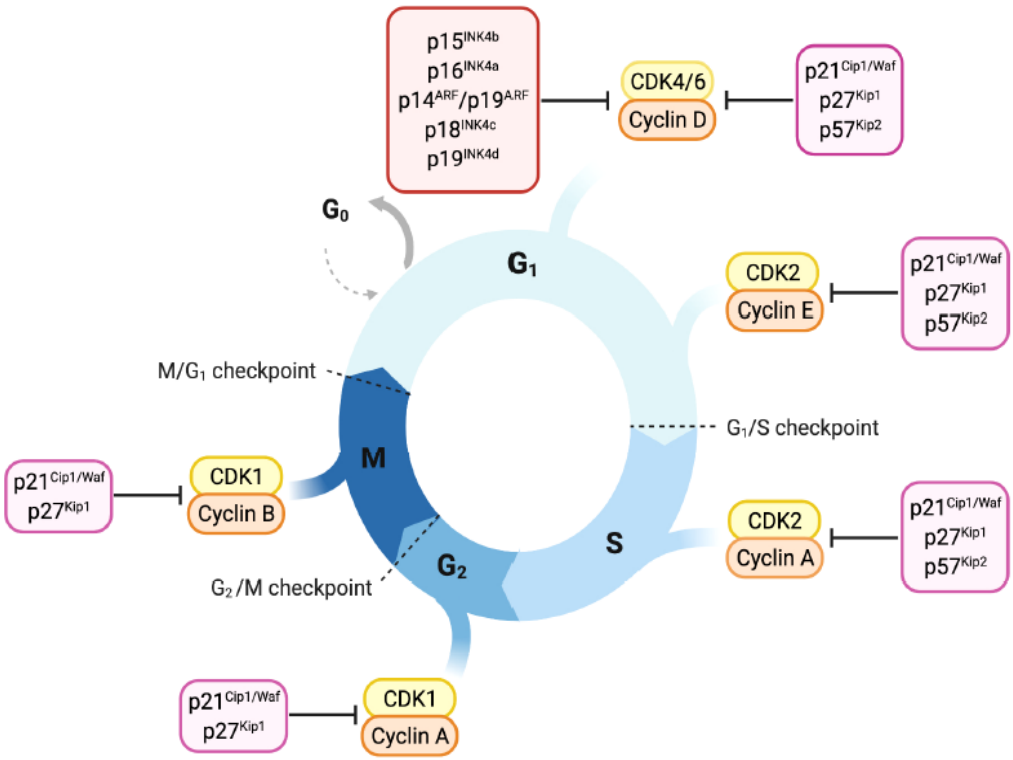

Fig.9 CDK4/6 control over G1/S cell cycle progression. From (*93*).

Although the most characterized role of CDK4/6 is the regulation of cell cycle progression, mounting evidence indicate that these kinases are implicated in the regulation of several other cellular functions, among which lysosome and mitochondria metabolism, oxidative phosphorylation and regulation of immune response (*92*).

In WDLS and DDLS, *CDK4* is often but not always included in the 12q13-15 amplicon (*94*). In these tumors, the increased levels of CDK4 lead to a constitutive inactivation of RB and, therefore, in an uncontrolled cell proliferation (*95*). The efficacy of CDK4/6 inhibitors for WDLS and DDLS treatment, both as single agents or in combination with MDM2 inhibitors (e.g. ribociclib plus siremadlin), is currently under clinical investigation (*96, 97*).

1.3.3. Additional genomic features

If the 12q13-15 pathognomonic amplification of WDLS and DDLS typically targets *MDM2*, *HMGA2* and *CDK4,* other genes mapping in proximity of these targets are reported to be occasionally included in the amplicon and contribute to LPS tumorigenesis (*9*). Among these, *YEATS4* (*GAS41*), a chromatin reader and component of the NuA4 histone acetyltransferase (HAT) complex that promotes gene transcriptional activation by acetylating H4 and H2A histones. Interestingly, it has been shown that the co-amplification of *YEATS* and *MDM2* in DDLS cooperates to repress the p53 pathway (*94, 98-100*). Also, *CPM,* located 11kb downstream *MDM2*, may be included in the amplicon. *CPM* encodes a glycosyl-phosphatidylinositol anchored membrane-bound carboxypeptidase that cleaves basic residues (Arginine or Lysine) located at the C-terminus of proteins and peptides. This proteolytic activity seems to be involved in the regulation of receptor signaling (*101*), in mesenchymal cell differentiation, as well as in the inflammation and coagulation processes (*101, 102*). Other genes occasionally co-amplified are *FRS2* (12q15) and *TSPAN31 (12q14.1)*. *FRS2* encodes an adaptor protein which exerts docking activity for FGFR and other receptor tyrosine kinases thus facilitating their signaling (*103*). *TSPAN31* encodes a transmembrane protein that belongs to the tetraspanin family. Both genes are implicated in cell proliferation and motility (*104*).

Other genetic aberrations reported in DDLS include *ATRX* (Xq21.1), *NF1* (17q11.2) and *CDKN2A* (9p21.3) deletions and amplifications of *JUN* (1p23), *MAP3K5* (6q23) and *TERT* (5p15.33) (*43*).

1.3.4. Heterologous differentiation of DDLS

In the progression from WDLS to DDLS cells lose manifest adipocytic characteristics (the adipocytic nature of a DDLS is inferred by the presence of scattered lipoblasts or associated areas of WDLS) and generally fail to show a defined lineage of differentiation. Nevertheless, the gain of features proper of other mesenchymal tissues may be observed in 5-10% of cases (*9, 22, 30*). This phenomenon, known as heterologous

differentiation, suggests a reactivation of a primitive differentiation program of mesenchymal stem cells (Fig.10).

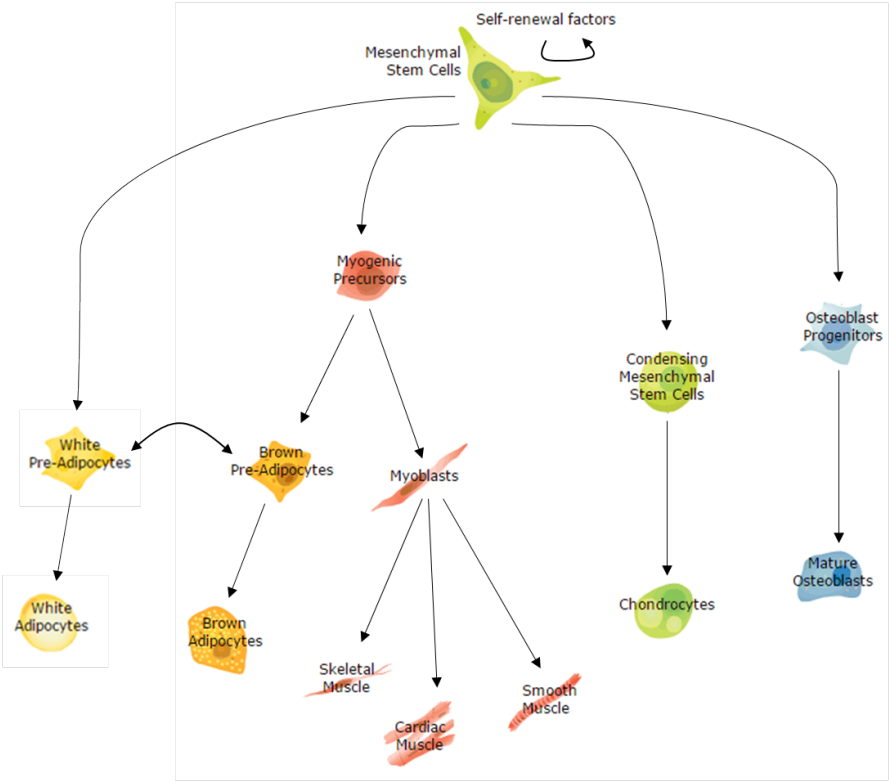

Fig.10 Mesenchymal stem cells differentiation routes**.** Adapted from R&D Systems, 2014.

DDLS undergoing heterologous differentiation may express osteogenic, chondrogenic or, most commonly, myogenic features (*105-108*).

The clinicopathological features of DDLS showing muscular heterologous differentiation were first reported by Binh and coworkers in 2007 (*109*) who found no difference in the clinical behavior of DDLS with muscle differentiation, either smooth or skeletal, vs conventional DDLS (*109*). Subsequently, Kurzawa and coworkers (*110*) confirmed the lack of correlation between clinical outcome and smooth muscle differentiation (positivity for desmin and smooth muscle actin α) (*110*). Both studies included both retroperitoneal DDLS as well as DDLS developed in other truncal sites. This may be a source of bias, as retroperitoneal tumors typically show a worst outcome compared to tumors developed in other truncal sites (*111*). On these grounds, Gronchi and coworkers

(*112*) focused specifically on retroperitoneal DDLS and demonstrated that retroperitoneal DDLS undergoing muscle dedifferentiation showed a worst prognosis compared to conventional DDLS (no defined lineage of differentiation). In particular, these authors demonstrated that DDLS with rhabdomyosarcomatous characteristics (rounded/oval rhabdoid cells with eosinophilic cytoplasm containing filamentous inclusions; atypical and eccentric nuclei with prominent nucleoli) and positive for myogenin, exhibited a particularly poor outcome (Fig.11).

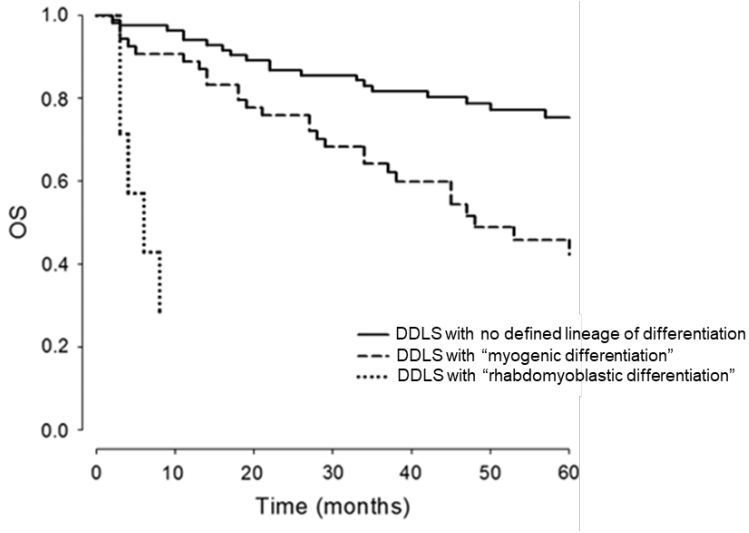

Fig.11 OS of retroperitoneal LPS. Dotted line: DDLS with rhabdomyoblastic differentiation (myogenin positive); dashed line: DDLS with generic myogenic differentiation but negative for myogenin; plain line: DDLS with no defined line of differentiation. Adapted from (*112*).

Subsequent studies (*113, 114*) corroborated these findings and supported the notion that the gain of muscular characteristics, especially towards the skeletal muscle lineage (rhabdomyoblastic differentiation), correlates with a particularly aggressive clinical course in DDLS originating in the retroperitoneum.

2. AIM

In this work we focused on retroperitoneal liposarcomas and exploited RNA-sequencing and targeted NGS omics approaches to investigate the molecular mechanisms underlying the malignant evolution of WDLS to DDLS and the genetic and transcriptional features of the particularly aggressive rhabdomyosarcomatous DDLS variant.

3. RESULTS

3.1. Transcriptome profiling of WDLS and DDLS

A series of 60 retroperitoneal liposarcomas, consisting of 18 WDLS and 42 DDLS, were retrieved from the pathological files of collaborating institutions and transcriptionally profiled by RNA-sequencing (Table 1).

Class	Sample_ID	Myogenin IHC	Paired sample
DDLS	D344	+	x
	D349	+	x
	D375	+	x
	D376	+	x
	D377	+	x
	D378	+	x
	D669	+	x
	D973	+	x
	D974	+	x
	D341	-	D399
	D345	-	D401
	D346	-	D402
	D348	-	D403
	D379	-	x
	D380	-	D408
	D381	-	D409
	D382	-	x
	D383	-	D410
	D510	-	D506
	D511	-	D507
	D512	-	D508
	D513	-	D509
	D514	-	x
	D515	-	D518
	D516	-	x
	D661	-	x
	D663	-	x
	D664	-	x
	D667	-	x
	D668	-	x
	D964	-	x
	D965	-	x
	D966	-	x
	D969	-	x
	D970	-	x
	D971	-	x
	D975	-	x
	D672	-	x
	D1066	-	x
	D1067	-	x
	D1068	-	x
	D1069	-	x

Class	Sample_ID	Myogenin IHC	Paired sample
WDLS	D399	-	D341
	D400	-	x
	D401	-	D345
	D402	-	D346
	D403	-	D348
	D404	-	x
	D405	-	x
	D406	-	x
	D407	-	x
	D408	-	D380
	D409	-	D381
	D410	-	D383
	D506	-	D510
	D507	-	D511
	D508	-	D512
	D509	-	D513
	D518	-	D515
	D972	-	x

Table 1 The study cohort composed of 60 DDLS and WDLS. The 12 cases in which the WDLS and DDLS components came from different areas of the same tumor mass are indicated as "paired samples".

Nine out of 42 DDLS showed rhabdomyoblastic differentiation as indicated by the positivity for myogenin at immunohistochemistry (myogenin IHC positive). Given their exceptional clinical-pathological characteristics, these 9 tumors were excluded from the first analysis that aimed to shed light on the molecular events implicated in the progression from WDLS to DDLS. This first analysis was then conducted on 51 cases, 18 WDLS and 33 DDLS. In 12 cases the WDLS and DDLS components came from different areas of the same tumor mass.

To get an overview of the molecular differences within this tumor series (51 cases), unsupervised transcriptional analyses were performed by Principal Component Analysis (PCA) and unsupervised hierarchical clustering analysis (UHCA). These algorithms are employed to identify, in an unbiased manner, differences or similarities in input data to highlight cryptic patterns or data groupings. In both instances the algorithms try to reduce the number of dimensions in the input dataset without losing important information. In the PCA, this reduction is graphically illustrated into a two or three-dimensional projection (principal components) and it is optimized to maintain as much as possible the variance in the original data set. In the UHCA, objects are partitioned into homogeneous groups, in a way that the similarities within each group are greater that the similarities between the groups. The graphical output of UHCA is usually a dendrogram, in which samples are organized in a hierarchical tree, and data are represented as a heatmap.

PCA, conducted on the top 500 genes with the highest variance in the whole liposarcoma series, showed a certain separation trend between WDLS and DDLS along the PC1, with a minor overlap between the two groups (Fig.12A). No clear pattern of clustering for the matched WDLS and DDLS components of the same tumor was observed (not shown).

Similarly, UHCA identified two major clusters: the first (cluster c) includes the majority of the WDLS samples whilst the second (cluster d) is mostly composed of DDLS (Fig.12B).

The visual inspection of the heatmap identified 2 gene sets whose expression clearly differs between the two clusters. Gene set 1 is mostly expressed in WDLS (cluster c) and includes genes involved in lipid storage and lipid response that are typical to fat cells.

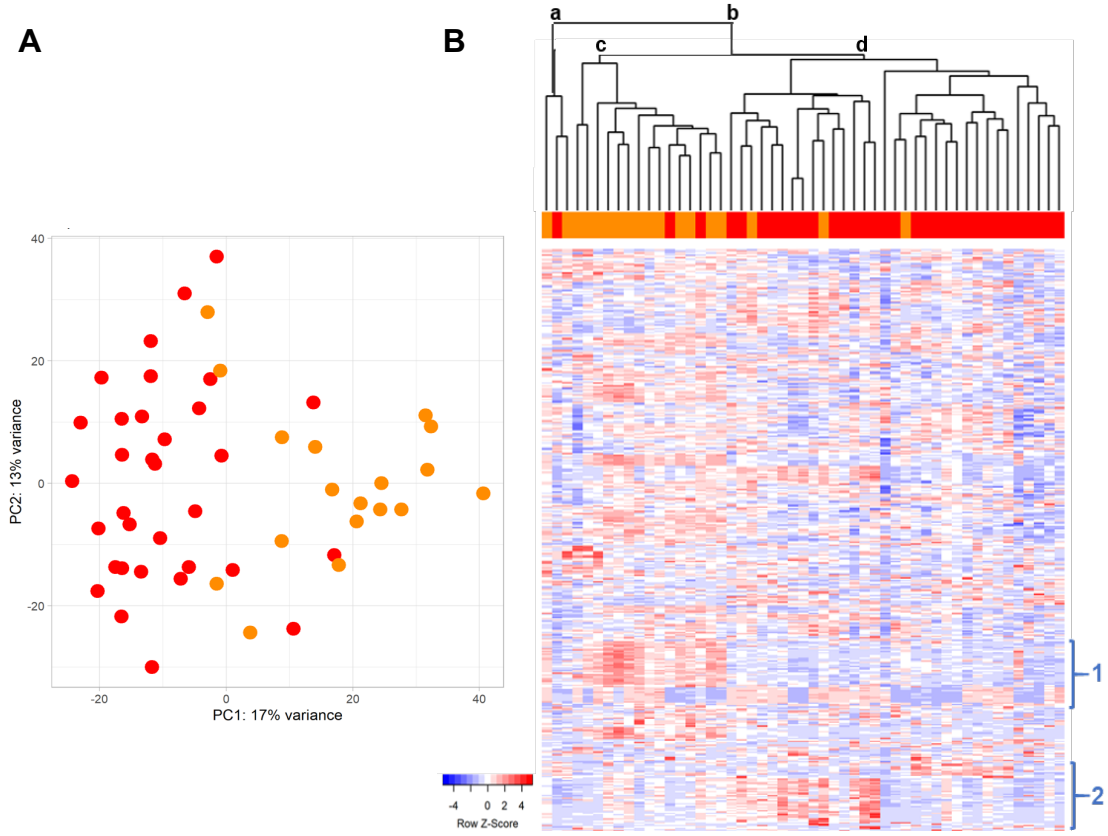

Fig.12 PCA (A) and unsupervised hierarchical clustering (B) of retroperitoneal DDLS and WDLS**.** DDLS are labelled in red; WDLS are labelled in dark orange.

Gene set 2 is mostly expressed in DDLS (cluster d) and includes genes involved in immune response.

Then we performed Differential Expression (DE) analysis by using the DESeq2 algorithm. DE analysis between DDLS vs WDLS identified 2399 differentially expressed genes, 1138 up-regulated and 1261 down-regulated.

Then DE genes were functionally annotated by Gene Set Enrichment Analysis (GSEA) and Over-Representation Analysis (ORA). GSEA was performed both in the classical mode and in the pre-ranked mode. GSEA, ran over the MSigDB Hallmark gene set, and the Biological Process (GOBP), from the Gene Ontology Consortium, highlighted an enrichment of pathways related to cell cycle, DNA repair and epithelial mesenchymal transition (EMT) in DDLS (Fig.13 left), and pathways related to adipogenesis and fat cell differentiation in WDLS (Fig.13 right).

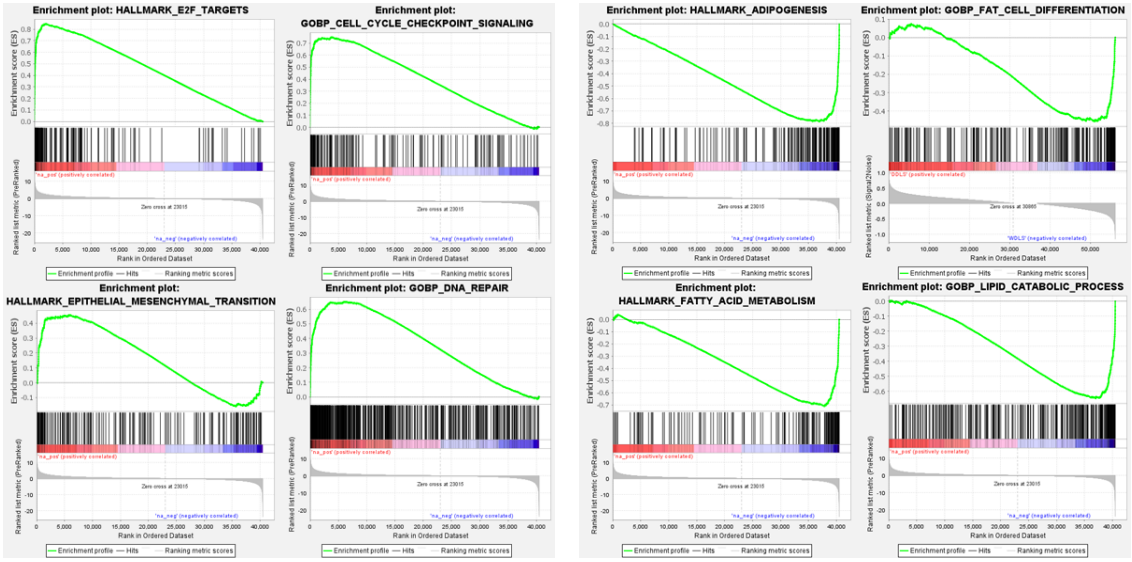

Fig.13 Enriched gene sets and processes in DDLS (left) and WDLS (right) as according to a preranked GSEA of differentially expressed genes. The green line highlights the enrichment of these pathways in DDLS (left, positive correlation) or WDLS (right, negative correlation). The enrichment score is indicated on the Y axis.

GSEA, ran against the MSigDB Oncogenic signatures highlighted several enrichments. Among the enriched signatures there were dataset associated with cell proliferation (Serum response, RB, E2F), Sonic Hedgheog pathway and YAP in DDLS (Fig.14).

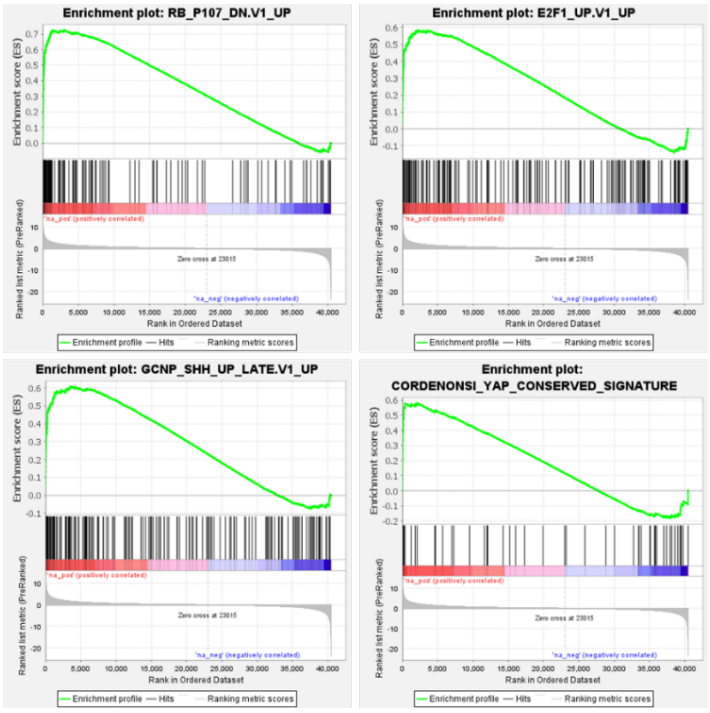

Fig.14 Enrichment of Oncogenic signatures in DDLS. GSEA was run on DE genes against Oncogenic gene sets.

DE genes were also functionally annotated by ORA. ORA is a statistical method that allows to establish whether a pre-defined list of genes (e.g. genes defining a specific pathway) are present more than expected (over-represented) in a group of samples compared to another group, irrespective of the extent of differential expression. This analysis confirmed the positive association of DDLS with cell proliferation (Fig.15 up), and of WDLS with adipogenesis, supporting their more differentiated phenotype (Fig.15 bottom).

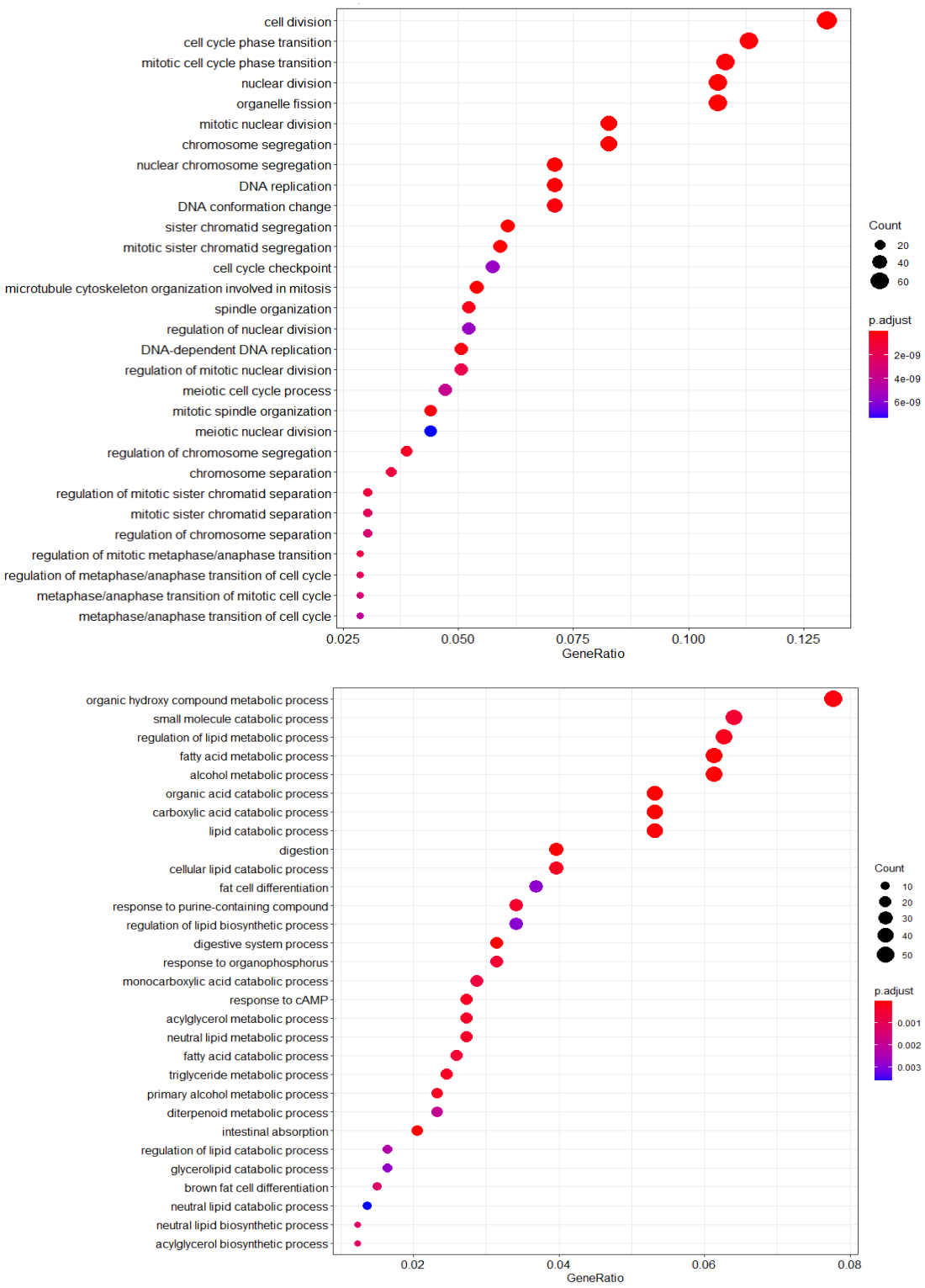

Fig.15 ORA analysis of DDLS and WDLS. The list of genes significantly up-regulated in DDLS (up) and in WDLS (bottom) were used to perform functional enrichment analysis against GOBP gene sets. The x axis labelled as GeneRatio indicates the ratio of input genes that are annotated in a term. The y axis shows the different GOBP annotated. The size of the dot is correlated to the count of gene that belong to a given gene-set. The color of dot is representative of the adjusted p value (p.adjust).

3.2. Mutation profiling and Copy number variation analysis of WDLS and DDLS

To gain further insights into the molecular mechanisms underlying the malignant evolution from WDLS to DDLS, DNA-sequencing was performed in a series of 49 tumor samples, 19 WDLS and 30 DDLS. For 13 of these cases, the WDLS and DDLS components were from different areas of the same tumor mass.

Massive parallel sequencing analysis was conducted using the TruSight 500 Oncology Panel which allows the analysis of 523 cancer-related genes. The genomic variants identified by the TruSight Oncology pipeline were first annotated using the OncoKB annotation tool (*115*), then filtered to identify the mutations with a more likely biological impact. Over 2827 different genomic variants were identified, after OncoKB annotation and filter application, 112 were selected for potential biological impact. No recurrent mutation or recurrently mutated gene (detected event in at least 20% of the whole series or in one of the two subsets, WDLS or DDLS), among the 523 cancer-related genes of the panel were identified (Fig.16).

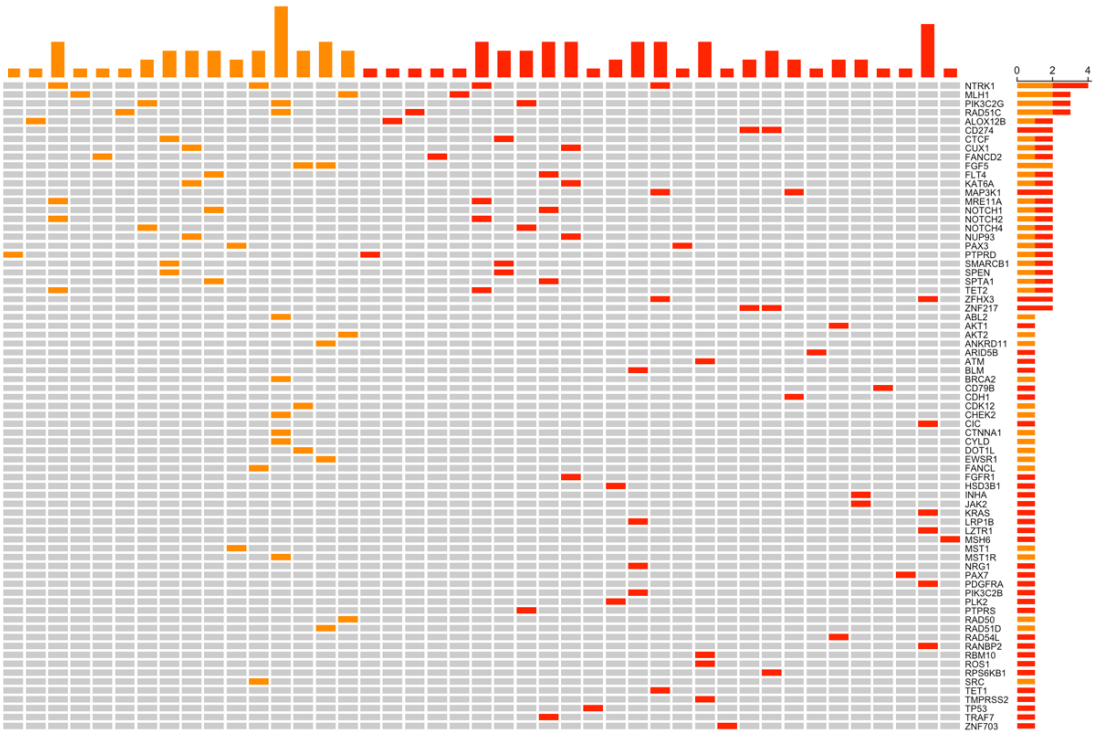

Fig.16 Oncoprint of mutational analysis of WDLS and DDLS. WDLS are labelled in dark orange; DDLS are labelled in red.

The TSO500 panel allows also the detection of copy number gains (CNG) in 59/523 genes. CNG analysis confirmed the pathognomonic amplification of *MDM2* (49/49) and *CDK4* (47/49) in both WDLS and DDLS. In DDLS, relatively common amplification events were detected in *RPS6KB1* (6/30, 20%), *FGFR1* and *CDK6* (5/30, 16%) (Fig.17).

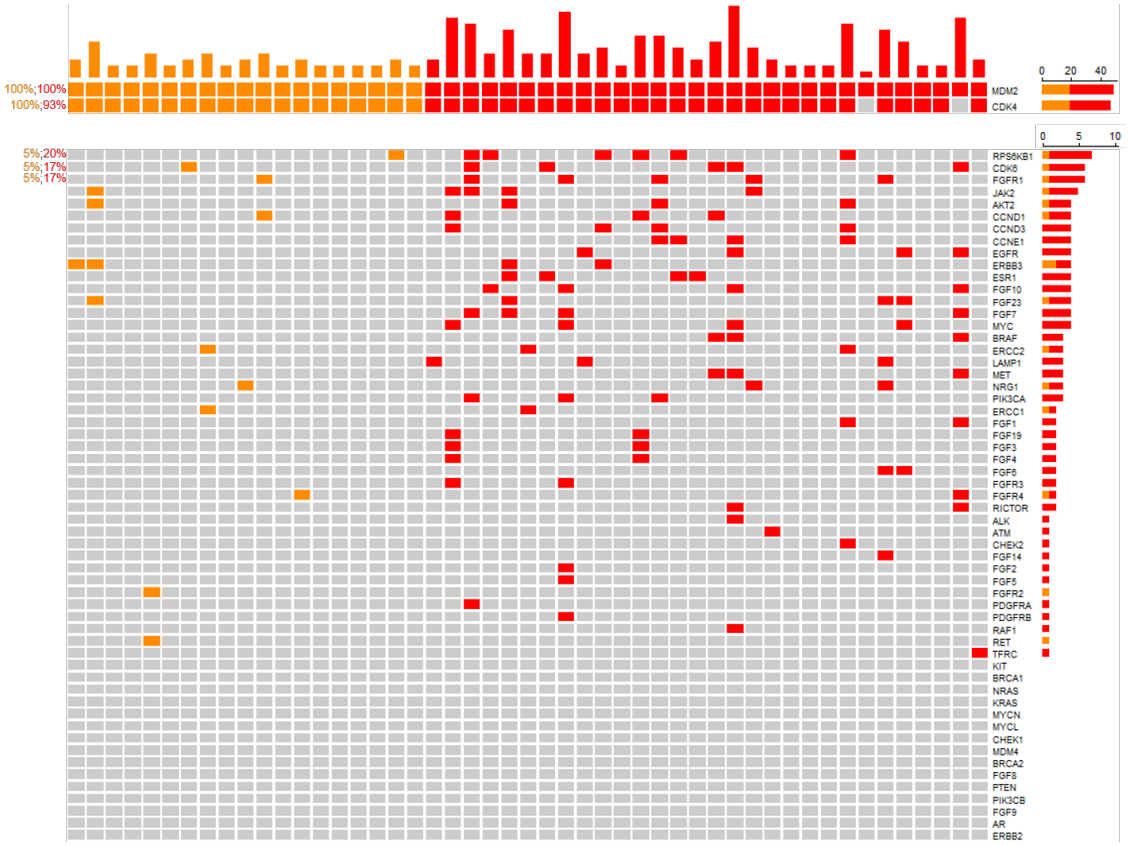

Fig.17 Oncoprint of CNG analysis of WDLS and DDLS. WDLS are labelled in dark orange; DDLS are labelled in red. The frequencies of the common events are reported on the left (dark orange for WDLS; red for DDLS).

Overall, the targeted mutational analysis failed to identify significant differences between WDLS and DDLS. Instead, a tendency towards a higher gene amplification rate in DDLS compared to WDLS was highlighted by CNG analysis.

3.3. Transcriptome profiling of DDLS: focus on rhabdomyosarcomatous DDLS

To gain insight into the aggressiveness of DDLS with rhabdomyoblastic differentiation we compared the transcriptional profile of the 9 DDLS with rhabdomyosarcomatous characteristics, positive for myogenin, and the series of 33 DDLS previously analyzed, negative for myogenin. Transcriptome data confirmed the expression of the *MYOG* gene was restricted to the 9 cases diagnosed as rhabdomyosarcomatous and immunohistochemically scored myogenin positive. We defined these tumors MYOG+ DDLS. All the other DDLS, in which the expression of *MYOG* was negative or negligible (possibly due to contaminant cells) were defined MYOG- DDLS.

Both PCA and UHCA, conducted on the top 500 genes with the highest variance, highlighted a net separation between MYOG+ and MYOG- DDLS, supporting the biological divergence between these two DDLS subtypes (Fig.18).

The two DDLS variants clearly separated in PCA along the PC1 and generated separate clusters in UHCA.

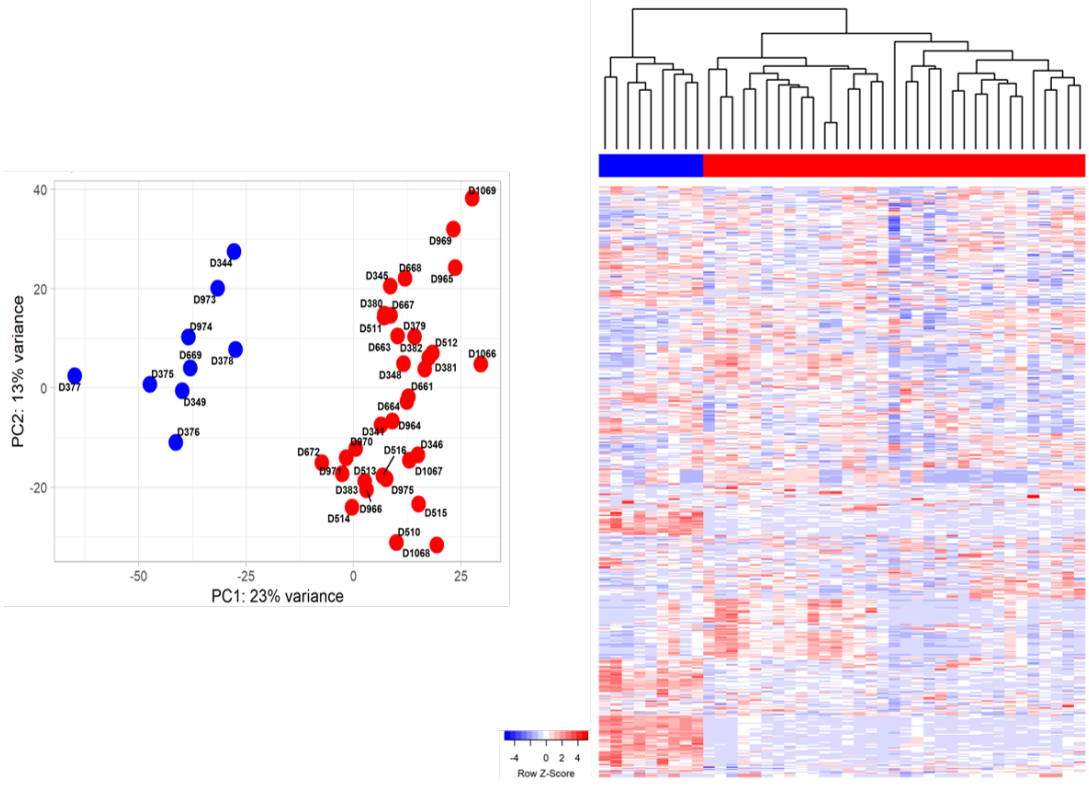

Fig.18 PCA (left) and UHCA (right) of retroperitoneal DDLS**.** MYOG+ DDLS are labelled in blue; MYOG- DDLS are in red.

These analyses supported the notion that retroperitoneal DDLS undergoing rhabdomyoblastic differentiation are characterized by peculiar transcriptional profile and *bona fide* represents a distinct biological entity. To better elucidate the biology of these DDLS, we performed DE analysis. The contrast MYOG+ vs MYOG- DDLS highlighted over two thousand DE genes, 1232 up-regulated and 1211 down-regulated.

DEGs were then functionally annotated by GSEA and ORA. Not surprisingly, the top enriched MSigDB Hallmark pathway in MYOG+ DDLS was myogenesis. Similar results were obtained by running GSEA against the GOBP dataset which indicated enrichment in striated muscle cell differentiation (Fig.19 up). Additionally, MYOG+ DDLS featured activation of E2F and MYC signaling pathways (Fig.19 bottom). Although *MYC* was not differentially expressed (*MYC*: log2FC 0.61; padj=2.9E-01), the two members of the MYC family, *MYCL* and *MYCN*, were definitively up-regulated in MYOG+ DDLS (*MYCL*: log2FC 2.3; padj=6.1E-05; *MYCN*: log2FC 2.3; padj=4.7E-02).

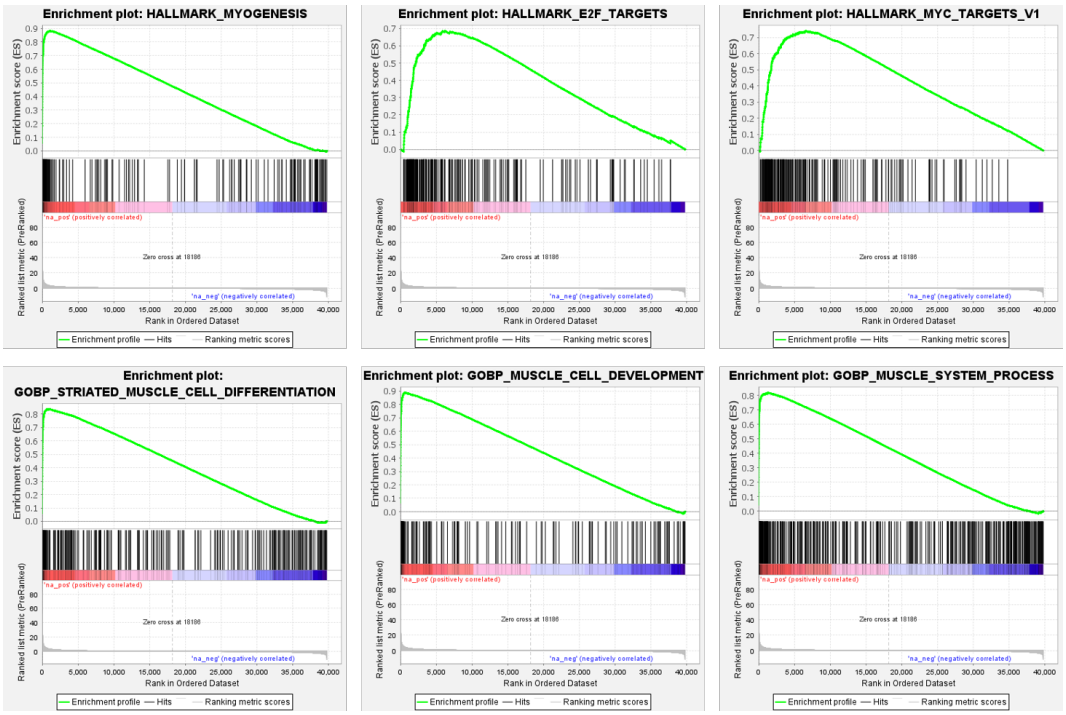

Fig.19 Enriched gene sets in MYOG+ DDLS. A preranked GSEA was run on DE genes against Hallmark gene sets (up) and GOBP gene sets (bottom). The green line summarizes the enrichment of the pathway in MYOG+ tumours (left, positive correlation) vs MYOG- tumours (right). The enrichment score is indicated on the Y axis.

Interestingly, in MYOG- DDLS, GSEA pointed at an enrichment for signatures related to immune response and inflammation (Fig.20).

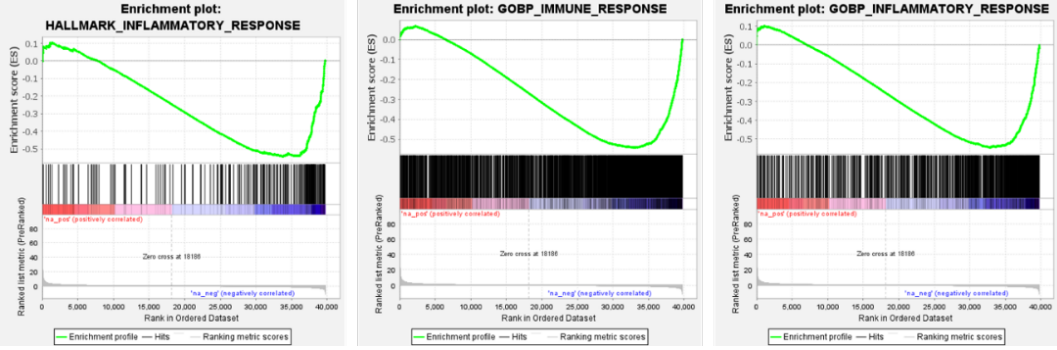

Fig.20 Enriched pathways in MYOG- DDLS. A preranked GSEA, run on DE genes against Hallmark and GOBP gene sets, indicated enrichment of immune-related signatures (green line) in MYOG- tumors (right, negative correlation).

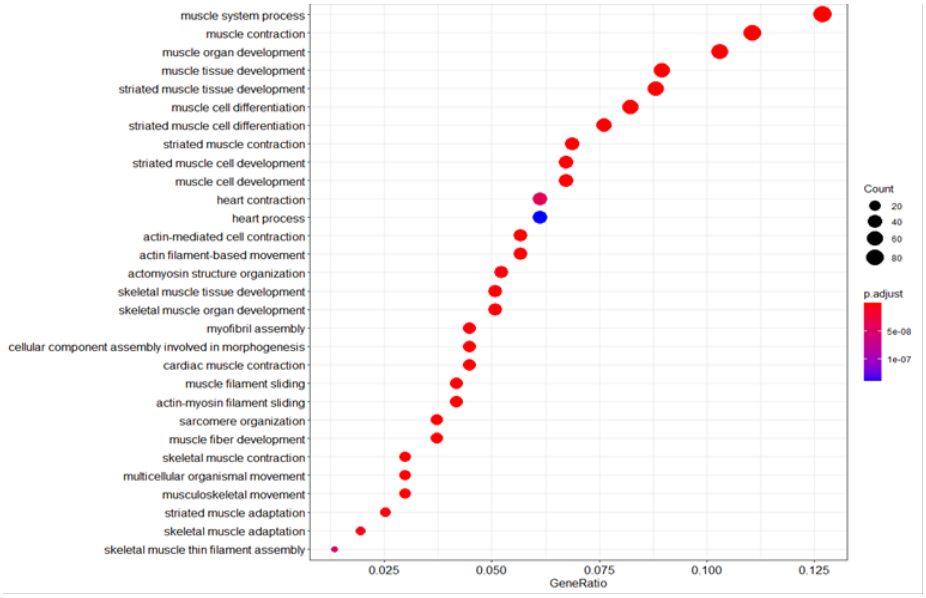

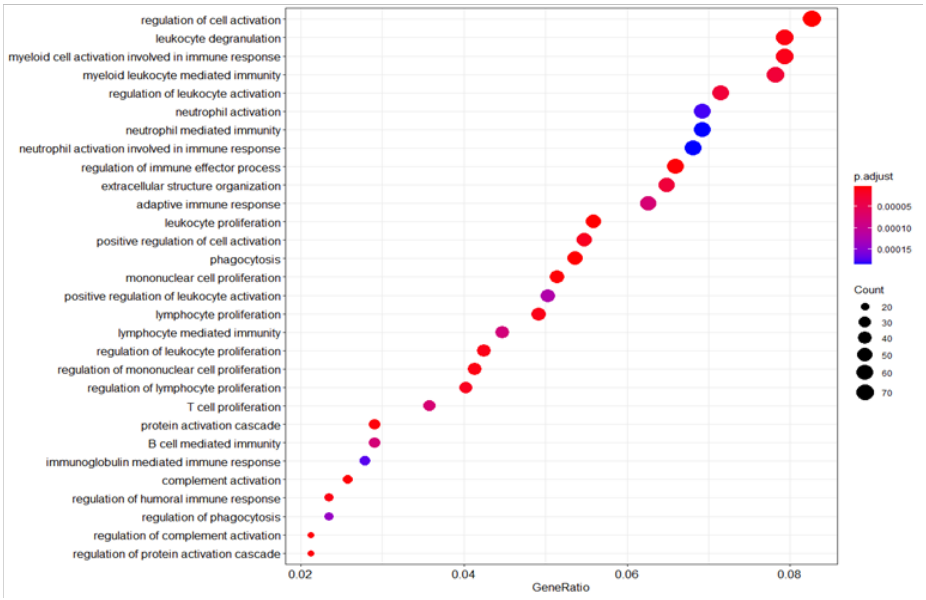

Fig.21 ORA analysis of MYOG+ (up) and MYOG- (bottom) DDLS. The list of genes significantly up regulated in MYOG+ (up) and in MYOG- (bottom) DDLS were used to perform functional enrichment analysis against GOBP gene sets. The x axis labelled as GeneRatio indicates the ratio of input genes that are annotated in a term. The y axis shows the different GOBP annotated. The size of the dot is correlated to the count of gene that belong to a given gene-set. The color of dot is representative of the adjusted p value (p.adjust).

Also, the over-representation analysis of the DE genes indicated a positive association of MYOG+ tumors with muscle-related pathways (Fig.21 up) and of MYOG- tumors with pathways related to the immune system (Fig.21 bottom).

Based on these results, we performed a closer inspection of the genes involved in myogenenic differentiation. Myogenesis process is driven by a sequential activation of myogenic-specific transcription factors. The process starts with induction in progenitor cells of *Pax3* and *Pax7*. These two genes mediate the entry in the myogenic program via the activation of the myogenic regulatory transcription factors *Myf5* and *Mrf4/Myf6*. *Myf5* activates *MyoD/MyoD1* and these two genes cooperate to eventually activate myogenin. The combination of *Myf5*, *MyoD* and myogenin, drives the terminal differentiation and the fusion of myocytes cells into myotubes (Fig.22) (*116*).

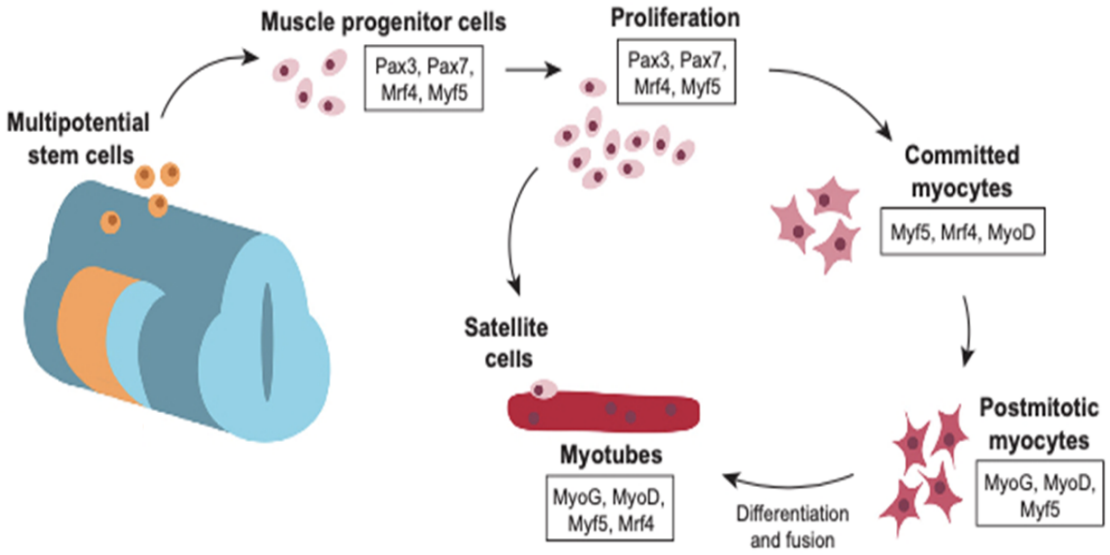

Fig.22 Myogenesis. Adapted from (*116*).

An inspection of the expression levels of these genes indicated that they were all expressed to variable extents in MYOG+ DDLS, with *MyoD1* and *MYOG* showing definitively the highest expression levels.

To investigate the extent of progress toward myogenic differentiation of MYOG+ DDLS, we then focused on known markers of advanced skeletal muscle differentiation (Fig.23), including key structural constituents of terminally differentiated myocytes (e.g. desmin, actin genes, tropomyosin and troponin, myosin heavy and light chain genes, myomesin and myotilin) (*117, 118*).

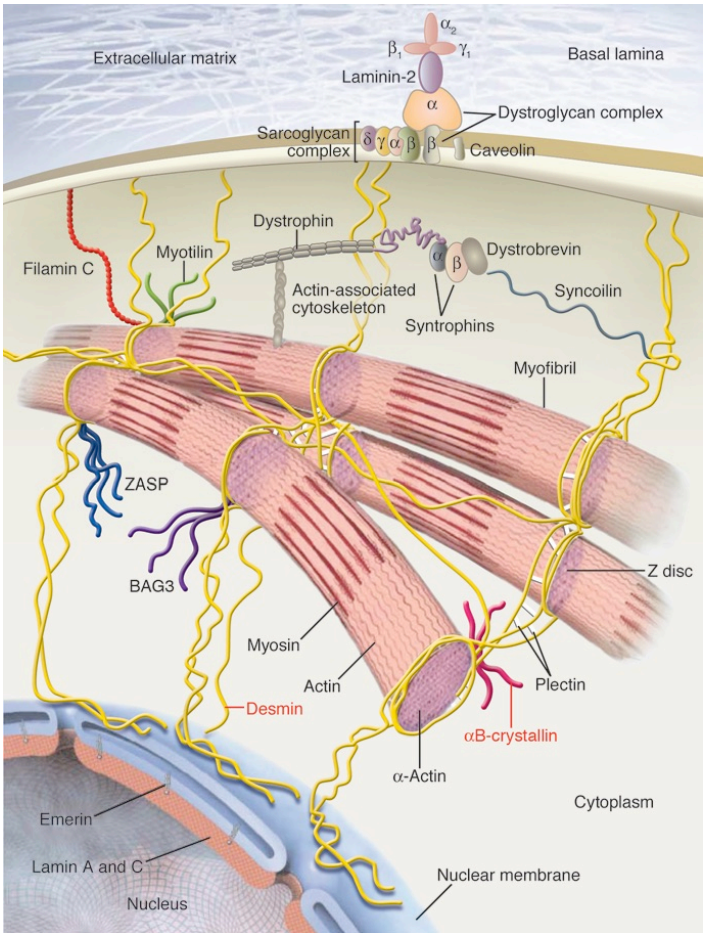

Fig.23 Key structural components of terminally differentiated myocytes. From (*117*).

These turned out to be expressed in MYOG+ DDLS, suggesting a late differentiation stage (Fig.24).

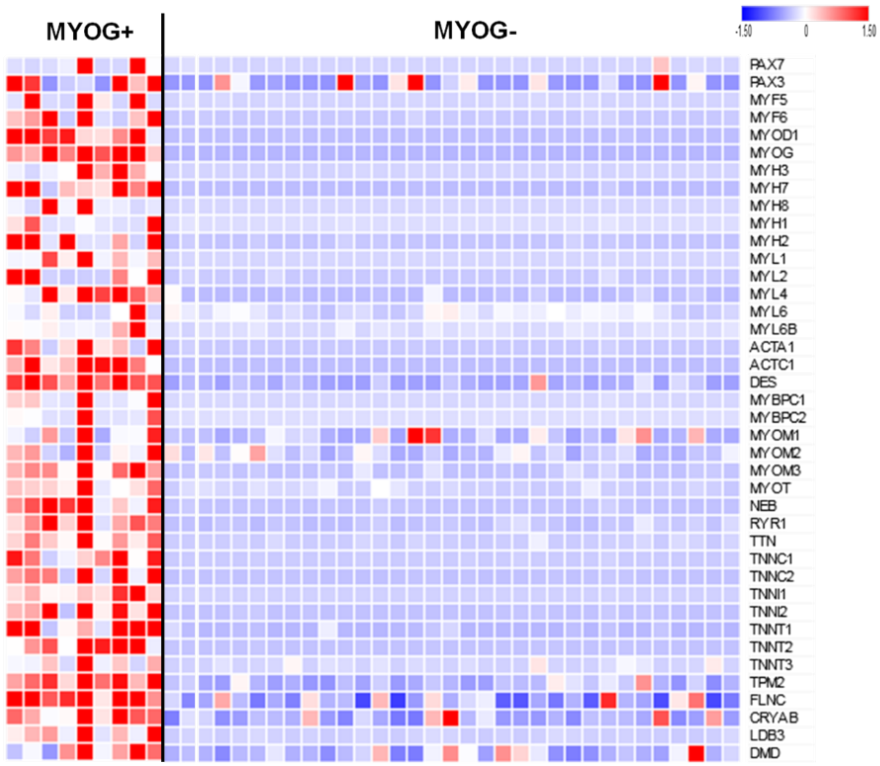

Fig.24 Heatmap of genes involved in myogenesis in MYOG+ and MYOG- DDLS. pTPM values of the indicated genes were used as input. The heat map was generated with the Morpheus web app (Broad institute).

Overall, these results indicate that DDLS undergoing rhabdomyoblastic differentiation feature a profound transcriptional rewiring towards the skeletal muscle lineage, accompanied by MYC pathway activation and a reduced immune cell infiltration.

3.4. Analysis of DDLS immune infiltration

Based on the transcriptome results indicating a reduced immune infiltration in MYOG+ DDLS, we sought to investigate in greater detail the immune contexture of DDLS by using different computational approaches including XCELL, CibersortX, TIMER, QUANTISEQ, and EPIC (*119-123*). These are deconvolution algorithms that infer the presence of immune cells from bulk transcriptome data by using dedicated immune cell-specific signatures. Some of these tools (XCELL and CibsersortX) also provide an overall estimate of immune cell infiltration as immune infiltration score (IIS).

According to these *in silico* approaches, DDLS presented a variable extent of immune infiltration, in line with literature data (*43*). Interestingly, MYOG+ DDLS showed immune infiltration scores significantly lower compared to MYOG- tumors (e.g. XCELL IIS mean values: MYOG+ = 0.04; MYOG- = 0.11; two-tailed t-test, p = 0.05; CibersortX IIS mean values: MYOG+= 1.26; MYOG-=1.69, two-tailed t-test, p=0.03) (Fig. 25 up), corroborating functional annotations of transcriptome data (GSEA and ORA). All the tools used for these analyses agreed that MYOG+ and MYOG- DDLS differ in particular for the extent of infiltration by macrophages (Fig.25 bottom).

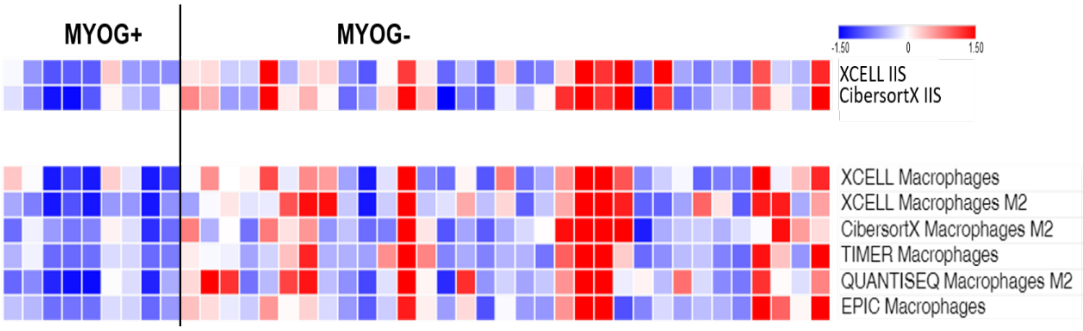

Fig.25 Heatmaps of XCELL and Cibersort overall immune infiltration scores (up) and prediction of macrophages distribution according to the different in silico infiltration calculators (XCELL, CibsersortX, TIMER, QUANTISEQ and EPIC (bottom). The comparison of MYOG+ vs MYOG- is statistically significant for all indicated signatures ($p \leq 0.05$).

Since the capacity of a cell to process and present antigens in the context of HLA molecules is mediated by a group of proteins that represent the antigen presenting machinery (APM) (*124, 125*), we explored the expression levels of these molecules and calculated an APM score, as the geometric mean of pTPM values (transcript per millions

of protein-coding genes). The main components of the APM machinery were overall less expressed in MYOG+ tumors compared to MYOG- DDLS, as indicated also by the significantly lower APM score (Fig.26).

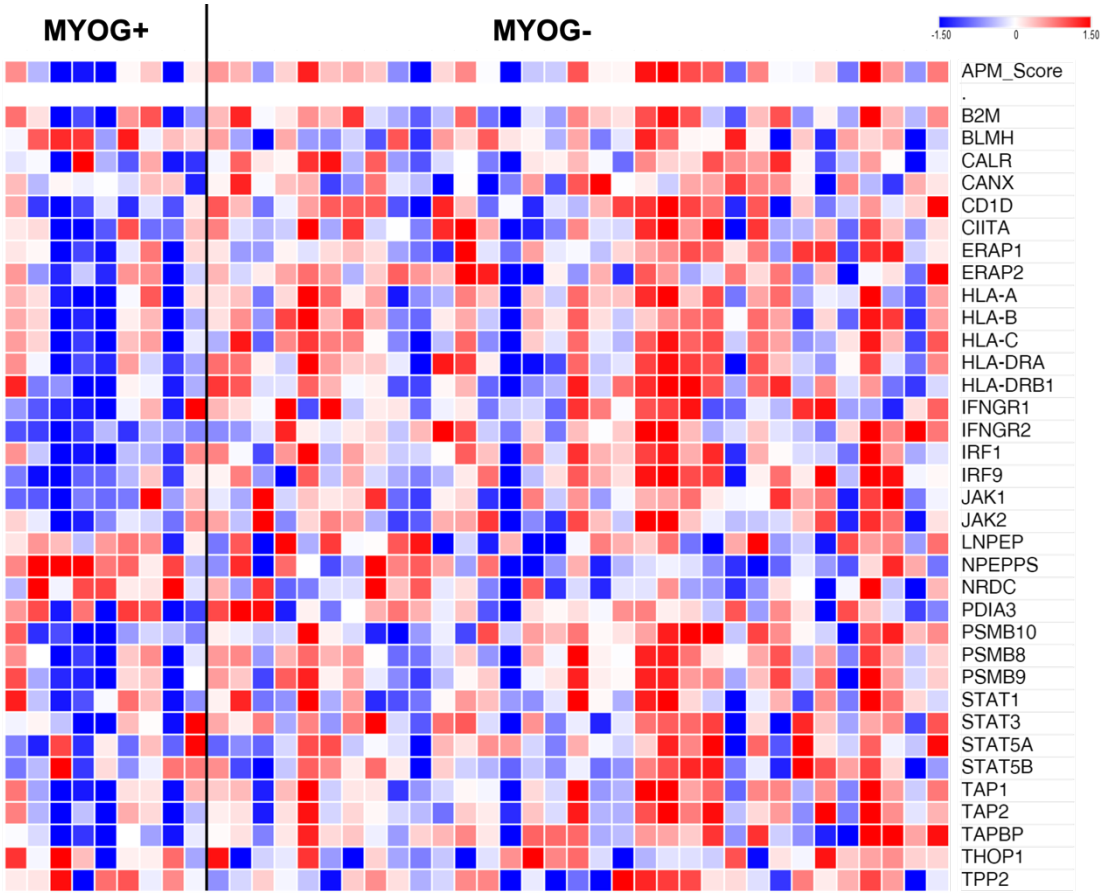

Fig.26 Heatmap of the APM score and pTPM of key APM components (represented as z-scores).

Altogether these *in silico* investigations supported the notion that MYOG+ DDLS feature an immune cold phenotype.

3.5. *In situ* evaluation of immune infiltrate

To validate the *in silico* prediction of a reduced immune infiltration of MYOG+ DDLS, subset of 20 DDLS, 6 MYOG+ and 14 MYOG- DDLS, was stained for the immune cell markers and the percentage of immunohistochemically positive cells over the whole cell population was analyzed and calculated. The following immune cell markers were used: CD14 and CD163 for monocytes/macrophages; CD3 for T cells; CD4 for CD4-positive T cells; CD20 (encoded by MS4A1) for B cells (Fig.27).

The fraction of immune cells infiltrating the tumor was significantly higher in MYOG- vs MYOG+ DDLS for all the markers (Fig.28). Moreover, immune cell counts and pTPM for the cognate marker were significantly correlated (cell count:pTPM spearman correlation values: CD14 $r_s = 0.64$; CD163 $r_s = 0.70$; CD3 $r_s = 0.82$; CD4 $r_s = 0.52$; CD20 $r_s = 0.70$). Overall, these data corroborate the *in silico* predictions that MYOG+ DDLS are less infiltrated by immune cells than MYOG- tumors. The immune cold phenotype of MYOG+ DDLS is likely to contribute to their aggressive behavior.

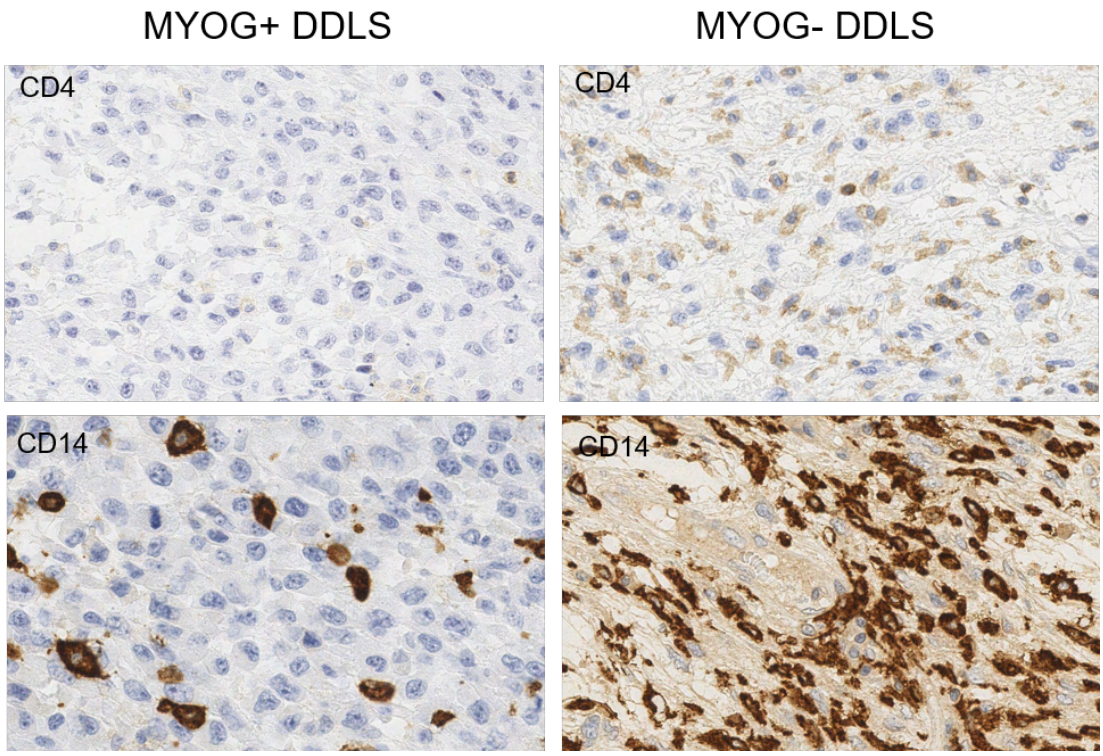

Fig.27 Representative IHC images for: CD4 T cells and CD14 monocytes/macrophages of a MYOG+ (left) and a MYOG- (right) DDLS sample.

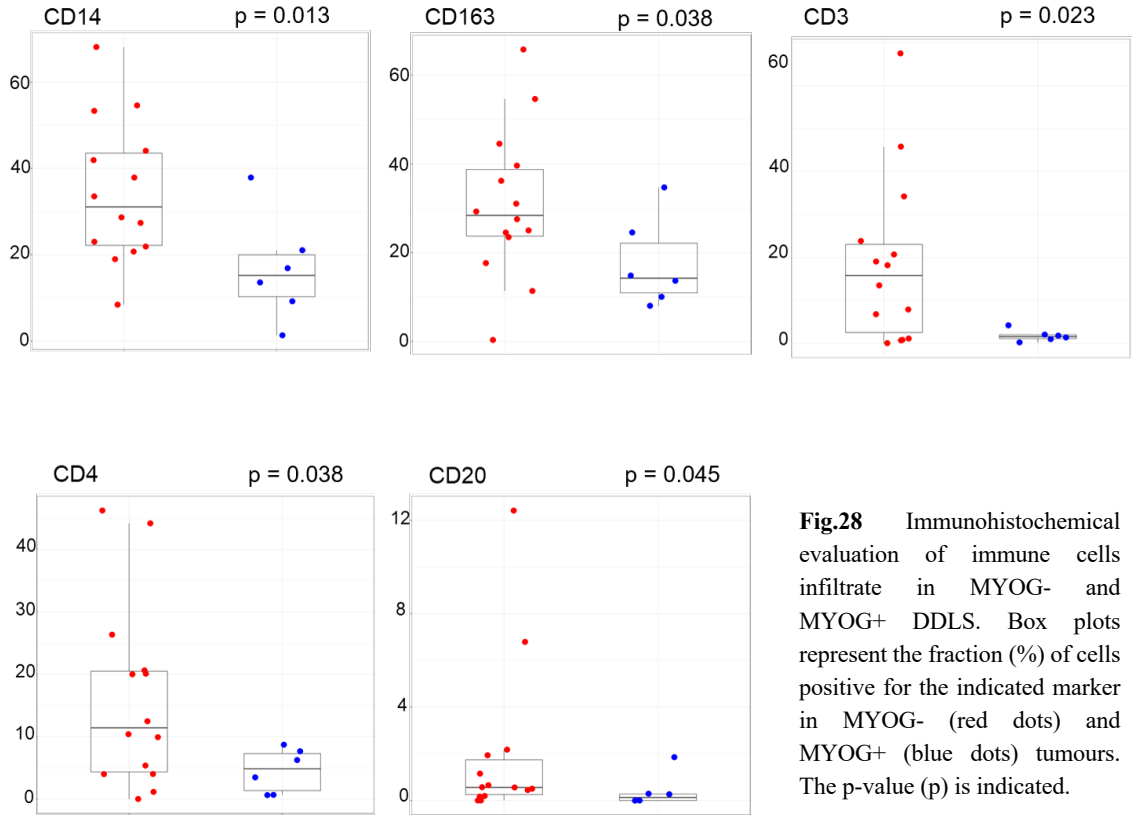

Fig.28 Immunohistochemical evaluation of immune cells infiltrate in MYOG- and MYOG+ DDLS. Box plots represent the fraction (%) of cells positive for the indicated marker in MYOG- (red dots) and MYOG+ (blue dots) tumours. The p-value (p) is indicated.

3.6. Mutation profiling and Copy number variation analysis of DDLS: focus on rhabdomyosarcomatous DDLS

To further investigate the molecular events possibly contributing to rhabdomyoblastic differentiation of retroperitoneal DDLS we compared the mutational pattern of the 9 MYOG+ vs the 30 MYOG- DDLS that we previously analyzed with the TSO500 panel and the OncoKB annotator. As previously discussed, no recurrent mutational event was detected in MYOG- DDLS. Instead, 2/9 (22%) MYOG+ tumors carried genomic variants in *BRCA2* (Fig.29). These *BRCA2* variants were classified based on mutation predictors as deleterious by SIFT and probably damaging by Polyphen, but the ClinVar mutation database classified them as "uncertain significance".

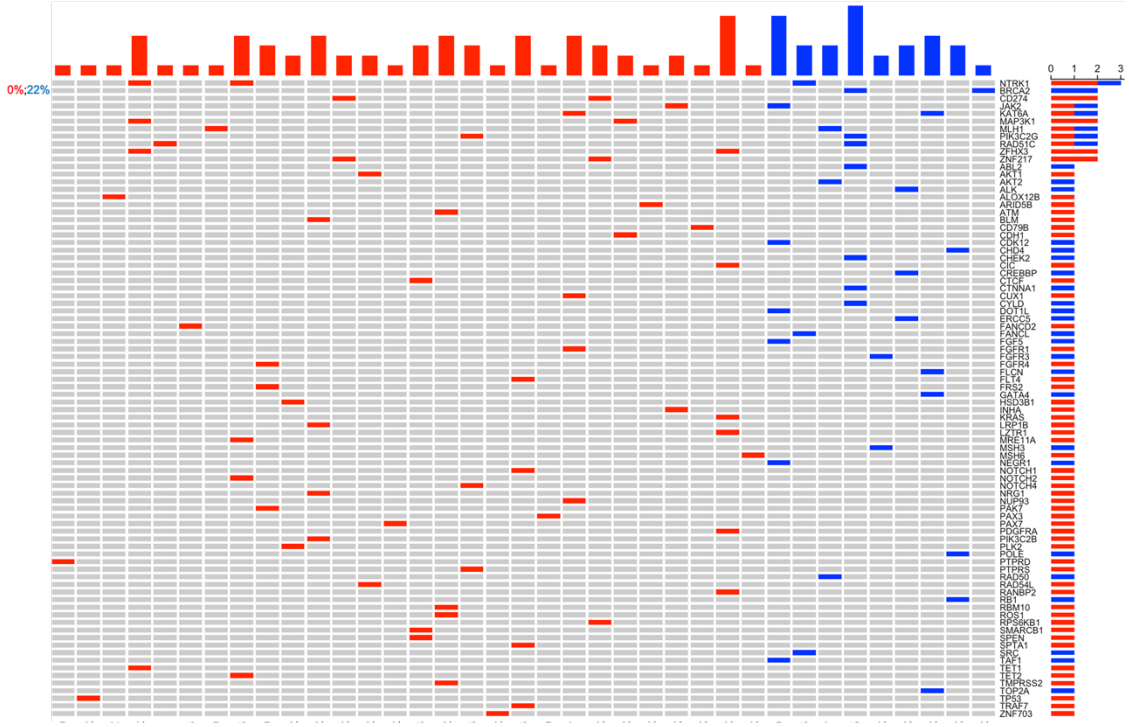

Fig.29 Oncoprint of mutational analysis of MYOG- and MYOG+ DDLS. MYOG- DDLS are labelled in red; MYOG+ DDLS are labelled in blue. The frequencies of the common events are reported on the left (in red for MYOG- and in blue for MYOG+ DDLS).

In the previous comparison of WDLS and DDLS (all MYOG-), copy number variation analysis indicated recurrent CNG of *RPS6KB1* in DDLS (20%). The same analysis here highlighted CNG of *MYC* and *MYCL* selectively in MYOG+ DDLS (*MYC*: 5/9 vs 4/30, p=0.02; *MYCL*: 3/9 vs 0/30; p=0.01, Fisher exact test). Also, *FGFR1* and *ERCC2* were tendentially more commonly gained in MYOG+ vs MYOG- tumors (*FGFR1*: 4/9 vs 5/30;

ERCC2: 2/9 vs 2/30), although the difference did not reach statistical significance (Fig.30).

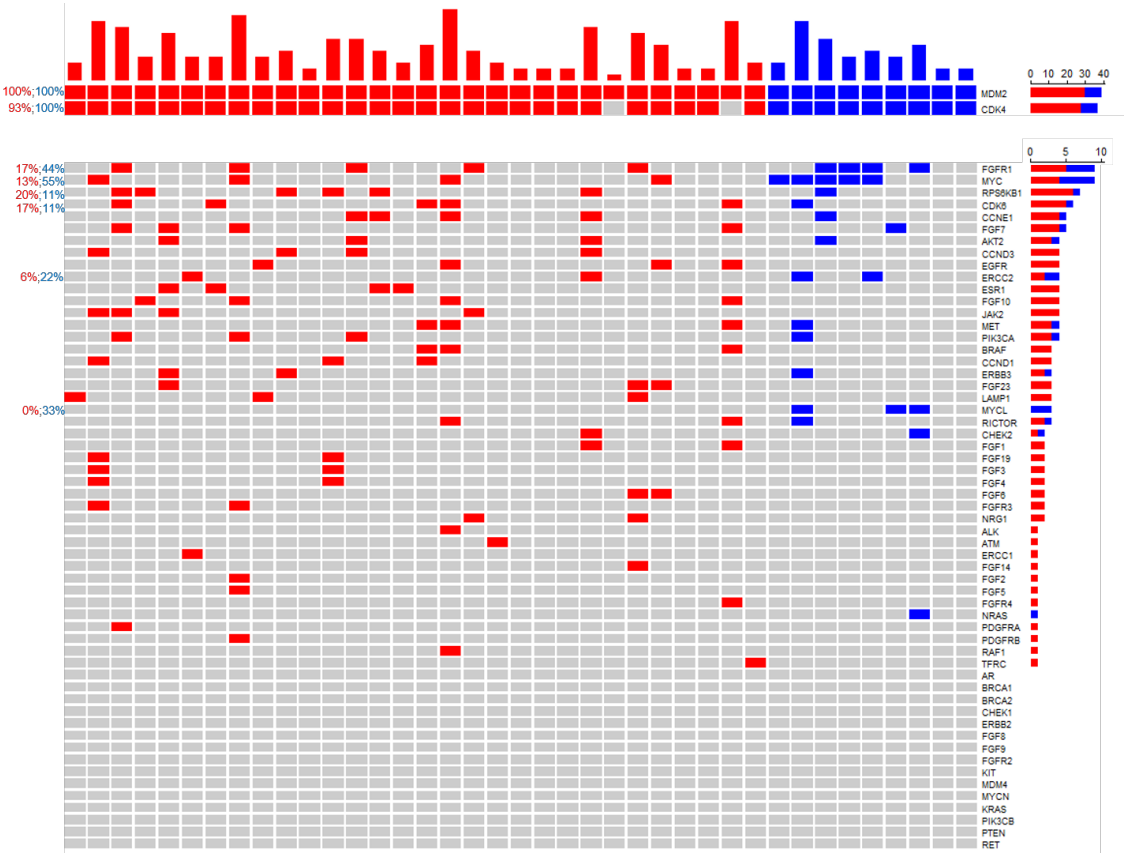

Fig.30 Oncoprint of CNG analysis of MYOG- and MYOG+ DDLS. MYOG- DDLS are labelled in red; MYOG+ DDLS are labelled in blue. The frequencies of the common events are reported on the left (in red for MYOG- and in blue for MYOG+ DDLS).

In conclusion, the CNG analysis demonstrated an amplification of *MYC* genes (*MYC* and *MYCL)* in MYOG+ DDLS, reinforcing the concept of an involvement of the MYC pathway in this DDLS subtype, as suggested by transcriptome analysis.

4. DISCUSSION

WDLS and DDLS of the retroperitoneum are the focus of this study. These tumors share the amplification of the 12q13-15 chromosomal region involving *MDM2*, *HMGA2* and *CDK4* genes. WDLS is a low grade adipocytic tumor that is considered the precursor of DDLS. This highly malignant tumor variant, besides losing adipocytic features, may gain characteristics proper of other mesenchymal tissues (heterologous differentiation), a phenomenon often associated with increased aggressiveness. Here we sought to investigate the molecular mechanisms underlying the malignant progression of DDLS.

To this end we performed transcriptional and mutational analysis by RNA-sequencing and targeted DNA-sequencing of a pathologically well annotated WDLS and DDLS series.

Functional annotation of the genes differentially expressed between the two liposarcoma variants underlined that during the progression from WDLS to DDLS, this latter variant loses adipogenic transcriptional features, as expected, while becomes enriched in the expression of genes involved in DNA replication, cell cycle, cell division, and DNA repair. These results are in line with the previous studies comparing WDLS and DDLS (*21, 126*).

Interestingly, although *YAP1* and *TAZ* were expressed at similar levels in WDLS and DDLS, we noticed an enrichment of the YAP1 signature in DDLS, suggesting an hyperactivation of the YAP1/TAZ pathway in DDLS. YAP and TAZ are post-transcriptionally regulated and the YAP1/TAZ signaling is known to be regulated by the stiffness of the extracellular matrix (*127*). Interestingly, the expression of molecules involved in EMT and matrix remodeling were also up-regulated in DDLS. Among the molecules of the EMT signature enriched in DDLS, we found *LOXL1* and *LOXL2*, two lysyl oxidases that are involved in matrix crosslinking and stiffness (*128*), Fibronectin, and the tissue inhibitor of metalloproteinase *TIMP1*, which are also associated with matrix stiffness (*129, 130*).

This suggests that the evolution from WDLS to DDLS is likely to be accompanied by the transition from a soft fat environment to a harder matrix contexture. This might trigger the YAP1/TAZ pathway that is notoriously associated with tumor progression (*127*), hence contributing to the malignant phenotype of DDLS. Accordingly, Fullenkamp and coworkers reported that the number of TAZ immunohistochemically-positive nuclei

(readout for YAP1/TAZ pathway activation) was greater in DDLS compared to WDLS (*131*).

To better unfold the mechanisms behind the malignant progression from WDLS to DDLS, we also performed targeted DNA-sequencing. The overall tumor mutational burden (TMB, expressed as Mutations/Megabases of coding genome covered by the assay) was low in WDLS and DDLS (WDLS=2.0; DDLS=3.5; conventional cutoff for low TMB <10Mut/Mb), in line with what reported about other sarcomas (*43*).

As about gene mutation pattern, previous studies reported some genes as recurrently mutated in either WDLS or DDLS, but results were not consistent. Only *BRCA1* was reported as mutated in two different studies (*132, 133*). No recurrent mutation in either WDLS or DDLS was found in our targeted NGS analysis and hence no significantly different mutation pattern emerged between the two subtypes. Although we failed to detected *BRCA1* mutations, *BRCA2* was altered in 1/19 WDLS and in 2/39 DDLS. We also found occasional alterations in other genes of the DNA repair pathway including *hMLH1* (2/19 WDLS and 2/39 DDLS) and *FANCD2* (1/19 WDLS and 1/39 DDLS), a fact suggesting that defects in the control of genome stability might contribute to the development of both types of liposarcoma.

If TMB in sarcoma is low, sarcomas are known to be more prone to undergo chromosome imbalance (*43*). In our series we found that DDLS in general show a higher number of copy number gains compared to WDLS (5.5% vs 1.3%, Chi-square p<10e-5). Specifically, besides *MDM2*, *HMGA2* and *CDK4*, relatively common amplification events detected in DDLS involves *FGFR1* (9/39, 23%), *RP6SKB1* (7/39), and *CDK6* (6/39).

FGFR1 is a receptor tyrosine kinase involved in cell proliferation, differentiation and migration (*134*). Amplification of *FGFR1* was reported in different cancer types and associated with poor prognosis (*134-137*). Amplification and overexpression of *FGFR1* were reported in about 17% of sarcomas (including DDLS), and sarcoma cell lines with such amplification demonstrated sensitivity to *FGFR1* inhibition, suggesting that FGFR targeting may represent a therapeutic avenue for these tumors (*138*).

RPS6KB1, a member of the S6 kinase family of serine/threonine kinases (*139, 140*), is known to regulate different cellular processes like mRNA processing, protein folding,

cell growth and survival (*141*). Dysregulation of the mTORC1-RPS6KB1 signaling pathway has been associated with cancer development (*142*) and amplification of *RPS6KB1* has been related to poor prognosis (*143-145*).

CDK6 is a paralog of *CDK4*, both key players in the transition through the G1/S phase of the cell cycle (*85-87*). Amplification of *CDK6* was reported in different tumors like intimal sarcoma and breast cancer (*146*). In breast cancer the amplification of *CDK6* seems to correlate with reduced sensitivity to CDK4/6 inhibitors (*147*). Since the efficacy of CDK4/6 inhibitors in the treatment of sarcomas is currently under clinical investigation (*148*), it will be interesting to assess whether the presence of *CDK6* amplification impairs the sensitivity to these inhibitors also in the DDLS context. Noteworthy, a DDLS with *CDK6* amplification was one of those uncommon DDLS cases reported in literature (*94*) that do not carry the common amplification of CDK4.

Overall, mutation and copy number variation analysis of our WDLS and DDLS series did not provide major insight into the transcriptional differences identified between WDLS and DDLS but confirms the low propensity of these tumors to undergo gene mutations and supports the notion that the evolution from WDLS to DDLS is accompanied by a progressive genomic imbalance.

A second step of our study was to investigate the molecular characteristics of DDLS with rhabdomyoblastic differentiation, a DDLS variant characterized by a particularly aggressive clinically course. Following this type of differentiation, DDLS gain characteristics proper of skeletal muscle cells including myogenin expression. The molecular trigger of this differentiative path occurring in DDLS is unknown as well as the reason that makes this tumor variant so clinically aggressive. Intriguingly, immunohistochemical positivity for myogenin is not necessarily diffused, but single myogenin-immunoreactive scattered liposarcoma cells are sufficient to classify a DDLS as rhabdomyosarcomatous.

The comparison of the transcriptional profile of DDLS with rhabdomyoblastic differentiation vs conventional DDLS indicated that rhabdomyosarcomatous cells of these tumors do not activate the expression of just myogenin but feature the activation of a plethora of myogenesis-related genes including master myogenic transcription factors (*Pax7, Myf5, MyoD1, Mrf4/Myf6, MyoG*), as well as other structural components of

terminally differentiated myocytes. Thus, myogenin positivity in rhabdomyosarcomatous DDLS is just the tip of the iceberg and subtends a very profound transcriptional reprogramming of this adipocytic tumor toward the striated muscle lineage.

Remarkably, adipocytes and muscle cells share a common embryonal origin from mesenchymal progenitors (*149, 150*). Adipose tissue is subdivided into white fat, mostly deriving from *Myf5*-negative mesenchymal progenitors, and brown fat, deriving from *Myf5*-positive progenitors. *Myf5*-positive progenitors are the cells from which muscle cells originate (*151*). Under some not fully clarified circumstances, white adipocytes may convert into brown adipocytes and vice versa, indicating the possibility of transition between the two lineages of adipose differentiation (*151, 152*). Thus, the conversion of an adipocytic tumor cell (DDLS) into a cell with muscular characteristics (MYOG+ DDLS) likely relies on the reactivation of a transcriptional program proper of the cell of origin.

In this "transdifferentiation" process MYOG+ DDLS maintain a high proliferative activity, with the activation of E2F and MYC signalings (in some cases associated with *MYC* or *MYCL* amplification) that support an aggressive clinical behavior (*153, 154*). Intriguingly, a correlation between the gain of myoid traits and poor outcome has been suggested also for other types of sarcomas (*155-158*).

An additional observation that emerged from the analysis of the transcriptome of DDLS undergoing rhabdomyoblastic differentiation was the transcriptional indication of a reduced immune infiltration if compared to conventional DDLS. This finding was confirmed by both deconvolution analyses with bioinformatic tools specifically designed to interrogate translational data for immune-related signatures as well as by *in situ* investigations of tumor section stained with diverse immune cell markers. The reduced extent of immune cells infiltrating rhabdomyosarcomatous DDLS was paralleled by a reduced expression of antigen presenting machinery genes. Suppression of the antigen presenting machinery and regulation of immune checkpoint molecules are mechanisms of immune evasion commonly deployed by tumor cells to resist to immune system control and propagate. Accordingly, these phenomena are associated with an aggressive phenotype (*159-161*). There are a number of factors that contribute to tumor persistence

via immune evasion, among which MYC, WNT/β-catenin and Sonic-Hedgehog signaling pathways (*153, 160, 162*).

Noteworthy, muscles are considered "immune privileged" organs, similarly to brain, retina and testis. In fact, they express very low levels of class I and class II HLA molecules and are scarcely populated by immune cells, including antigen presenting cells (*163, 164*). Conversely, adipose tissue is one of the tissues with the highest expression levels of HLA molecules (*164*). Thus, it is tempting to speculate that the differentiation drift toward the muscle lineage may represent the strategy exploited by DDLS cells to overcome immune attack, gaining in parallel a more aggressive phenotype.

Immune-based therapies, such as monoclonal antibodies and immune checkpoint inhibitors, represent one of the most promising anti-cancer treatments (*165*). Tumor types characterized by elevated immune infiltration (e.g. melanoma and non-small cell lung cancer) are particularly sensitive to immune therapies (*166*). Sarcomas are in general scarcely infiltrated and, although very few responses were achieved in series of sarcomas treated with immune checkpoint inhibitors, responsive cases included DDLS (*167-169*). Our findings suggest that non-rhabdomyosarcomatous DDLS are more likely to respond to these treatments.

5. CONCLUSIONS AND FUTURE DIRECTIONS

Overall, this study supports the notion that the malignant progression of retroperitoneal liposarcomas is accompanied by hyperactivation of pathways related to cell proliferation and downregulation of signaling related to the adipose cell lineage. Although mutational analysis failed to pinpoint recurrent genetic events supporting this evolution, the intriguing activation of the YAP1/TAZ pathway in DDLS suggests that matrix stiffness may play a role in this transition. The fact that a WDLS may recur as a DDLS and, in turn, a DDLS may recur as a WDLS (*24*) suggests that this transition may be reversible and influenced by external factors. *In vitro* experiments aimed at addressing whether matrix stiffness may play a role into WDLS to DDLS transition and viceversa will be performed.

Also, our study indicates that the rhabdomyoblastic differentiation of a DDLS is characterized by a profound transcriptional rewiring possibly due to the reactivation of a transcriptional program intrinsic to the cell of origin. Intriguingly, rhabdomyosarcomatous DDLS show an "immune excluded" phenotype, a phenomenon correlated with a reduced expression of components of the APM machinery.
We are designing *in vitro* experiments in which WDLS and DDLS cell lines will be engineered to ectopically express *MYOG* or *MYOD1* in order to ascertain whether the expression of these myogenic transcription factors impacts on cell growth and migration capabilities and whether it dampens the expression of APM genes.

Moreover, we are in the process of performing microRNA profiling to elucidate the role of these epigenetic regulators in the malignant evolution from WDLS to DDLS and in in rhabdomyoblastic differentiation.

6. MATERIALS AND METHODS

6.1. Case series

Archival Formalin-Fixed Paraffin-Embedded (FFPE) blocks from 51 retroperitoneal DDLS, including 33 DDLS and 18 WDLS were retrieved from the pathology files of CRO biobank and collaborating institutions. The entire series includes 12 matched WDLS and DDLS and an additional 27 samples, of which 21 sample were available only for the DDLS component and 6 sample were available only for the WDLS component. Moreover, the DDLS series includes 9 MYOG+ DDLS and 33 MYOG- DDLS samples. Only specimens with a tumor cell fraction greater than 70% were used in the study.

6.2. RNA extraction

RNA was extracted from FFPE samples by using the Qiagen deparaffinization solution (Qiagen). The Ambion RecoverAll Nucleic Acid isolation kit (ThermoFisher Scientific) or the FFPE RNA Purification kit (Norgen) were employed for RNA recovery, according to the manufacturer's instructions. RNA was quantified with a fluorometer using the Qubit RNA HS Assay Kit (ThermoFischer Scientific). The fluorometer determines the sample concentration using a curve-fitting algorithm, based on a calibration curve generated with standard samples with known concentrations. RNA quality was evaluated by electrophoresis using the RNA Assay Kit (Agilent Technologies) on the Agilent 2200 TapeStation instrument.

6.3. RNA profiling and data processing

Fifty to 250 nanograms of total RNA were used for the generation of RNA-sequencing libraries with Illumina Stranded Total RNA Library Prep kits (TruSeq or Ribo-Zero Plus) (Illumina), according to the manufacturer's protocol and as illustrated in (Fig.31). Briefly, RNA was first depleted form ribosomal RNA (rRNA) by using rRNA depletion reagents; then it was converted into double-stranded cDNA with the incorporation of dUTP in place of dTTP during the synthesis of the second strand. cDNA fragments were then adenylated

at the 3’ end. After ligation of adapters, libraries were amplified by polymerase chain reaction (PCR) with concomitant incorporation of indexes.

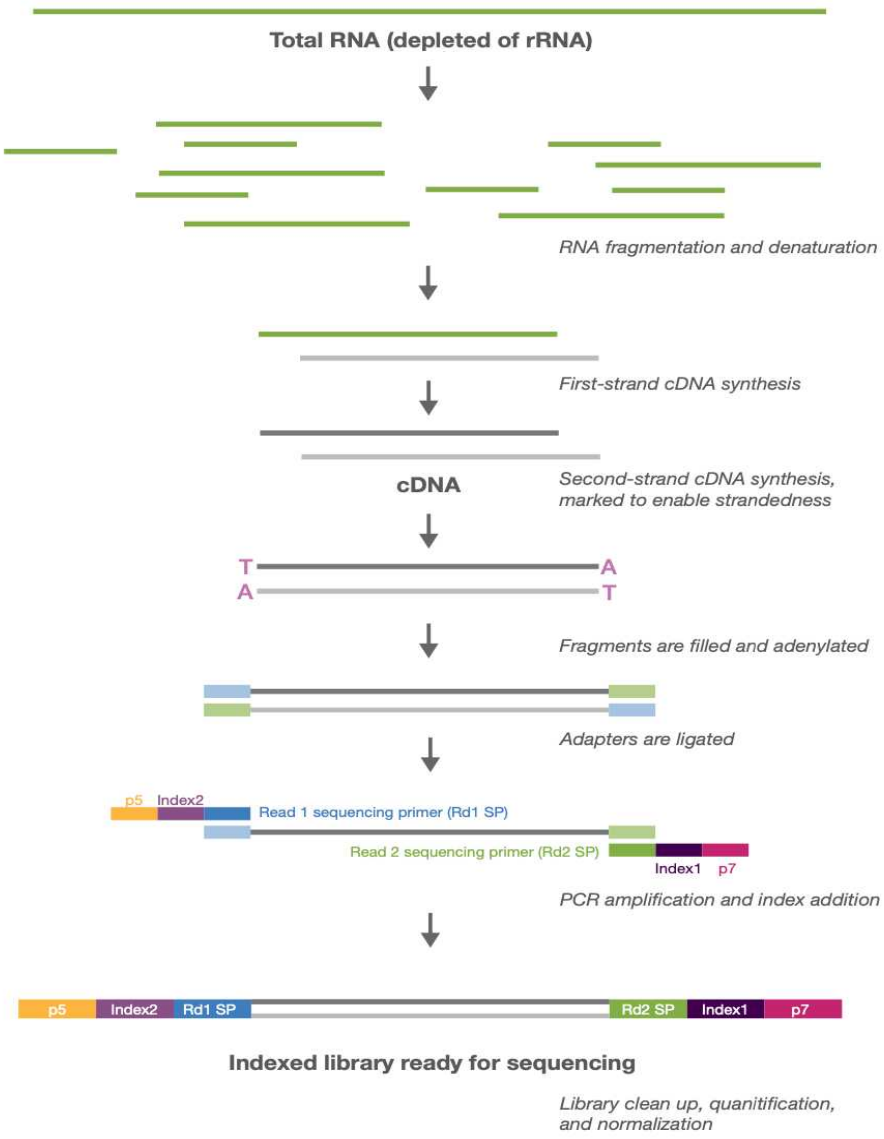

Fig.31 Illumina Stranded Total RNA Prep steps for the generation of RNA-seq libraries.

RNA libraries were “stranded libraries” as, due to the presence of dUTP in the second strand of the cDNA, which prevents its duplication by the Taq DNA polymerase, only the first strand is employed as a template in the PCR library amplification step. Libraries were quantified by a fluorometric assay (Qubit dsDNA High Sensitivity Assay Kit, ThermoFischer Scientific) and evaluated for size and purity (absence of PCR dimers) by

TapeStation electrophoresis (D1000 Assay Kit, Agilent Technologies). Libraries were considered suitable if fragments were roughly 260bp long. Finally, libraries were diluted, pooled (in pools of 12 libraries/pool) to a 2 nM total concentration and loaded to an Illumina Hiseq 1000 platform using the Hiseq Rapid PE Cluster v2 Kit (Illumina, San Diego, CA, USA) to reach a sequencing depth ≥ 50 million paired-end reads per sample. Once sequencing was completed, data (in the form of bcl files) were converted into FASTQ files using the bcl2fastq software (Illumina). FastQC (version 0.11.9), MultiQC (version 1.0), and Trimmomatic (version 0.39) softwares were used for FASTQ sequence quality measurements and trimming.

The obtained sequences (named reads) were then aligned to the human genome reference sequence hg38 (GRCh38.p13) (https://www.ncbi.nlm.nih.gov/grc) using the STAR algorithm (version 2.7.10a) (*170*). The RSEM tool (version 1.3.1) (*171*) was used for reads quantification and GENCODE v.27 (*172*) was employed for gene annotation. To attenuate possible batch effects due to the different rRNA depletion strategies were employed by the two library preparation kits used, genes targeted by the probes used for rRNA depletion were in silico uniformly depleted from all counts. This resulted in a total number of measurable genes equal to 57729, 19807 of which protein-coding. GENCODE annotation v.27 and hg38 were retrieved from the GATK resource bundle (https://gatk.broadinstitute.org/hc/en-us/articles/360035890811-Resource-bundle). Raw data (read counts from RSEM) were finally converted into normalized read counts using the Variance Stabilizing Transformation (VST) function in DESeq2 package (version 1.26) (*173*) run in R (version 3.6.2). Transcripts per million for all genes (TPM) were calculated using the RSEM tool and are a normalized measure of the relative expression level of each transcript (expressed per 1 million transcripts). This measure takes into account sequencing depth and gene length and it is useful to compare gene expression in different samples (*171, 174, 175*). To calculate the TPM of protein-coding genes (pTPM) the TPM values calculated for all genes were filtered for protein-coding genes and renormalized to 1 million. To calculate the APM score, pTPM of key components of the APM machinery were log2-converted as [(log2 pTPM+1)+0.01] to eventually compute the geometric mean of the corresponding values.

Principal Component Analysis (PCA) and unsupervised hierarchical clustering analysis (UHCA) were performed using the normalized read counts of the top 500 genes with

highest variance. PCA is a mathematical algorithm used to reduce the dimensionality of the data, while preserving as much as possible of the variation (*176*). Specifically, in PCA, data are linearly transformed into a coordinate system where the majority of the variance of the original data is expressed with fewer dimensions, commonly two, the principal component 1 and 2 (PC1 and PC2) (*177, 178*). We used the plotPCA function built in DESeq2 to perform PCA analysis and the ggplot2 package (version 3.3.6) for graphical representation.

UHCA is an algorithm that is designed to group together data (objects) that are somehow "close" to one another. The graphical outcome of this analysis is a dendrogram deriving by a reiterated calculation of the distance between data (objects) and between clusters once data (objects) are being grouped into clusters. The “Euclidian” method to calculate distance, and the “complete linkage method” to compute the hierarchical clustering were employed.

Also, UHCA was generated from the top 500 genes with highest variance by using DESeq2 and ggplot2 packages.

Differential expression analysis was performed using the DESeq2 R package. Genes expressed at a very low level (raw sum of the counts <10) were excluded from the analysis. Genes were considered differentially expressed (DE) if the absolute value of the log2 Fold Change (log2FC) was ≥ 1 and the adjusted p-value was ≤ 0.05 ($|\log2(FC)| \geq 1$ and $padj \leq 0.05$).

6.4. Functional data annotation

Functional annotation analyses of RNA-sequencing data were performed on a whole set of normalized counts using the GSEA desktop app (version 4.1.0) of the Gene Set Enrichment Analysis (GSEA) algorithm. GSEA is a computational method that allows to establish whether a reference, pre-defined gene set, shows statistically significance and concordant differences between two conditions (e.g. phenotypes). MSigDB Hallmark pathways (Hallmarks) (h.allv2022.1.Hs.symbols.gmt) (https://www.gsea-msigdb.org/gsea/msigdb/human/genesets.jsp?collection=H), Gene Ontology Biological

Processes (GOBP) (c5.go.bp.v2022.1.Hs.symbols.gmt) (https://www.gsea-msigdb.org/gsea/msigdb/human/genesets.jsp?collection=GO:BP), and Oncogenic signatures (c6.all.v2022.1.Hs.symbols.gmt) (https://www.gsea-msigdb.org/gsea/msigdb/human/genesets.jsp?collection=C6) were used as reference datasets. An analysis was conducted by first defining the two set of samples (phenotype) compared (DDLS and WDLS), and then using the following parameters: number of permutations = 1000; enrichment statistic = weighted; minimum size = 3; maximum size = 2000; collapse/remap to gene symbols = no collapse. Using the same signatures and parameters mentioned above, we performed also a preranked GSEA (*179, 180*). Preranked GSEA uses the list of DE genes that are ranked according to the statistical significance and fold change. To rank our list of DE genes we used the formula [-log10(p-value)*(sign of log2(Fold-Change))] as in (*181*).

Functional annotation of DE genes was also performed by over-representation analysis (ORA). To this end we used clusterProfiler v.4.0 R package against the gene ontology biological processes, and the hyper-geometric test was used to calculate the enrichment of GOBP terms (*182*). Genes up and down-regulated were annotated separately.

6.5. DNA extraction

FFPE samples were dewaxed using the QIAGEN deparaffinization solution and total DNA was extracted by using either the QIAamp DNA FFPE Tissue Kit (QIAGEN) or the FFPE RNA/DNA Purification Plus Kit (Norgen), according to the manufacturer's instructions. DNA was quantified with a fluorometer using the Qubit DNA BR Assay Kit (ThermoFischer Scientific). DNA quality was assessed by electrophoresis using gDNA Assay Kit (Agilent Technologies) on the Agilent 2200 TapeStation instrument.

6.6. DNA profiling and data processing

Forty to 110 ng of total DNA were used for the generation of DNA-sequencing libraries using the hybrid capture-based TruSight Oncology 500 Library Preparation Kit (Illumina, San Diego, CA). Briefly, DNA fragmentation was performed using the Covaris M220

focused-ultrasonicator (Woburn, MA) with a setting of 25 W peak incident power, 40% as duty factor, 1000 cycles per burst, at 10°C to the end to obtain 230-280 bp gDNA fragments. The efficacy of sonication was evaluated by electrophoresis using HSD1000 Assay Kit (Agilent Technologies) on the Agilent 2200 TapeStation instrument. gDNA fragments were then end repaired and adenylated at the 3' end. Next, adapters containing UMIs were ligated to the ends of the DNA fragments and libraries were amplified by PCR with concomitant incorporation of indexes for sample multiplexing (required for cluster generation). After two probe-hybridization steps performed to capture the target sequences (523 genes), the enriched libraries were finally amplified by PCR. Amplified libraries were then quantified (Qubit dsDNA High Sensitivity Assay Kit, ThermoFischer Scientific), normalized to ensure a uniform representation of the libraries and pooled in pools of 8 libraries/pool. After denaturation, pooled libraries were loaded on an Illumina NextSeq 550 platform. The High Output Kit v2.5 (Illumina, San Diego, CA, USA) was used for sequencing run (read length of 2 x 101 bp; 300 cycles).
To analyze sequencing output, the TruSight Oncology 500 v2.2 Local App was used. This includes the FASTQ file generation (BCLConvert software); the alignment to the human genome reference sequence hg19 (GRCh37) with the Burrows-Wheeler Aligner (BWA-MEM) of the SAM Tools utility; the somatic variant calling with Pisces (https://github.com/Illumina/Pisces) and primary annotation with Nirvana (*183*); to detect CNV the app uses the CRAFT copy number variant caller which performs counts bin normalization, calculates fold change values for each gene and determines CNV status. The tumor mutational burden (TMB) score was generated using TMBRaider, and represents the number of tumor mutations per megabase of DNA calculated as follows: eligible variants/ effective panel size in Mb.

After variant identification with the TruSight Oncology 500 v2.2 Local App, variants were functionally annotated using the OncoKB annotation database (*115*). OncoKB is a comprehensive knowledge base for precision oncology that provides information on somatic mutations and structural alterations present in tumor samples. It contains biological, clinical, and therapeutic information from multiple resources and includes 3405 alterations in 418 cancer-associated genes (*115*). The output of OncoKB functional annotation was then filtered using the following criteria: VAF (Variant

Allele_Frequency) ≥10%; AF (which represents non-reference allele and frequency of existing variant in 1000 Genomes): ≤ 0.01 or missing value; gnomAD_NFE_AF (which represents the frequency of existing variant in gnomAD exomes Non-Finnish European population): ≤ 0.01 or missing value; IMPACT (which represents the severity of the consequence): moderate or high; CLIN_SIG (which represents the clinical significance of variant per ClinVar): pathogenic, likely pathogenic, conflicting interpretations of pathogenicity, uncertain significance, or not provided; SIFT: deleterious, deleterious_low_confidence, or tolerated_low_confidence; PolyPhen: possibly damaging, probably damaging, unknown, or missing value; FILTER (which represents false-positive filtering status): pass.

For each gene, the frequency of mutations or CNV in each class was calculated as 100*(number of mutations or CNV / total cases of the class). Mutations/CNV were arbitrarily defined "recurrent" if their frequency in a class was ≥ 20%.

For graphical representation of mutations and CNV, the OncoPrint function built in ComplexHeatmap packages in R was used.

6.7. Transcriptome analysis of immune infiltration of DDLS series

Transcriptome data were interrogated with immune-specific signatures to infer the possible presence of immune infiltrate within our DDLS cohort. To this end we used interrogated CibersortX as well as the Timer2 web tool (a comprehensive resource that provides immune infiltration estimations from expression profiles by XCELL, TIMER, QUANTISEQ, and EPIC) (*120, 184*) by using pTPM as input. CibersortX is a machine learning method that infers an overall absolute estimate of immune cell infiltration and cell type-specific abundance (22 cell types) from RNA profiles (*120*). XCELL, TIMER, QUANTISEQ and EPIC are algorithms performing enrichment analysis from gene expression for a variable number of immune cell types by using deconvolution approaches (*121, 123, 185*). XCELL generates also an overall immune score (*119*).

The antigen presenting machinery score (APM score) was calculated as the geometric mean of log2-converted pTPM values ([log2 pTPM+1]+0.01) of 35 key components of APM machinery.

Data were Z-score normalized and the computed Z-scores used to generate the heatmap plots using the Morpheus web app (https://software.broadinstitute.org/morpheus).

6.8. Immunohistochemical analysis of DDLS samples

Immunohistochemical staining was conducted by pathologists of collaborating institutions (University of Padova and Fondazione IRCCS Istituto Nazionale dei Tumori of Milano).

The F5D mouse monoclonal antibody (MoAb) (Dako) was used for myogenin staining. Immune cell infiltration was evaluated using the following immune cell markers: CD3 (rabbit polyclonal antibody, Dako); CD4 (clone 4B12 MoAb, Novocastra); CD14 (clone 7 MoAb, Lab Vision); CD20 (clone L26 MoAv, Dako); CD163 (clone 10D6 MoAb, Novocastra).

For *in situ* evaluation of immune cell infiltration extent, stained slides were computationally magnified at 40X magnification and at least 500 cells, including stained and unstained cells, were counted in 4 random fields. The percentage of each immune cell type was calculated as the ratio between marker positive cells on total number of counted cells on the 4 random fields. Data were plotted as box and whiskers plots using the ggplot2 package in R. In these plots, the box is delimited by the upper (Q3) and lower (Q1) quartile; the median value (Q2, middle quartile) is the inner line. Whiskers mark the minimum and maximum observation.

6.9. Statistical analysis

T test (Student's T test) is a parametric inferential statistical test that is applied to determine whether there is a statistically significant difference between the means of two groups. T test is applied when the series of data meets the criteria of continuous variables, normal distribution of data, independent measurements, and homogeneity of variance. Once verified the conditions above, the T test (two tailed) was applied to estimate the

statistical difference in the enrichment scores obtained from XCELL and CibersortX of the groups MYOG+ and MYOG- DDLS.

The Mann-Whitney U test is a non-parametric test that is used to compare the statistical significance in the means of two groups when the conditions for the application of a T test are not met. Having assessed that the counts of immune infiltrating cells were not following a normal distribution, we applied the Mann-Whitney U test (one-tailed) to ascertain whether the *in silico* prediction of a differential immune infiltration between MYOG+ and MYOG- tumors was verified also *in situ*.

The Spearman non-parametric correlation test (rs) was employed to measure, for each immune cell marker, the association between the percentage of immune cell marker positive cells and the pTPM of the cognate gene. The value of rs ranges from -1 (negative association) to 1 (positive association), with rs equal to 0 meaning no association.

The Chi-square test and Fisher's exact test (used if one class was ≤ 5) are non-parametric tests used to determine whether the frequency distribution of a categorical variable is different from the expectation or whether two categorical variables are related to each other. These tests were used to investigate distribution of gene copy gains between WDLS and DDLS and between MYOG+ and MYOG- DDLS.

7. REFERENCES

References

1. L. J. Helman, P. Meltzer, Mechanisms of sarcoma development. *Nat Rev Cancer* **3**, 685-694 (2003).
2. A. Mariño-Enríquez, J. V. Bovée, Molecular Pathogenesis and Diagnostic, Prognostic and Predictive Molecular Markers in Sarcoma. *Surg Pathol Clin* **9**, 457-473 (2016).
3. B. A. Nacev *et al.*, Clinical sequencing of soft tissue and bone sarcomas delineates diverse genomic landscapes and potential therapeutic targets. *Nat Commun* **13**, 3405 (2022).
4. Z. Burningham, M. Hashibe, L. Spector, J. D. Schiffman, The epidemiology of sarcoma. *Clin Sarcoma Res* **2**, 14 (2012).
5. R. L. Siegel, K. D. Miller, A. Jemal, Cancer statistics, 2018. *CA Cancer J Clin* **68**, 7-30 (2018).
6. J. M. Brownstein, T. F. DeLaney, Malignant Soft-Tissue Sarcomas. *Hematol Oncol Clin North Am* **34**, 161-175 (2020).
7. S. W. Weiss, J. R. Goldblum, A. L. Folpe, *Enzinger and Weiss's soft tissue tumors*. (Elsevier Health Sciences, 2007).
8. A. Jemal *et al.*, Cancer statistics, 2003. *CA Cancer J Clin* **53**, 5-26 (2003).
9. WHO, *Soft Tissue and Bone Tumours*. (International Agency for Research on Cancer, 2020).
10. W.-L. Wang, A. J. Lazar, in *Practical Soft Tissue Pathology: a Diagnostic Approach (Second Edition),* J. L. Hornick, Ed. (Elsevier, Philadelphia, 2019), pp. 513-556.
11. J. V. Bovée, P. C. Hogendoorn, Molecular pathology of sarcomas: concepts and clinical implications. *Virchows Arch* **456**, 193-199 (2010).
12. G. Lahat, A. Lazar, D. Lev, Sarcoma epidemiology and etiology: potential environmental and genetic factors. *Surg Clin North Am* **88**, 451-481, v (2008).
13. B. S. Taylor *et al.*, Advances in sarcoma genomics and new therapeutic targets. *Nat Rev Cancer* **11**, 541-557 (2011).
14. E. C. Borden *et al.*, Soft tissue sarcomas of adults: state of the translational science. *Clin Cancer Res* **9**, 1941-1956 (2003).

15. B. Amadeo *et al.*, Incidence and time trends of sarcoma (2000-2013): results from the French network of cancer registries (FRANCIM). *BMC Cancer* **20**, 190 (2020).
16. T. M. Mack, Sarcomas and other malignancies of soft tissue, retroperitoneum, peritoneum, pleura, heart, mediastinum, and spleen. *Cancer* **75**, 211-244 (1995).
17. J. Henze, S. Bauer, Liposarcomas. *Hematol Oncol Clin North Am* **27**, 939-955 (2013).
18. S. M. Gadgeel, L. C. Harlan, C. A. Zeruto, M. Osswald, A. G. Schwartz, Patterns of care in a population-based sample of soft tissue sarcoma patients in the United States. *Cancer* **115**, 2744-2754 (2009).
19. V. Y. Jo, C. D. Fletcher, WHO classification of soft tissue tumours: an update based on the 2013 (4th) edition. *Pathology* **46**, 95-104 (2014).
20. A. M. Crago, S. Singer, Clinical and molecular approaches to well differentiated and dedifferentiated liposarcoma. *Curr Opin Oncol* **23**, 373-378 (2011).
21. H. C. Beird *et al.*, Genomic profiling of dedifferentiated liposarcoma compared to matched well-differentiated liposarcoma reveals higher genomic complexity and a common origin. *Cold Spring Harb Mol Case Stud* **4**, (2018).
22. M. Kind, N. Stock, J. M. Coindre, Histology and imaging of soft tissue sarcomas. *Eur J Radiol* **72**, 6-15 (2009).
23. C. N. Johnson, A. S. Ha, E. Chen, D. Davidson, Lipomatous Soft-tissue Tumors. *J Am Acad Orthop Surg* **26**, 779-788 (2018).
24. A. P. D. Dei Tos, *Soft Tissue Sarcomas*. (Cambridge University Press, 2018).
25. M. P. Powers *et al.*, Detection of myxoid liposarcoma-associated FUS-DDIT3 rearrangement variants including a newly identified breakpoint using an optimized RT-PCR assay. *Mod Pathol* **23**, 1307-1315 (2010).
26. J. Han *et al.*, ER stress signalling through eIF2α and CHOP, but not IRE1α, attenuates adipogenesis in mice. *Diabetologia* **56**, 911-924 (2013).
27. S. Brenner, Z. Bercovich, Y. Feiler, R. Keshet, C. Kahana, Dual Regulatory Role of Polyamines in Adipogenesis. *J Biol Chem* **290**, 27384-27392 (2015).
28. J. C. Schwartz, T. R. Cech, R. R. Parker, Biochemical Properties and Biological Functions of FET Proteins. *Annu Rev Biochem* **84**, 355-379 (2015).

29. L. Wang, W. Ren, X. Zhou, W. Sheng, J. Wang, Pleomorphic liposarcoma: a clinicopathological, immunohistochemical and molecular cytogenetic study of 32 additional cases. *Pathol Int* **63**, 523-531 (2013).
30. M. Sbaraglia, A. P. Dei Tos, in *Practical Soft Tissue Pathology: a Diagnostic Approach (Second Edition),* J. L. Hornick, Ed. (Elsevier, Philadelphia, 2019), pp. 311-340.
31. A. T. J. Lee, K. Thway, P. H. Huang, R. L. Jones, Clinical and Molecular Spectrum of Liposarcoma. *J Clin Oncol* **36**, 151-159 (2018).
32. R. Conyers, S. Young, D. M. Thomas, Liposarcoma: molecular genetics and therapeutics. *Sarcoma* **2011**, 483154 (2011).
33. WHO-Pediatric, A Summary of the Inaugural WHO Classification of Pediatric Tumors: Transitioning from the Optical into the Molecular Era. *Cancer Discov* **12**, 331-355 (2022).
34. R. Alaggio *et al.*, Liposarcomas in young patients: a study of 82 cases occurring in patients younger than 22 years of age. *Am J Surg Pathol* **33**, 645-658 (2009).
35. D. Creytens *et al.*, Myxoid pleomorphic liposarcoma-a clinicopathologic, immunohistochemical, molecular genetic and epigenetic study of 12 cases, suggesting a possible relationship with conventional pleomorphic liposarcoma. *Mod Pathol* **34**, 2043-2049 (2021).
36. A. Vijay, L. Ram, Retroperitoneal liposarcoma: a comprehensive review. *Am J Clin Oncol* **38**, 213-219 (2015).
37. K. Thway, Well-differentiated liposarcoma and dedifferentiated liposarcoma: An updated review. *Semin Diagn Pathol* **36**, 112-121 (2019).
38. D. R. Lucas, A. G. Nascimento, B. K. Sanjay, M. G. Rock, Well-differentiated liposarcoma. The Mayo Clinic experience with 58 cases. *Am J Clin Pathol* **102**, 677-683 (1994).
39. J. M. Coindre, F. Pédeutour, A. Aurias, Well-differentiated and dedifferentiated liposarcomas. *Virchows Arch* **456**, 167-179 (2010).
40. H. L. Evans, Liposarcoma: a study of 55 cases with a reassessment of its classification. *Am J Surg Pathol* **3**, 507-523 (1979).

41. P. Sun *et al.*, Pathological prognostic factors of retroperitoneal liposarcoma: comprehensive clinicopathological analysis of 124 cases. *Ann Transl Med* **9**, 574 (2021).
42. C. J. Chouairy, F. W. Abdul-Karim, G. T. MacLennan, Retroperitoneal liposarcoma. *J Urol* **177**, 1145 (2007).
43. Cancer-Genome-Atlas-Research-Network, Comprehensive and Integrated Genomic Characterization of Adult Soft Tissue Sarcomas. *Cell* **171**, 950-965.e928 (2017).
44. B. J. Kukull *et al.*, Low-grade Osteosarcomatous Dedifferentiation of an Atypical Lipomatous Tumor in a Pediatric Patient. *Pediatr Dev Pathol* **23**, 240-246 (2020).
45. J. Rosai *et al.*, Combined morphologic and karyotypic study of 59 atypical lipomatous tumors. Evaluation of their relationship and differential diagnosis with other adipose tissue tumors (a report of the CHAMP Study Group). *Am J Surg Pathol* **20**, 1182-1189 (1996).
46. P. Dal Cin *et al.*, Cytogenetic and fluorescence in situ hybridization investigation of ring chromosomes characterizing a specific pathologic subgroup of adipose tissue tumors. *Cancer Genet Cytogenet* **68**, 85-90 (1993).
47. F. Pedeutour *et al.*, Structure of the supernumerary ring and giant rod chromosomes in adipose tissue tumors. *Genes Chromosomes Cancer* **24**, 30-41 (1999).
48. J. Momand, G. P. Zambetti, D. C. Olson, D. George, A. J. Levine, The mdm-2 oncogene product forms a complex with the p53 protein and inhibits p53-mediated transactivation. *Cell* **69**, 1237-1245 (1992).
49. A. J. Levine, p53: 800 million years of evolution and 40 years of discovery. *Nat Rev Cancer* **20**, 471-480 (2020).
50. D. P. Lane, Cancer. p53, guardian of the genome. *Nature* **358**, 15-16 (1992).
51. F. Kruiswijk, C. F. Labuschagne, K. H. Vousden, p53 in survival, death and metabolic health: a lifeguard with a licence to kill. *Nat Rev Mol Cell Biol* **16**, 393-405 (2015).
52. L. Collavin, A. Lunardi, G. Del Sal, p53-family proteins and their regulators: hubs and spokes in tumor suppression. *Cell Death Differ* **17**, 901-911 (2010).

53. F. Mantovani, L. Collavin, G. Del Sal, Mutant p53 as a guardian of the cancer cell. *Cell Death Differ* **26**, 199-212 (2019).
54. E. R. Kastenhuber, S. W. Lowe, Putting p53 in Context. *Cell* **170**, 1062-1078 (2017).
55. P. H. Kussie *et al.*, Structure of the MDM2 oncoprotein bound to the p53 tumor suppressor transactivation domain. *Science* **274**, 948-953 (1996).
56. J. Lin, J. Chen, B. Elenbaas, A. J. Levine, Several hydrophobic amino acids in the p53 amino-terminal domain are required for transcriptional activation, binding to mdm-2 and the adenovirus 5 E1B 55-kD protein. *Genes Dev* **8**, 1235-1246 (1994).
57. M. V. Poyurovsky *et al.*, The C terminus of p53 binds the N-terminal domain of MDM2. *Nat Struct Mol Biol* **17**, 982-989 (2010).
58. P. Chène, Inhibiting the p53-MDM2 interaction: an important target for cancer therapy. *Nat Rev Cancer* **3**, 102-109 (2003).
59. M. H. Kubbutat, S. N. Jones, K. H. Vousden, Regulation of p53 stability by Mdm2. *Nature* **387**, 299-303 (1997).
60. F. Toledo, G. M. Wahl, Regulating the p53 pathway: in vitro hypotheses, in vivo veritas. *Nat Rev Cancer* **6**, 909-923 (2006).
61. J. C. Marine, G. Lozano, Mdm2-mediated ubiquitylation: p53 and beyond. *Cell Death Differ* **17**, 93-102 (2010).
62. M. Nilbert, A. Rydholm, F. Mitelman, P. S. Meltzer, N. Mandahl, Characterization of the 12q13-15 amplicon in soft tissue tumors. *Cancer Genet Cytogenet* **83**, 32-36 (1995).
63. C. Tovar *et al.*, MDM2 small-molecule antagonist RG7112 activates p53 signaling and regresses human tumors in preclinical cancer models. *Cancer Res* **73**, 2587-2597 (2013).
64. I. Ray-Coquard *et al.*, Effect of the MDM2 antagonist RG7112 on the P53 pathway in patients with MDM2-amplified, well-differentiated or dedifferentiated liposarcoma: an exploratory proof-of-mechanism study. *Lancet Oncol* **13**, 1133-1140 (2012).

65. K. L. Bill *et al.*, SAR405838: A Novel and Potent Inhibitor of the MDM2:p53 Axis for the Treatment of Dedifferentiated Liposarcoma. *Clin Cancer Res* **22**, 1150-1160 (2016).
66. R. S. Traweek *et al.*, Targeting the MDM2-p53 pathway in dedifferentiated liposarcoma. *Front Oncol* **12**, 1006959 (2022).
67. S. Jeay *et al.*, Dose and Schedule Determine Distinct Molecular Mechanisms Underlying the Efficacy of the p53-MDM2 Inhibitor HDM201. *Cancer Res* **78**, 6257-6267 (2018).
68. A. M. Klein, R. M. de Queiroz, D. Venkatesh, C. Prives, The roles and regulation of MDM2 and MDMX: it is not just about p53. *Genes Dev* **35**, 575-601 (2021).
69. S. K. Mungamuri *et al.*, USP7 Enforces Heterochromatinization of p53 Target Promoters by Protecting SUV39H1 from MDM2-Mediated Degradation. *Cell Rep* **14**, 2528-2537 (2016).
70. P. Hallenborg *et al.*, MDM2 facilitates adipocyte differentiation through CRTC-mediated activation of STAT3. *Cell Death Dis* **7**, e2289 (2016).
71. L. Gopinathan, D. B. Hannon, J. M. Peters, J. P. Vanden Heuvel, Regulation of peroxisome proliferator-activated receptor-alpha by MDM2. *Toxicol Sci* **108**, 48-58 (2009).
72. H. S. Park *et al.*, PPARγ neddylation essential for adipogenesis is a potential target for treating obesity. *Cell Death Differ* **23**, 1296-1311 (2016).
73. E. Saâda-Bouzid *et al.*, Prognostic value of HMGA2, CDK4, and JUN amplification in well-differentiated and dedifferentiated liposarcomas. *Mod Pathol* **28**, 1404-1414 (2015).
74. A. Anand, K. Chada, In vivo modulation of Hmgic reduces obesity. *Nat Genet* **24**, 377-380 (2000).
75. J. Henriksen *et al.*, Identification of target genes for wild type and truncated HMGA2 in mesenchymal stem-like cells. *BMC Cancer* **10**, 329 (2010).
76. A. R. Young, M. Narita, Oncogenic HMGA2: short or small? *Genes Dev* **21**, 1005-1009 (2007).
77. B. Mansoori *et al.*, HMGA2 as a Critical Regulator in Cancer Development. *Genes (Basel)* **12**, (2021).

78. R. Reeves, M. S. Nissen, The A.T-DNA-binding domain of mammalian high mobility group I chromosomal proteins. A novel peptide motif for recognizing DNA structure. *J Biol Chem* **265**, 8573-8582 (1990).
79. B. Noro *et al.*, Molecular dissection of the architectural transcription factor HMGA2. *Biochemistry* **42**, 4569-4577 (2003).
80. L. A. Meza-Zepeda *et al.*, Ectopic sequences from truncated HMGIC in liposarcomas are derived from various amplified chromosomal regions. *Genes Chromosomes Cancer* **31**, 264-273 (2001).
81. C. Mayr, M. T. Hemann, D. P. Bartel, Disrupting the pairing between let-7 and Hmga2 enhances oncogenic transformation. *Science* **315**, 1576-1579 (2007).
82. Y. S. Lee, A. Dutta, The tumor suppressor microRNA let-7 represses the HMGA2 oncogene. *Genes Dev* **21**, 1025-1030 (2007).
83. D. O. Morgan, Cyclin-dependent kinases: engines, clocks, and microprocessors. *Annu Rev Cell Dev Biol* **13**, 261-291 (1997).
84. C. J. Sherr, Cancer cell cycles. *Science* **274**, 1672-1677 (1996).
85. M. Malumbres, M. Barbacid, To cycle or not to cycle: a critical decision in cancer. *Nat Rev Cancer* **1**, 222-231 (2001).
86. M. Meyerson, E. Harlow, Identification of G1 kinase activity for cdk6, a novel cyclin D partner. *Mol Cell Biol* **14**, 2077-2086 (1994).
87. H. Matsushime *et al.*, Identification and properties of an atypical catalytic subunit (p34PSK-J3/cdk4) for mammalian D type G1 cyclins. *Cell* **71**, 323-334 (1992).
88. P. D. Adams, Regulation of the retinoblastoma tumor suppressor protein by cyclin/cdks. *Biochim Biophys Acta* **1471**, M123-133 (2001).
89. C. Giacinti, A. Giordano, RB and cell cycle progression. *Oncogene* **25**, 5220-5227 (2006).
90. S. P. Chellappan, S. Hiebert, M. Mudryj, J. M. Horowitz, J. R. Nevins, The E2F transcription factor is a cellular target for the RB protein. *Cell* **65**, 1053-1061 (1991).
91. R. A. Weinberg, The retinoblastoma protein and cell cycle control. *Cell* **81**, 323-330 (1995).

92. A. Fassl, Y. Geng, P. Sicinski, CDK4 and CDK6 kinases: From basic science to cancer therapy. *Science* **375**, eabc1495 (2022).
93. A. Schirripa, V. Sexl, K. Kollmann, Cyclin-dependent kinase inhibitors in malignant hematopoiesis. *Front Oncol* **12**, 916682 (2022).
94. A. Italiano *et al.*, HMGA2 is the partner of MDM2 in well-differentiated and dedifferentiated liposarcomas whereas CDK4 belongs to a distinct inconsistent amplicon. *Int J Cancer* **122**, 2233-2241 (2008).
95. T. Assi *et al.*, Targeting CDK4 (cyclin-dependent kinase) amplification in liposarcoma: A comprehensive review. *Critical Reviews in Oncology/Hematology* **153**, 103029 (2020).
96. A. R. Abdul Razak *et al.*, Co-Targeting of MDM2 and CDK4/6 with Siremadlin and Ribociclib for the Treatment of Patients with Well-Differentiated or Dedifferentiated Liposarcoma: Results from a Proof-of-Concept, Phase Ib Study. *Clin Cancer Res* **28**, 1087-1097 (2022).
97. Z. Gahvari, A. Parkes, Dedifferentiated Liposarcoma: Systemic Therapy Options. *Curr Treat Options Oncol* **21**, 15 (2020).
98. J. H. Park, R. G. Roeder, GAS41 is required for repression of the p53 tumor suppressor pathway during normal cellular proliferation. *Mol Cell Biol* **26**, 4006-4016 (2006).
99. J. Barretina *et al.*, Subtype-specific genomic alterations define new targets for soft-tissue sarcoma therapy. *Nat Genet* **42**, 715-721 (2010).
100. Y. Li *et al.*, AF9 YEATS domain links histone acetylation to DOT1L-mediated H3K79 methylation. *Cell* **159**, 558-571 (2014).
101. C. J. Denis, K. Deiteren, D. Hendriks, P. Proost, A. M. Lambeir, Carboxypeptidase M in apoptosis, adipogenesis and cancer. *Clin Chim Acta* **415**, 306-316 (2013).
102. K. Deiteren, D. Hendriks, S. Scharpé, A. M. Lambeir, Carboxypeptidase M: Multiple alliances and unknown partners. *Clin Chim Acta* **399**, 24-39 (2009).
103. X. Wang *et al.*, High-resolution genomic mapping reveals consistent amplification of the fibroblast growth factor receptor substrate 2 gene in well-differentiated and dedifferentiated liposarcoma. *Genes Chromosomes Cancer* **50**, 849-858 (2011).

104. M. E. Hemler, Tetraspanin proteins promote multiple cancer stages. *Nat Rev Cancer* **14**, 49-60 (2014).
105. R. P. Salzano, Z. Tomkiewicz, W. A. Africano, Dedifferentiated liposarcoma with features of rhabdomyosarcoma. *Conn Med* **55**, 200-202 (1991).
106. G. Tallini, R. A. Erlandson, M. F. Brennan, J. M. Woodruff, Divergent myosarcomatous differentiation in retroperitoneal liposarcoma. *Am J Surg Pathol* **17**, 546-556 (1993).
107. W. H. Henricks, Y. C. Chu, J. R. Goldblum, S. W. Weiss, Dedifferentiated liposarcoma: a clinicopathological analysis of 155 cases with a proposal for an expanded definition of dedifferentiation. *Am J Surg Pathol* **21**, 271-281 (1997).
108. H. L. Evans, K. K. Khurana, B. L. Kemp, A. G. Ayala, Heterologous elements in the dedifferentiated component of dedifferentiated liposarcoma. *Am J Surg Pathol* **18**, 1150-1157 (1994).
109. M. B. Binh *et al.*, Dedifferentiated liposarcomas with divergent myosarcomatous differentiation developed in the internal trunk: a study of 27 cases and comparison to conventional dedifferentiated liposarcomas and leiomyosarcomas. *Am J Surg Pathol* **31**, 1557-1566 (2007).
110. P. Kurzawa *et al.*, Prognostic Value of Myogenic Differentiation in Dedifferentiated Liposarcoma. *Am J Surg Pathol* **44**, 799-804 (2020).
111. J. Gootee, S. Aurit, C. Curtin, P. Silberstein, Primary anatomical site, adjuvant therapy, and other prognostic variables for dedifferentiated liposarcoma. *J Cancer Res Clin Oncol* **145**, 181-192 (2019).
112. A. Gronchi *et al.*, Myogenic differentiation and histologic grading are major prognostic determinants in retroperitoneal liposarcoma. *Am J Surg Pathol* **39**, 383-393 (2015).
113. A. Agaimy, M. Michal, L. Hadravsky, Dedifferentiated liposarcoma composed predominantly of rhabdoid/epithelioid cells: a frequently misdiagnosed highly aggressive variant. *Hum Pathol* **77**, 20-27 (2018).
114. G. O. Dorian Yarih *et al.*, Myogenic dedifferentiation is associated with poor outcomes in retroperitoneal dedifferentiated liposarcomas. *Rare Tumors* **13**, 2036361320986655 (2021).

115. D. Chakravarty *et al.*, OncoKB: A Precision Oncology Knowledge Base. *JCO Precision Oncology*, 1-16 (2017).
116. K. Weskamp, B. B. Olwin, R. Parker, Post-Transcriptional Regulation in Skeletal Muscle Development, Repair, and Disease. *Trends Mol Med* **27**, 469-481 (2021).
117. L. G. Goldfarb, M. C. Dalakas, Tragedy in a heartbeat: malfunctioning desmin causes skeletal and cardiac muscle disease. *J Clin Invest* **119**, 1806-1813 (2009).
118. C. E. Ha, N. Bhagavan, *Essentials of medical biochemistry: with clinical cases*. (Academic Press, 2011).
119. D. Aran, Z. Hu, A. J. Butte, xCell: digitally portraying the tissue cellular heterogeneity landscape. *Genome Biol* **18**, 220 (2017).
120. A. M. Newman *et al.*, Determining cell type abundance and expression from bulk tissues with digital cytometry. *Nat Biotechnol* **37**, 773-782 (2019).
121. J. Racle, D. Gfeller, EPIC: A Tool to Estimate the Proportions of Different Cell Types from Bulk Gene Expression Data. *Methods Mol Biol* **2120**, 233-248 (2020).
122. T. Li *et al.*, TIMER: A Web Server for Comprehensive Analysis of Tumor-Infiltrating Immune Cells. *Cancer Res* **77**, e108-e110 (2017).
123. F. Finotello *et al.*, Molecular and pharmacological modulators of the tumor immune contexture revealed by deconvolution of RNA-seq data. *Genome Med* **11**, 34 (2019).
124. Z. Eroglu *et al.*, High response rate to PD-1 blockade in desmoplastic melanomas. *Nature* **553**, 347-350 (2018).
125. S. Wang, Z. He, X. Wang, H. Li, X. S. Liu, Antigen presentation and tumor immunogenicity in cancer immunotherapy response prediction. *Elife* **8**, (2019).
126. M. Hirata *et al.*, Integrated exome and RNA sequencing of dedifferentiated liposarcoma. *Nat Commun* **10**, 5683 (2019).
127. S. Piccolo, T. Panciera, P. Contessotto, M. Cordenonsi, YAP/TAZ as master regulators in cancer: modulation, function and therapeutic approaches. *Nat Cancer*, (2022).
128. S. Ishihara, H. Haga, Matrix Stiffness Contributes to Cancer Progression by Regulating Transcription Factors. *Cancers (Basel)* **14**, (2022).

129. S. Wu *et al.*, Matrix stiffness-upregulated LOXL2 promotes fibronectin production, MMP9 and CXCL12 expression and BMDCs recruitment to assist pre-metastatic niche formation. *J Exp Clin Cancer Res* **37**, 99 (2018).
130. C. H. Luo *et al.*, High levels of TIMP1 are associated with increased extracellular matrix stiffness in isocitrate dehydrogenase 1-wild type gliomas. *Lab Invest* **102**, 1304-1313 (2022).
131. C. A. Fullenkamp *et al.*, TAZ and YAP are frequently activated oncoproteins in sarcomas. *Oncotarget* **7**, 30094-30108 (2016).
132. D. Kanojia *et al.*, Genomic landscape of liposarcoma. *Oncotarget* **6**, 42429-42444 (2015).
133. R. Tyler *et al.*, A review of retroperitoneal liposarcoma genomics. *Cancer Treat Rev* **86**, 102013 (2020).
134. N. Turner, R. Grose, Fibroblast growth factor signalling: from development to cancer. *Nat Rev Cancer* **10**, 116-129 (2010).
135. J. M. Bae *et al.*, Fibroblast Growth Factor Receptor 1 (FGFR1) Amplification Detected by Droplet Digital Polymerase Chain Reaction (ddPCR) Is a Prognostic Factor in Colorectal Cancers. *Cancer Res Treat* **52**, 74-84 (2020).
136. Y. Wang *et al.*, Prognostic and clinicopathological significance of. *Ann Transl Med* **7**, 669 (2019).
137. R. Erber *et al.*, Impact of fibroblast growth factor receptor 1 (FGFR1) amplification on the prognosis of breast cancer patients. *Breast Cancer Res Treat* **184**, 311-324 (2020).
138. P. Chudasama *et al.*, Targeting Fibroblast Growth Factor Receptor 1 for Treatment of Soft-Tissue Sarcoma. *Clin Cancer Res* **23**, 962-973 (2017).
139. S. Kaeser-Pebernard *et al.*, mTORC1 controls Golgi architecture and vesicle secretion by phosphorylation of SCYL1. *Nat Commun* **13**, 4685 (2022).
140. G. Y. Liu, D. M. Sabatini, mTOR at the nexus of nutrition, growth, ageing and disease. *Nat Rev Mol Cell Biol* **21**, 183-203 (2020).
141. B. Magnuson, B. Ekim, D. C. Fingar, Regulation and function of ribosomal protein S6 kinase (S6K) within mTOR signalling networks. *Biochem J* **441**, 1-21 (2012).

142. S. Faivre, G. Kroemer, E. Raymond, Current development of mTOR inhibitors as anticancer agents. *Nat Rev Drug Discov* **5**, 671-688 (2006).
143. C. S. Sinclair, M. Rowley, A. Naderi, F. J. Couch, The 17q23 amplicon and breast cancer. *Breast Cancer Res Treat* **78**, 313-322 (2003).
144. J. Bostner *et al.*, S6 kinase signaling: tamoxifen response and prognostic indication in two breast cancer cohorts. *Endocr Relat Cancer* **22**, 331-343 (2015).
145. M. Bärlund *et al.*, Detecting activation of ribosomal protein S6 kinase by complementary DNA and tissue microarray analysis. *J Natl Cancer Inst* **92**, 1252-1259 (2000).
146. C. Koelsche *et al.*, Intimal sarcomas and undifferentiated cardiac sarcomas carry mutually exclusive MDM2, MDM4, and CDK6 amplifications and share a common DNA methylation signature. *Mod Pathol* **34**, 2122-2129 (2021).
147. C. Yang *et al.*, Acquired CDK6 amplification promotes breast cancer resistance to CDK4/6 inhibitors and loss of ER signaling and dependence. *Oncogene* **36**, 2255-2264 (2017).
148. J. Y. Hsu, N. D. Seligson, J. L. Hays, W. O. Miles, J. L. Chen, Clinical Utility of CDK4/6 Inhibitors in Sarcoma: Successes and Future Challenges. *JCO Precis Oncol* **6**, e2100211 (2022).
149. E. Parra-Peralbo, A. Talamillo, R. Barrio, Origin and Development of the Adipose Tissue, a Key Organ in Physiology and Disease. *Front Cell Dev Biol* **9**, 786129 (2021).
150. C. F. Bentzinger, Y. X. Wang, M. A. Rudnicki, Building muscle: molecular regulation of myogenesis. *Cold Spring Harb Perspect Biol* **4**, (2012).
151. S. Pani, S. Dey, B. Pati, U. Senapati, N. C. Bal, Brown to White Fat Transition Overlap With Skeletal Muscle During Development of Larger Mammals: Is it a Coincidence? *J Endocr Soc* **6**, bvac151 (2022).
152. V. Gilsanz, H. H. Hu, S. Kajimura, Relevance of brown adipose tissue in infancy and adolescence. *Pediatr Res* **73**, 3-9 (2013).
153. R. Dhanasekaran *et al.*, The MYC oncogene - the grand orchestrator of cancer growth and immune evasion. *Nat Rev Clin Oncol* **19**, 23-36 (2022).

154. D. Williamson *et al.*, Relationship between MYCN copy number and expression in rhabdomyosarcomas and correlation with adverse prognosis in the alveolar subtype. *J Clin Oncol* **23**, 880-888 (2005).
155. S. C. Kamran *et al.*, Malignant peripheral nerve sheath tumors: prognostic impact of rhabdomyoblastic differentiation (malignant triton tumors), neurofibromatosis 1 status and location. *Eur J Surg Oncol* **39**, 46-52 (2013).
156. D. Massi, G. Beltrami, R. Capanna, A. Franchi, Histopathological re-classification of extremity pleomorphic soft tissue sarcoma has clinical relevance. *Eur J Surg Oncol* **30**, 1131-1136 (2004).
157. A. T. Deyrup *et al.*, Myoid differentiation and prognosis in adult pleomorphic sarcomas of the extremity: an analysis of 92 cases. *Cancer* **98**, 805-813 (2003).
158. B. Liegl, J. L. Hornick, C. R. Antonescu, C. L. Corless, C. D. Fletcher, Rhabdomyosarcomatous differentiation in gastrointestinal stromal tumors after tyrosine kinase inhibitor therapy: a novel form of tumor progression. *Am J Surg Pathol* **33**, 218-226 (2009).
159. S. Jhunjhunwala, C. Hammer, L. Delamarre, Antigen presentation in cancer: insights into tumour immunogenicity and immune evasion. *Nat Rev Cancer* **21**, 298-312 (2021).
160. S. Spranger, T. F. Gajewski, Impact of oncogenic pathways on evasion of antitumour immune responses. *Nat Rev Cancer* **18**, 139-147 (2018).
161. J. Galon, D. Bruni, Approaches to treat immune hot, altered and cold tumours with combination immunotherapies. *Nat Rev Drug Discov* **18**, 197-218 (2019).
162. S. C. Casey, V. Baylot, D. W. Felsher, The MYC oncogene is a global regulator of the immune response. *Blood* **131**, 2007-2015 (2018).
163. C. Sciorati, E. Rigamonti, A. A. Manfredi, P. Rovere-Querini, Cell death, clearance and immunity in the skeletal muscle. *Cell Death Differ* **23**, 927-937 (2016).
164. S. Boegel *et al.*, HLA and proteasome expression body map. *BMC Med Genomics* **11**, 36 (2018).
165. C. García-Fernández, A. Saz, C. Fornaguera, S. Borrós, Cancer immunotherapies revisited: state of the art of conventional treatments and next-generation nanomedicines. *Cancer Gene Ther* **28**, 935-946 (2021).

166. A. M. Eggermont, M. Maio, C. Robert, Immune checkpoint inhibitors in melanoma provide the cornerstones for curative therapies. *Semin Oncol* **42**, 429-435 (2015).
167. E. Z. Keung *et al.*, Correlative Analyses of the SARC028 Trial Reveal an Association Between Sarcoma-Associated Immune Infiltrate and Response to Pembrolizumab. *Clin Cancer Res* **26**, 1258-1266 (2020).
168. F. Petitprez *et al.*, B cells are associated with survival and immunotherapy response in sarcoma. *Nature* **577**, 556-560 (2020).
169. A. Dufresne *et al.*, Specific immune landscapes and immune checkpoint expressions in histotypes and molecular subtypes of sarcoma. *Oncoimmunology* **9**, 1792036 (2020).
170. A. Dobin *et al.*, STAR: ultrafast universal RNA-seq aligner. *Bioinformatics* **29**, 15-21 (2013).
171. B. Li, C. N. Dewey, RSEM: accurate transcript quantification from RNA-Seq data with or without a reference genome. *BMC Bioinformatics* **12**, 323 (2011).
172. A. Frankish *et al.*, GENCODE 2021. *Nucleic Acids Res* **49**, D916-D923 (2021).
173. M. I. Love, W. Huber, S. Anders, Moderated estimation of fold change and dispersion for RNA-seq data with DESeq2. *Genome Biol* **15**, 550 (2014).
174. A. Conesa *et al.*, A survey of best practices for RNA-seq data analysis. *Genome Biol* **17**, 13 (2016).
175. Y. Zhao *et al.*, TPM, FPKM, or Normalized Counts? A Comparative Study of Quantification Measures for the Analysis of RNA-seq Data from the NCI Patient-Derived Models Repository. *J Transl Med* **19**, 269 (2021).
176. H. HOTELLING, RELATIONS BETWEEN TWO SETS OF VARIATES*. *Biometrika* **28**, 321-377 (1936).
177. M. Ringnér, What is principal component analysis? *Nat Biotechnol* **26**, 303-304 (2008).
178. I. T. Jolliffe, J. Cadima, Principal component analysis: a review and recent developments. *Philos Trans A Math Phys Eng Sci* **374**, 20150202 (2016).
179. V. K. Mootha *et al.*, PGC-1alpha-responsive genes involved in oxidative phosphorylation are coordinately downregulated in human diabetes. *Nat Genet* **34**, 267-273 (2003).

180. A. Subramanian *et al.*, Gene set enrichment analysis: a knowledge-based approach for interpreting genome-wide expression profiles. *Proc Natl Acad Sci U S A* **102**, 15545-15550 (2005).
181. S. B. Plaisier, R. Taschereau, J. A. Wong, T. G. Graeber, Rank-rank hypergeometric overlap: identification of statistically significant overlap between gene-expression signatures. *Nucleic Acids Res* **38**, e169 (2010).
182. G. Yu, L. G. Wang, Y. Han, Q. Y. He, clusterProfiler: an R package for comparing biological themes among gene clusters. *OMICS* **16**, 284-287 (2012).
183. M. Stromberg *et al.*, in *Proceedings of the 8th ACM International Conference on Bioinformatics, Computational Biology, and Health Informatics*. (2017), pp. 596-596.
184. T. Li *et al.*, TIMER2.0 for analysis of tumor-infiltrating immune cells. *Nucleic Acids Res* **48**, W509-W514 (2020).
185. B. Li *et al.*, Comprehensive analyses of tumor immunity: implications for cancer immunotherapy. *Genome Biol* **17**, 174 (2016).

8. ACKNOWLEDGEMENT

I would like to thank our external collaborators: Dr. A. Gronchi (Fondazione IRCCS Istituto Nazionale dei Tumori, Milan, Italy); Dr. Prof. Angelo P. Dei Tos (University of Padua School of Medicine, Padua, Italy) and Dr. Marta Sbaraglia (Azienda Ospedale Università Padova, Padua, Italy).

A special thanks go to my supervisor, Dr. Roberta Maestro, for accepting me into her lab, for her guidance during these three years of my PhD, for teaching me what it means to do research, for her patience, and for sharing her passion for this challenging but wonderful work.
A heartfelt thank you also go to Dr. Dominga Racanelli, who shared her knowledge with me during the first year of my PhD and for her guidance, albeit briefly, along on this path.
Additional thanks go to all the people I have met in the unit of Oncogenetics and Functional Oncogenomics, who provided me with advice and support when I needed it.
In particular, I would like to thank Dr. Elisa Del Savio, who stood by me in the happiest and most difficult moments of these three years of my PhD, for her patience and endless kindness.
A special thanks also go to Dr. Maria Elena Ciuffetti, for me simply Ciuffy, who helped me a lot in this last year of my PhD.
I would also like to thank Dr. Davide Baldazzi, whose support has been crucial for the bioinformatics analyses and beyond, for his ability to always make me laugh even in the most difficult moments, for his patience, especially in this last year, and for his support and encouragement.

My thanks go to all the people I have met during these years of doctoral study, both those who have accompanied me during the three years and those whom I have met in the course and with whom I have shared cheerful moments. I would also like to thank all my distant friends who have always supported me despite the distance.
Finally, I would like to thank my family who supported me throughout my journey; I dedicate the achievement of this goal mainly to them, my mother, who taught me never to give up and that it is never too late to change course and improve, my father who was always been there for me and supported me, my sister Giulia and her husband Stefano

who always managed to make me smile in times of need. I would also like to thank Ewelina who supported me.

I dedicate this work especially to my grandmother Lina and my grandparents, who are no longer with us, but to whom I always feel close despite everything.

Finally, I dedicate this work to Prof. Guglielmo Longo who, besides my family, was the first to always believed in me.

9. PUBLISHED ARTICLES

cancers

MDPI

Article

Crosstalk between Macrophages and Myxoid Liposarcoma Cells Increases Spreading and Invasiveness of Tumor Cells

Michele Minopoli [1,†], Sabrina Sarno [1,†], Lucia Cannella [2], Salvatore Tafuto [2], Gosuè Scognamiglio [3], Michele Gallo [4], Flavio Fazioli [4], Rosa Azzaro [5], Gaetano Apice [2], Biagio De Angelis [6], Elena Tamborini [7], Cecilia Garofalo [8], Ymera Pignochino [9,10], Laura Mercatali [11], Toni Ibrahim [11], Rita Falcioni [12], Beatrice Valenti [13], Roberta Maestro [13], Katia Scotlandi [14], Annarosaria De Chiara [3,‡] and Maria Vincenza Carriero [1,*,‡]

[1] Neoplastic Progression Unit, Istituto Nazionale Tumori IRCCS 'Fondazione G. Pascale', 80131 Naples, Italy; m.minopoli@istitutotumori.na.it (M.M.); sabrina.sarno@istitutotumori.na.it (S.S.)
[2] Medical Oncology Unit, Istituto Nazionale Tumori IRCCS 'Fondazione G. Pascale', 80131 Naples, Italy; l.cannella@istitutotumori.na.it (L.C.); s.tafuto@istitutotumori.na.it (S.T.); g.apice@istitutotumori.na.it (G.A.)
[3] Pathology Unit, Istituto Nazionale Tumori IRCCS 'Fondazione G. Pascale', 80131 Naples, Italy; giosue.scognamiglio@istitutotumori.na.it (G.S.); a.dechiara@istitutotumori.na.it (A.D.C.)
[4] Musculoskeletal Surgery Unit, Istituto Nazionale Tumori IRCCS 'Fondazione G. Pascale', 80131 Naples, Italy; m.gallo@istitutotumori.na.it (M.G.); f.fazioli@istitutotumori.na.it (F.F.)
[5] Transfusion Medicine Unit, Istituto Nazionale Tumori IRCCS 'Fondazione G. Pascale', 80131 Naples, Italy; r.azzaro@istitutotumori.na.it
[6] Department of Onco-Haematology and Cell and Gene Therapy Unit, Bambino Gesù Children's Hospital, IRCCS, 00165 Rome, Italy; biagio.deangelis@opbg.net
[7] Department of Pathology, Fondazione IRCCS Istituto Nazionale dei Tumori, 20133 Milan, Italy; Elena.Tamborini@istitutotumori.mi.it
[8] Advanced Translational Research Laboratory, Veneto Institute of Oncology IOV—IRCCS, 35128 Padua, Italy; cecilia.garofalo@iov.veneto.it
[9] Department of Clinical and Biological Sciences, University of Turin, 10124 Torino, Italy; ymera.pignochino@ircc.it
[10] Division of Medical Oncology, Candiolo Cancer Institute, FPO-IRCCS, 10060 Candiolo, Italy
[11] Osteoncology and Rare Tumors Center, Istituto Romagnolo per lo Studio dei Tumori "Dino Amadori" (IRST) IRCCS, 47010 Meldola, Italy; laura.mercatali@irst.emr.it (L.M.); toni.ibrahim@irst.emr.it (T.I.)
[12] Department of Research, Diagnosis and Innovative Technology, IRCCS Regina Elena National Cancer Institute, 00128 Rome, Italy; rita.falcioni@ifo.gov.it
[13] Oncogenetics and Functional Oncogenomics, Centro di Riferimento Oncologico di Aviano (CRO Aviano) IRCCS, National Cancer Institute, 33081 Aviano, Italy; beatrice.valenti@cro.it (B.V.); rmaestro@cro.it (R.M.)
[14] Laboratory of Experimental Oncology, IRCCS Istituto Ortopedico Rizzoli, 40136 Bologna, Italy; katia.scotlandi@ior.it
* Correspondence: m.carriero@istitutotumori.na.it; Tel.: +39-081-5903569
† Michele Minopoli and Sabrina Sarno contributed equally to this article.
‡ These authors share senior authorship and should be considered co-last authors.

Citation: Minopoli, M.; Sarno, S.; Cannella, L.; Tafuto, S.; Scognamiglio, G.; Gallo, M.; Fazioli, F.; Azzaro, R.; Apice, G.; De Angelis, B.; et al. Crosstalk between Macrophages and Myxoid Liposarcoma Cells Increases Spreading and Invasiveness of Tumor Cells. *Cancers* **2021**, *13*, 3298. https://doi.org/10.3390/cancers13133298

Academic Editor: Mario Del Rosso

Received: 11 June 2021
Accepted: 26 June 2021
Published: 30 June 2021

Simple Summary: Myxoid liposarcoma (MLPS) is the second most common subtype of liposarcoma, occurs predominantly in the extremities, and tends either to recur locally and metastasize to unusual soft tissue locations. To date, the mechanisms of invasion and metastasis of MLPS remain unclear, and yet, there is a high need to identify new prognostic biomarkers to enable the development of novel targeted therapeutic strategies. This study firstly aimed to assess the role of immune cellular components that infiltrate MLPS tissues. Our data show that high grade, heavily vascularized MLPS tissues exhibit T lymphocyte-poor and M2-like macrophage-rich phenotypes, while low grade MLPS tissues are mainly infiltrated by T lymphocytes. In line with these findings, evidence is shown that a crosstalk occurring between MLPS cells and macrophages exists as MLPS cells drive an M2-like phenotype in monocytes which in turn, increase the invasive capability of MLPS cells.

Abstract: Myxoid liposarcoma (MLPS) is the second most common subtype of liposarcoma and has tendency to metastasize to soft tissues. To date, the mechanisms of invasion and metastasis of MLPS remain unclear, and new therapeutic strategies that improve patients' outcomes are expected. In

this study, we analyzed by immunohistochemistry the immune cellular components and microvessel density in tumor tissues from patients affected by MLPS. In order to evaluate the effects of primary human MLPS cells on macrophage polarization and, in turn, the ability of macrophages to influence invasiveness of MLPS cells, non-contact and 3D organotypic co-cultures were set up. High grade MLPS tissues were found heavily vascularized, exhibited a CD3, CD4, and CD8 positive T lymphocyte-poor phenotype and were massively infiltrated by CD163 positive M2-like macrophages. Conversely, low grade MLPS tissues were infiltrated by a discrete amount of CD3, CD4, and CD8 positive T lymphocytes and a scarce amount of CD163 positive macrophages. Kaplan–Meier analysis revealed a shorter Progression Free Survival in MLPS patients whose tumor tissues were highly vascularized and heavily infiltrated by CD163 positive macrophages, indicating a clear-cut link between M2-like macrophage abundance and poor prognosis in patients. Moreover, we documented that, in co-culture, soluble factors produced by primary human MLPS cells induce macrophage polarization toward an M2-like phenotype which, in turn, increases MLPS cell capability to spread into extracellular matrix and to cross endothelial monolayers. The identification of M2-like polarization factors secreted by MLPS cells may allow to develop novel targeted therapies counteracting MLPS progression.

Keywords: myxoid liposarcoma; tumor microenvironment; tumor associated macrophages; tumor-infiltrating lymphocytes

1. Introduction

Myxoid Liposarcoma (MLPS) is the second most common type of liposarcoma, representing 20–30% of all liposarcomas and an about 5% of all adult soft tissue sarcomas. These tumors occur not only in adults but also in a younger population, with a peak of incidence in the fourth and fifth decade of life and equal distribution between men and women [1,2]. Histologically, MLPS is characterized by a mixture of round to oval non-lipogenic cells and small ring lipoblasts dispersed in an abundant myxoid matrix stroma with a thin, delicate, so called "chicken wire" capillary network [3]. Different factors have been evaluated in an effort to predict the prognosis at initial diagnosis of MLPS, including patient age, tumor size and depth, vascularization, grading, necrosis, mitotic rate, and p53 overexpression [4–6]. Nowadays, the hyper-cellularity is considered the most important one affecting the development of distant metastases, and a greater amount of round cells well correlate with a higher histologic grade and poorer prognosis. A cellular overlap > 5%, decreased myxoid matrix, increased nuclear grade, and high mitotic activity hallmark high-grade MLPS [2]. The recurrent (12;16) (q13;p11) chromosome translocation that results in the *FUS-DDIT3* gene fusion has a 95% incidence, while the variant (12;22)(q13;q12), in which *DDIT3* rearranges with *EWSR1,* occurs in only 5% of MLPS cases [7,8]. More than 50% of cases carry *TERT* promoter mutations [9]. Other less frequent genetic aberrations described in MLPS include *PI3KCA* mutations [10,11], homozygous loss of PTEN, high expression of RET, IGF1R and IGF2 [12,13]. The metastatic behavior of MLPS is characterized by a propensity of tumor cells to spread to extra-pulmonary locations with a predilection to the bone, particularly spine and abdominal cavity [14,15]. Metastases occur in 30–60% of MLPS cases, and the prognosis of these patients remains poor [16]. Actually, wide surgical resection, combined with or without radiotherapy, is the treatment of choice for localized disease, whereas several clinical trials with molecular targeted agents are currently under investigation for patients with advanced or metastatic disease [17–19]. Based on these considerations, the identification of new biomarker of tumor progression as well as new therapeutic strategies are an unmet need, especially for patients with advanced disease.

Some evidence indicates that trabectedin may be a therapeutic option for MLPS patients. The mechanism of action of this drug is complex, and it seems to rely not only on

DNA damage but also on modulation of tumor microenvironment, including infiltrating macrophages and intra-tumor vascularization [20].

In the last ten years, the emerging role of tumor microenvironment (TME) in cancer progression induced researchers to consider solid tumors as complex ecosystems, in which the TME immune cells may both counteract or promote tumor progression, depending on their nature and their functional state [21,22]. It has been shown in several solid tumors that cytokines and chemokines secreted by cancer cells may recruit circulating leukocytes from blood into the neoplastic tissues, and initiate a complex cross-talk with tumor cells, exerting cytotoxic or, alternatively, pro-tumor activity [23–25]. In this regard, several reports highlight that immune cells infiltrating solid tumors impact on clinical outcomes of patients. High levels of CD8 + cytotoxic T lymphocytes and CD4+ helper T cells are in general favorable prognostic indicators whereas other immune cells, such as regulatory T cells and tumor-associated macrophages (TAM)s, may promote tumor progression [26]. More recently, molecular profiling studies allowed to identify a number of immune therapeutic targets in bone sarcomas [27]. Otherwise, most of soft tissue sarcomas are considered non-immunogenic [1], few reports investigating the composition of TME in soft tissue sarcomas have been published, and clinical responses in trials with checkpoint inhibitors still remain unsatisfactory [28–32].

The main focus of this study was to quantify and characterize the cellular composition of the tumor immune infiltrate in a large cohort of MLPS cases and to explore the association of cell subtype with the histologic grade, microvessel density, and the Progression Free Survival (PFS). Moreover, the contribution of primary human MLPS cells in affecting macrophages polarization toward an M2-like phenotype and, in turn, the macrophage ability to modulate spreading and invasiveness of MLPS cells have been investigated by non-contact and organotypic co-cultures.

2. Materials and Methods

2.1. Patients and Tissue Samples

We retrospectively retrieved MLPS patients' information from the established database at the Istituto Nazionale Tumori IRCCS "Fondazione G. Pascale". Fifty eligible formalin-fixed paraffin-embedded (FFPE) specimens collected between the years 2001 and 2020 were taken into account. All patients had provided written informed consent for the use of tissue samples according to the institutional regulations. The study was approved by the Ethics Committee of the Istituto Nazionale Tumori IRCCS 'Fondazione G. Pascale". Histopathological diagnoses were reviewed according to the 2020 WHO classification criteria [2], based on clinical information, morphological criteria, and *DDIT3* break-apart FISH. Medical records were reviewed, and up-to-date information was collected to assess PFS.

2.2. Immunohistochemistry

Immunohistochemistry (IHC) was performed on 4 μm thin FFPE tissue sections as previously described [29], using automated slide stainers BenchMark (Ventana Medical System-Roche) and Leica Bond-III, (Leica Biosystems,), according to manufacturer's instructions. To characterize lymphocytic infiltrate, CD3 (clone 2GV6, ready to use), CD4 (clone SP35, ready to use), and CD8 (clone SP57, ready to use) monoclonal antibodies (Roche) were applied on tissue sections for 15 min at 25 °C. Monoclonal antibody directed to nuclear transcription factor forkhead box P3 (FOXP3) (clone D2W8E, 1:250, Cell Signaling Technology) was utilized to identify regulatory T cells. CD68 (clone KP-1, ready to use, Roche), and CD163 (clone MRQ-26, Roche) monoclonal antibodies were employed to identify macrophages and M-2 like macrophages, respectively [33]. Intra-tumoral vascularization was assessed by using CD31 monoclonal antibody (clone JC70A, ready to use, Dako). Sections were counterstained with hematoxylin.

2.3. Image Analysis

Slides were recorded by a light microscope connected to a video camera and analyzed by using the Axiovision 4.4 software (Carl Zeiss, Oberkochen, Germany). Quantitative analysis of immune infiltrates was conducted by two independent molecular pathologists (M.V.C., S.S.), blinded to clinical information. Sections were scored based on the average counts of positive cells or microvessels counted in the tumor areas, in five randomly selected fields/sample, each field having area of 0.785 mm^2, at 200-x magnification.

2.4. Primary MLPS Cell Culture

A representative sample (~1 cm × 1 cm) from the tumor excision of the high grade #37, #47, and low grade #48 and #50 MLPS patients were immediately minced with a scalpel under sterile conditions, incubated with 1 mg/mL collagenase XI (Sigma-Aldrich, #9407 Saint Louis, MO, USA) for 3 h at 37 °C under gentle agitation, and subsequently subject to filtration with sterile nylon filters (40μm mesh) as described [34]. After recovering, cells were cultured in 6-well multi-dish plates in Dulbecco Modified Essential Medium (DMEM,Cytiva HyClone™ #SH30081.01, (Cytiva, Marlborough, MA, USA) with the addition of 10% fetal bovine serum (FBS, Cytiva HyClone™ #SV30160.03), penicillin (100 U/mL, and streptomycin (100 μg/mL, Cytiva HyClone™ #SV30010, Cytiva, Marlborough, MA, USA). Isolated cell clusters obtained from only #37 and #47 high grade tumor tissues were further amplified in growth medium until an adherent, homogeneous, round population was obtained. Mesenchymal phenotype was identified by the lack of staining for cytokeratin AE1/AE3 (sc-81714) and by the positive staining for vimentin (Clone V9, sc-6260), all antibodies being purchased by Santa Cruz (Dallas, TX, USA). For in vitro experiments, the #37 and #47 primary MLPS cells were amplified for further eight and fifteen passages, respectively.

2.5. Isolation of Blood Monocytes

Buffy coats were obtained from healthy blood donors at Transfusion Medicine of the National Cancer Institute of Naples, after informed written consent. Peripheral blood mononuclear cells (PBMC)s, and serum were individually collected. PBMCs were harvested by density gradient centrifugation as previously described [29], using the Lympholyte-poly Cell Separation Media (Cedarlane Laboratories, #CL5015, Cedarlane, Burlington, ON, Canada) according to the manufacturer's instructions. Monocytes were isolated from PBMCs by positive selection of CD14+ cells using the Monocyte Isolation Kit II purchased by Miltenyi Biotec, #130-091-153 (79% pure by visual and cytofluorimetric analysis) and transferred to tissue culture plates in RPMI-1640 medium (Cytiva HyClone™ #SH30096.01, Cytiva, Marlborough, MA, USA), supplemented with 10% autologous human serum, penicillin (100 U/mL), and streptomycin (100 μg/mL).

2.6. Non-Contact Co-Cultures and Collection of Conditioned Media

Non-Contact co-cultures were carried out as described [29], using 24-multiwell plates and transwell polyethylene terephthalate permeable supports that allow the exchange of soluble factors purchased by Corning (Falcon®, #353095, NY USA). Briefly, human monocytes (1×10^6 cells/well) were seeded in the lower compartment in RPMI-1640 medium supplemented with 10% heat inactivated human serum. MLPS cells (2×10^5 cells/well) suspended in growth medium were seeded on the filter top and incubated for 72 h, at 37 °C with 5% CO_2, changing medium every other day. Then, MLPS cells were removed, and conditioned medium (CM) from monocytes was achieved by adding serum-free RPMI-1640 medium. After 18 h, CM was recovered, centrifuged twice at 2200 rpm for 5 min at 4 °C, and aliquots stored at −80 °C.

2.7. Cytofluorimetric Analysis

Monocytes recovered from co-cultures with/without MLPS cells were analyzed by flow cytometry as described [29], using PE-conjugated anti-CD68 REAfinity™ (Miltenyi Biotec #130-114-460) and APC-conjugated anti-CD163 REAfinity™ (Miltenyi Biotec, #130-112–129, Bergisch Gladbach, Germany) antibodies. Samples were acquired with the BD FACSCanto II (BD Biosciences, Franklin Lakes, NJ, USA), and data analyzed by the FlowJo v10.0.7 software (Tree Star, Inc, Ashland, OR, USA), after gating on the myeloid population in the FSC/SSC plot. Values were expressed as the percentage of each specific marker over median fluorescence intensity of the unstained cells.

2.8. Dot Blot Array

The relative levels of CC-chemokine ligand 2 (CCL2), IL-10 and IL-12 in CMs secreted by monocytes after co-culturing with primary MLPS cells were analyzed using the dot blot Human Cytokine Array Kit (#ARY005, R&D Systems, Milan Italy), according to the manufacturer's instructions. Briefly, 500 mL CM were applied on each membrane, and signals were detected using the streptavidin-horseradish peroxidase and chemiluminescent detection reagents as described [29].

2.9. Invasion Kinetic of MLPS Cells Monitored in Real Time

Cell invasion assay was assessed using the xCELLigence Real Time Cell Analysis (RTCA) technology (Acea Bioscience) and E-16-well plates (#05469830001) as described [35]. Bottom wells were coated with 20 μg/well matrigel (Corning® #356231) diluted in serum-free medium. Matrigel was allowed to polymerize for 1 h at 37 °C prior to seed MLPS cells (1×10^4 cells/well) suspended in CM from monocytes pre-cultured with MLPS cells or CM from monocytes alone, the last employed as a control. In both cases, CMs were supplemented with 10% heat-inactivated human serum. Cells that cross matrigel adhere to the bottom of plates causing impedance changes which are proportional to the number of invading cells. The impedance value of each well was automatically monitored in real-time for 18 h and expressed as a cell index value.

2.10. 3D Organotypic Co-Cultures

Organotypic co-cultures of MLPS with monocytes were carried out as previously described [29]. Briefly, MLPS spheroids were obtained by pipetting MLPS cell suspension ($5x10^3$ cells in 40 μl growth medium/well) into a Perfecta 3D Hanging Drop Plate (SigmaAldrich #HDP1096, Saint Louis, USA). Collagen/fibroblast matrix was obtained by suspending human dermal fibroblasts (Lonza #CC-2511) (1×10^5 cells/sample) in 250 μL alpha Minimum Essential Medium (Cytiva HyClone™ #SH30024.01, Cytiva, Marlborough, MA, USA), containing 250 μl heat-inactivated serum and 2 mg/mL Type I Collagen (Cell Application Inc., #124–25, San Diego, CA, USA), with/without monocytes (1×10^5 cells/well). MLPS spheroids were embedded into the collagen/fibroblast mixture, and images were acquired with an inverted microscope at 50× magnification for 7-days.

2.11. MLPS Cell Proliferation

This assay was performed using the xCELLigence RTCA technology as described [36]. MLPS cells (2×10^3/well) were seeded in 16-well E-plates in serum-free medium, CM from human monocytes pre-cultured with MLPS cells or CM from monocytes alone, the last as control. In all cases, media were supplemented with 2,5% heat-inactivated human serum. Gold microelectrodes placed on the bottom of plates detect impedance changes, which are proportional to the number of adherent cells and are expressed as Cell Index. The impedance value of each well was automatically monitored for 96 h and expressed as a Cell Index value.

2.12. Rans-Endothelial Migration

Trans-endothelial migration assays were performed using the xCELLigence RTCA technology as described [35]. Human Umbilical Vein Endothelial Cells (HUVEC)s, purchased by Lonza (#CC-2519), were employed between the third and the seventh passage and grown in Eagle Basal Medium (#CC31-56) supplemented with 4% FBS, 0.1% gentamicin, 1μg/mL hydrocortisone, 10 μg/mL epidermal growth factor, and 12 μg/mL bovine brain extract packaged together (EGM-2 Endothelial Cell Growth Medium-2 BulletKit (LONZA #CC-3162, Basel, Switzerland). HUVECs (2×10^4 cells/well) suspended in growth medium, were plated on E-16-well plates and allowed to grow for ~25 h until they formed a confluent monolayer, prior to seeding primary MLPS cells (2×10^3 cells/well) suspended in serum-free medium, CM from human monocytes pre-cultured with MLPS cells, or in CM from monocytes alone. Medium and CMs were supplemented with 10% serum. When HUVECs are challenged with crossing cells, there is a drop in electrical resistance which is monitored in real-time for 5 h as the cell index changes due to crossing of the endothelial monolayer. The experiments were performed twice in quadruplicate.

2.13. Statistical Analysis

Data are expressed as the means ± SD of the number of the indicated determinations. Statistically significant differences were defined as $p < 0.05$. Multiple comparisons were performed by one-way ANOVA post hoc Dunnett t-test. Pearson's correlation test was used to analyze the occurrence of any correlation between patient age, max tumor size, average counts of CD3, CD4, CD8, CD68, and CD163 positive cells and CD31 positive microvessels in tumor tissues from MLPS patients by using the SPSS 20.0 software (SPSS Inc., IBM New York, NY, USA). Kaplan–Meier analysis was used as appropriate to evaluate the PFS.

2.14. Ethics Statement

All experimental protocols were performed in accordance with guidelines of the Istituto Nazionale Tumori "Fondazione G. Pascale" IRCCS (Quality System n. LRC 6019486/QMS/U/IT-2015 certificated in conformity with UNI EN ISO 9001:2008). The research work with primary cell lines and MLPS tissues has been approved by Institutional Ethical Committee of Istituto Nazionale Tumori "Fondazione G. Pascale"-IRCCS, Naples, Italy (protocol 258/18, December 2018).

3. Results

3.1. Phenotypic Characterization of Immune Cells Infiltrating MLPS Tissues

To identify and quantify the cellular composition of the MLPS tissue immune infiltrates and tumor vascularization, fifty-patients collected between the years 2001 and 2020 were included in the study. At the time of diagnosis, the median age of patients was 51 years (range, 21–77 years), and their clinical-pathological characteristics are shown in Table 1 and Table S1. Patients had not received neo-adjuvant chemotherapy or radiotherapy before to be subjected to surgical resection. Histopathological diagnoses were reviewed according to the 2020 WHO classification criteria [2], based on clinical information, morphological criteria, and *DDIT3* break-apart FISH. Tumor tissues derived from the resection of primary tumors with the exception of one recurrence and two metastases and included twenty-six low grade and twenty-four high grade MLPS. Median tumor size was 13.8 cm, ranging between 2 and 35 cm (Table 1 and Table S1). Metastatic lesions occurred in two MLPS patients and six MLPS patients died of causes unrelated to the disease. PFS was calculated by reviewing the medical records of forty-three patients enrolled between 2001 and 2010, the others being enrolled between 2012 and 2020. IHC carried out on FFPE tissue sections allowed us to identify, quantify, and assess spatial distribution of tumor-infiltrating CD3+ T, CD4+ T helper and CD8+ T cytotoxic lymphocytes, FOXP3+ Treg lymphocytes, CD68+ macrophages, CD163+ alternatively activated M2-like macrophages, and

CD31 positive microvessels. Both low and high grade MLPS tissues appeared infiltrated by T lymphocytes and macrophages, although to a different extent (Figure 1a,b). For each tissue sample, positive T cells, macrophages and microvessels were counted in five randomly selected fields/sample acquired at 200× magnification and the averages of lymphocytes macrophages and microvessels for each MLPS tissue (Table S2) were subjected to statistical analysis. High grade tumors were mainly infiltrated by CD68+ and CD163+ macrophages, whereas discrete amounts of CD3+ T, CD4+ T helper, and CD8+ T cytotoxic lymphocytes were observed in the perivascular areas of low grade MLPS (Figure 1a,b and Table S2).

Table 1. Clinical and histologic findings of enrolled MLPS patients.

Myxoid Liposarcomas	Primary	47 (94%)
	Recurrence	1 (2%)
	Metastasis	2 (4%)
Age (years)	Mean	51.66
	<60	33 (66%)
	>60	17 (34%)
Sex	Male	27 (54%)
	Female	23 (46%)
Size (cm)	Mean	138.302
	<10 cm	14 (28%)
	>10 cm	30 (60%)
	Unknown	6 (12%)
Tumor location	Axilla	3 (6%)
	Chest wall	1 (2%)
	Abdomen	1 (2%)
	Pelvis	1 (2%)
	Gluteus	2 (4%)
	Thigh	29 (58%)
	Knee	1 (2%)
	Leg	12 (24%)
Histological grade	Low	26 (52%)
	High	24 (48%)
Follow up (ten years)	None	18 (36%)
	Recurrence	25 (50%)
	Unknown	7 (14%)

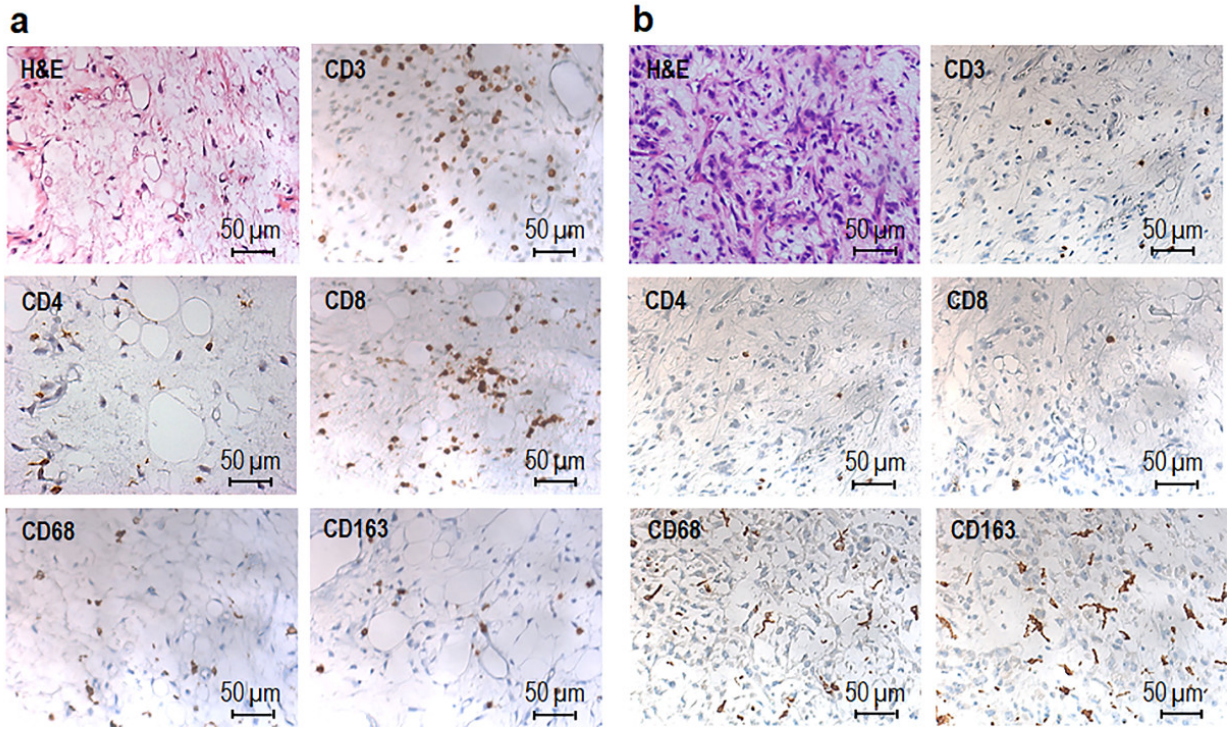

Figure 1. Immunohistochemical characterization of immune infiltrate in MLPS tissues. Representative images of H&E and IHC staining of CD3+, CD4+, CD8+, CD68+, and CD163+ positive cells in FFPE sections from a low grade MLPS (**a**) from patient #21 and high grade. MLPS tissues (**b**) from patient #4, acquired at 200× magnification.

As shown in the Figure 2, statistically significant differences were found between the mean number of T lymphocytes counted in low grade MLPS tissues (n.54 CD3+, n.41 CD4+, and n.32 CD8+ cells/field), compared to high grade ones (n.24 CD3, n.14 CD4, and n.16 CD8 positive cells/field). Moreover, the differences assessed between the average counts of macrophages in high grade (n.91 CD68+ and n.140 CD163+ cells/field) versus low grade (n.41 CD68+ and n.44 CD163+ cells/field) MLPS tissues were statistically significant with $p < 0.001$ (Figure 2).

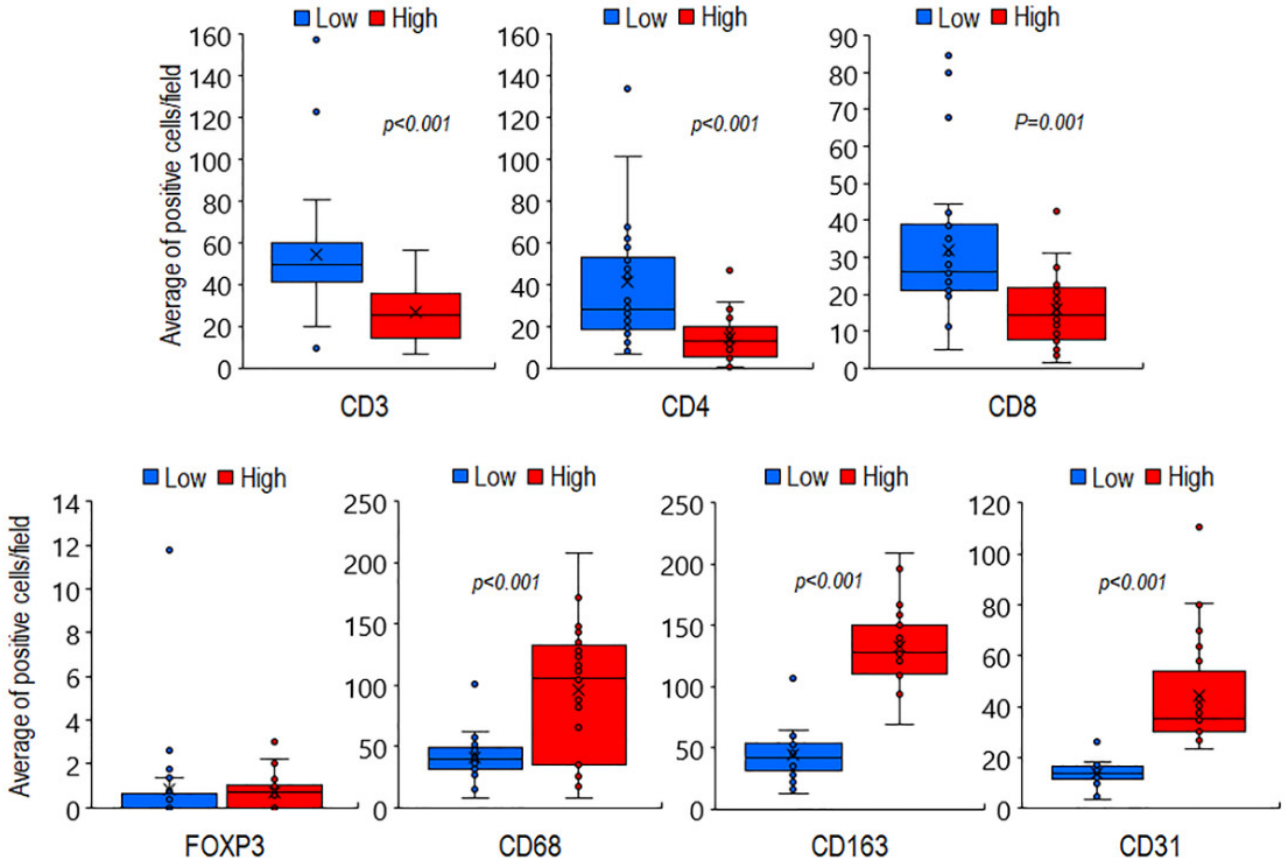

Figure 2. Correlation between immune cell infiltration and microvessel density in 26 low grade versus 24 high grade MLPS tissues. Box plots, showing variation in the average count of CD3+, CD4+, CD8+, FOXP3+, CD68+, and CD163+ cells as well as CD31 positive microvessels according to low or high histologic grade. Dark horizontal lines indicate the medians. Circles indicate outliers.

Of note, few Treg lymphocytes were found to infiltrate both low and high grade MLPS tissues (Table S2), whereas a statistically significant increase of capillary network was found in high grade MLPS sections (median: 129 microvessels/field), compared with low grade tumors (median: 42 microvessels/field) (Figure 2 and Table S2). Since the number of infiltrating CD163 positive macrophages appeared to better discriminate high grade from low grade MLPS tissues, the occurrence of any relationship between CD163+ macrophages and patient age, maximal tumor size as well as average counts/field of CD3+, CD4+, CD8+, and CD68+ cells were subjected to Pearson correlation analysis (Table S3). We found that CD163+ macrophage counts positively correlated with CD68+ macrophages, microvessel densities (Figure 3) as well as with patient age, but negatively with CD3+, CD4+, and CD8+ lymphocyte counts (Figure 3 and Table S3).

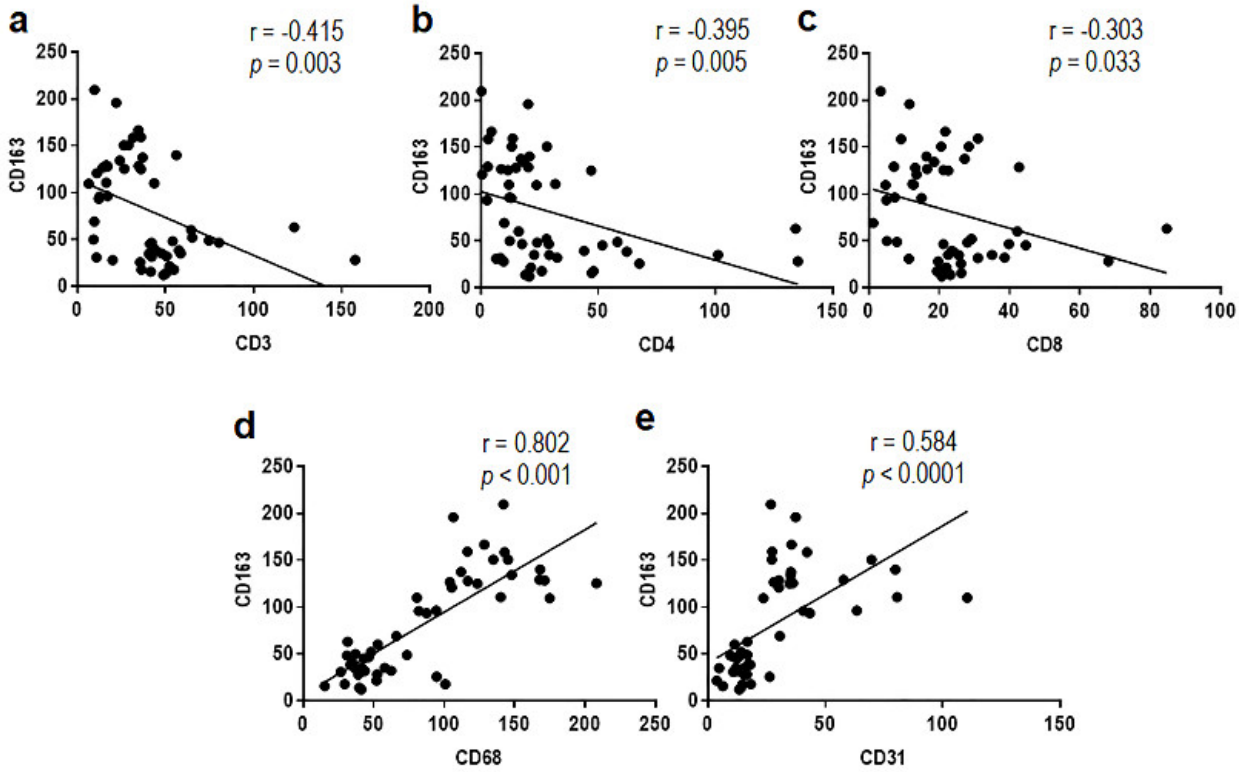

Figure 3. Pearson correlation between the average count of CD163+ macrophages and (**a**) CD3+ T lymphocytes, (**b**) CD4+ T helper lymphocytes, (**c**) CD8+ cytotoxic lymphocytes, (**d**) CD68+ macrophages, and (**e**) CD31+ microvessels in 50 MLPS tissue sections. Pearson correlation coefficients (r) are indicated.

Interestingly, patient ages were found to directly correlate with CD163+ macrophages but inversely with CD3+, CD4+, and CD8+ lymphocyte counts (Table S3). No correlation between tumor size and immune cell infiltration was found. (Table S3). Collectively, these observations seem to indicate that the aggressiveness of MLPS is modulated by its immune environment and that the alternatively activated M2 macrophages could support growth and invasive capability of MLPS cells.

To further investigate on the relationship occurring between paucity of cytotoxic T-lymphocytes and abundance of alternatively activated M2 macrophages, the PFS of MLPS patients was subjected to Kaplan–Meier analysis (Log-rank, Mantel–Cox test). Average counts of CD8+ lymphocytes, CD163+ macrophages, and CD31+ microvessels were dichotomized as poorly infiltrated, negative (0–20 CD8+, 0–50 CD163+ average cell count/field or 0–25 CD31+ microvessels/field), or highly infiltrated, positive (>20 CD8+, >50 CD163+ average cell counts/field or >25 microvessels/field). PFS time was defined as the interval between the date of diagnosis and the date of first disease recurrence or, in the absence of any recurrence, that of last follow-up visit. Kaplan–Meier analysis revealed that patients whose tissues were mainly infiltrated by cytotoxic T lymphocytes displayed a trend toward a better PFS (HR = 1.452, $p = 0.228$) whereas a shorter PFS was associated to patients whose tissues were highly vascularized (HR = 3.135, $p = 0.057$) and/or massively infiltrated by CD163 positive macrophages (HR = 3.774, $p = 0.052$) (Figure 4), indicating that a relationship between the number of TAMs infiltrating tumor tissues and poor prognosis of MLPS patients does exist.

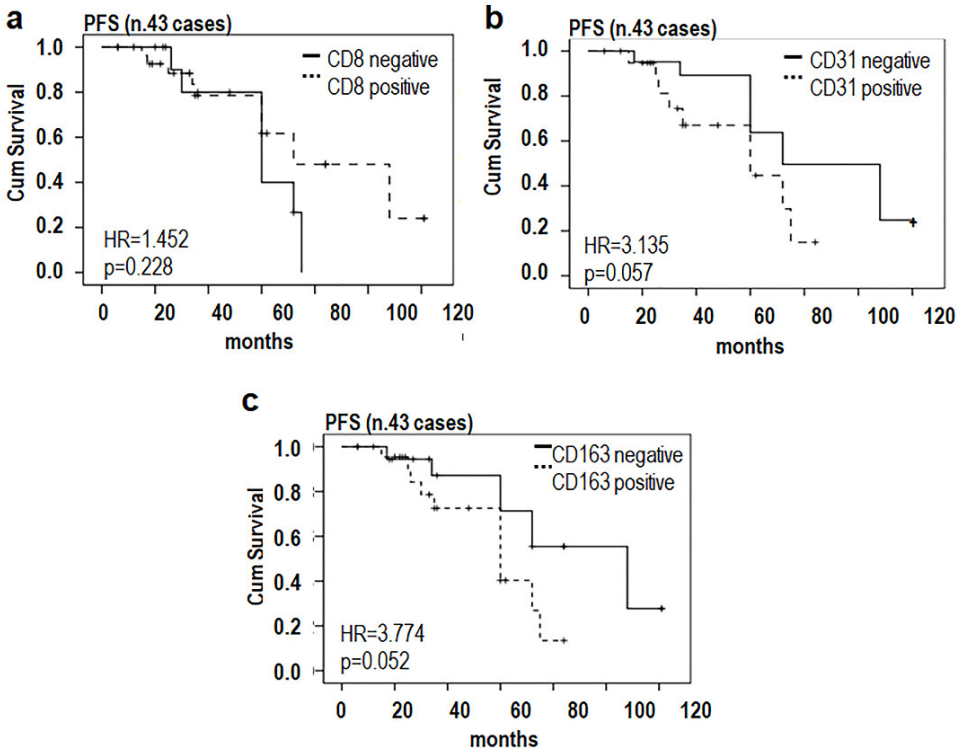

Figure 4. Prognostic implication of macrophages and microvessel density in MLPS. Kaplan–Meier analysis (Log-rank, Mantel–Cox test) used to evaluate the PFS, based on tumor-infiltrating CD8+ (**a**), CD31+ microvessels (**b**) and CD163+ cells (**c**) in 43 MLPS cases. Patients who were lost to clinical follow-up were censored from PFS at time lost to clinical follow-up (nine low and three high grade MLPS cases censored). Time was defined as the interval between the date of diagnosis and the date of disease recurrence or that of the last follow-up visit. HR, hazard ratio.

3.2. MLPS Cells Polarize Macrophages toward an M2-Like Pro-Tumor Phenotype

Cancer cells have been recognized to polarize tissue infiltrating macrophages toward an M2-like pro-tumor phenotype that, in turn, orchestrates many steps of tumor progression by secreting proteases and growth and angiogenic factors, as well as cytokines and chemokines [29,37–39]. To investigate whether MLPS cells engage a crosstalk with monocyte/macrophages, co-cultures of primary MLPS cells and monocytes from healthy donors were set up. Representative MLPS high grade tumor samples from patients #37 (Figure 5a) and #47 (Figure 5b) were subjected to enzymatic digestion and the recovered cells amplified until two adherent and homogeneous cell populations were obtained (Figure 5c,d, left). The mesenchymal phenotype of both primary MLPS cells was assessed by the lack of staining for cytokeratin AE1/AE3 and by the positive staining for vimentin (Figure 5c,d, right). Primary #37 and #47 MLPS cells were co-cultured with human monocytes in an in vitro non-contact co-culture system. After 72 h co-culture, monocytes were recovered and analyzed by flow cytometry using CD68 and CD163 Abs that recognize macrophages and alternatively activated M2 macrophages, respectively, [29]. After co-culture with either #37 (Figure 5e) or #47 (Figure 5f) primary MLPS cells, monocytes express high levels of CD68 and significantly higher levels of CD163 as compared to control monocytes (Figure S1a,b and Figure 5e,f). Polarized M2-like-macrophages are documented to secrete higher levels of CCL2 and IL-10 and lower levels of IL-12, as compared to macrophages [40]. Accordingly, higher levels of the CCL2 and IL-10 as well as lower levels of IL-12 were found in the CM from monocytes pre-co-cultured with either #37 and #47 primary MLPS cells, compared to CM from control monocytes (Figure S1c,d and Figure 5g,h), supporting the notion that MLPS cells effectively promote M2-like polarization.

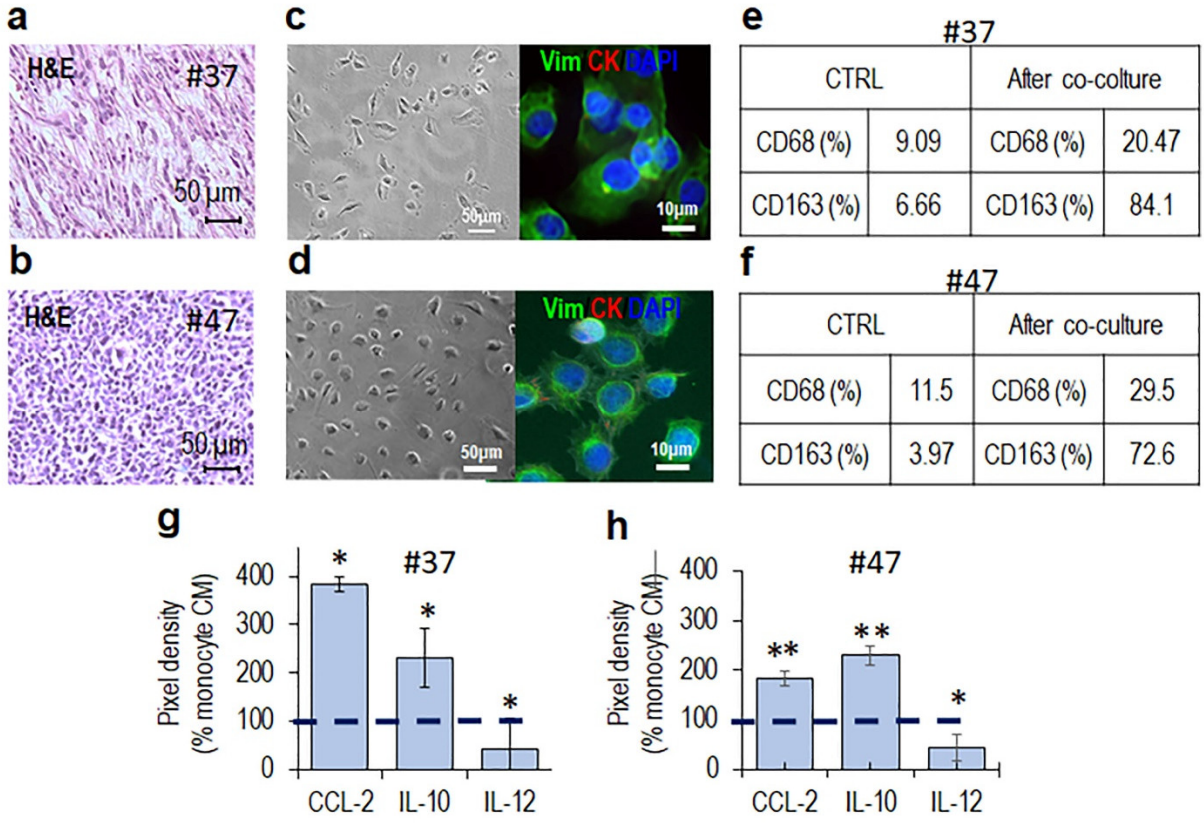

Figure 5. MLPS cells trigger M2-like polarization of monocytes in non-contact co-cultures. (**a**,**b**) Representative images of H&E staining of FFPE sections from #37 (**a**) and #47 (**b**) MLPS tissues acquired at 200× magnification. (**c**,**d**) Primary MLPS cells obtained by enzymatic digestion of 37 (**c**) and #47 (**d**) tumor tissues, visualized by phase contrast microscopy (left) and fluorescent microscopy after immunostaining with anti-vimentin and anti-cytokeratin Abs (right). Nuclei were stained blue with DAPI. Original magnifications: 200× (left) and 400× (right). (**e**,**f**) Human monocytes were co-cultured with #37 (**e**) and #47 (**f**) primary MLPS cells in an in vitro non-contact co-culture for 72 h and then analyzed for CD68 and CD163 expression by flow cytometry. (**e**,**f**) Percent variation of CD68 and CD163 on monocytes collected after non-contact co-culture, compared to control monocytes. (**g**,**h**) After co-cultures with #37 (**g**) and #47 (**h**) primary MLPS cells, CMs from monocytes were analyzed for the content of CC2, IL-10, and IL-12 by a dot plot assay. The pixel density of each spot was measured using NIH Image J 2.0 software developed by the US NIH, USA and positive control spots were used to normalize results between the membranes. The intensity of each spot was averaged over the duplicate spots and expressed as percentage of each cytokine or chemokine spontaneously secreted by control monocytes (monocyte CM), considered as 100% (dashed line). Data represent mean ± SD from three experiments performed in duplicate with * $p < 0.05$, ** $p < 0.005$.

3.3. Monocytes Increase Spreading and Invasive Ability of MLPS Cells

To understand whether monocytes/macrophages exert some effect on invasiveness of MLPS cells, we first determined the matrigel invasion rates of #37 and #47 primary MLPS cells exposed to CM from monocytes pre-cultured with MLPS cells or CM from control monocytes (CTRL CM), all supplemented with 10% heat-inactivated human serum, using the xCelligence technology. As shown in in Figure 6a,b CM from monocytes pre-cultured with #37 (Figure 6a) or #47 (Figure 6b) primary MLPS cells elicited a dramatic increase of MLPS cell invasion ability, as compared to CM from monocytes alone. Notably, the increase of MLPS cell invasiveness induced by soluble factors secreted by monocytes pre-exposed to MPLS cells is not due to cell proliferation increase, since cell index values recorded by proliferating MLPS cells exposed to diluents, CM from monocytes pre-cultured with MPLS cells or CM from control monocytes, all supplemented with 2.5% serum, generated overlapping curves (Figure S2). To further assess whether MLPS cells engage a crosstalk with monocyte/macrophages, organotypic 3D co-cultures that more accurately recapitulates key aspects of the architecture of solid cancers re-establishing morphological and functional features of the corresponding tissue in vivo, were set up.

Primary #37 and #47 MLPS cells were allowed to form spheroids for 72 h. Once obtained, MLPS spheroids and monocytes were incorporated in a semi-solid matrix containing dermal fibroblasts. Then, spreading of MLPS cells into matrices and size of MLPS spheroids were monitored for 7 days. Fibroblast-dependent matrix deposition allowed spheroids to grow in control samples. Remarkably, the inclusion of monocytes cells into organoids caused a dramatic, time-dependent increase of #37 and #47 MLPS cell spreading and size of MLPS spheroids (Figure 6c). Measurement of spheroid volumes after 7 days, revealed that monocytes caused an about 35% increase of spheroid sizes (Figure 6d).

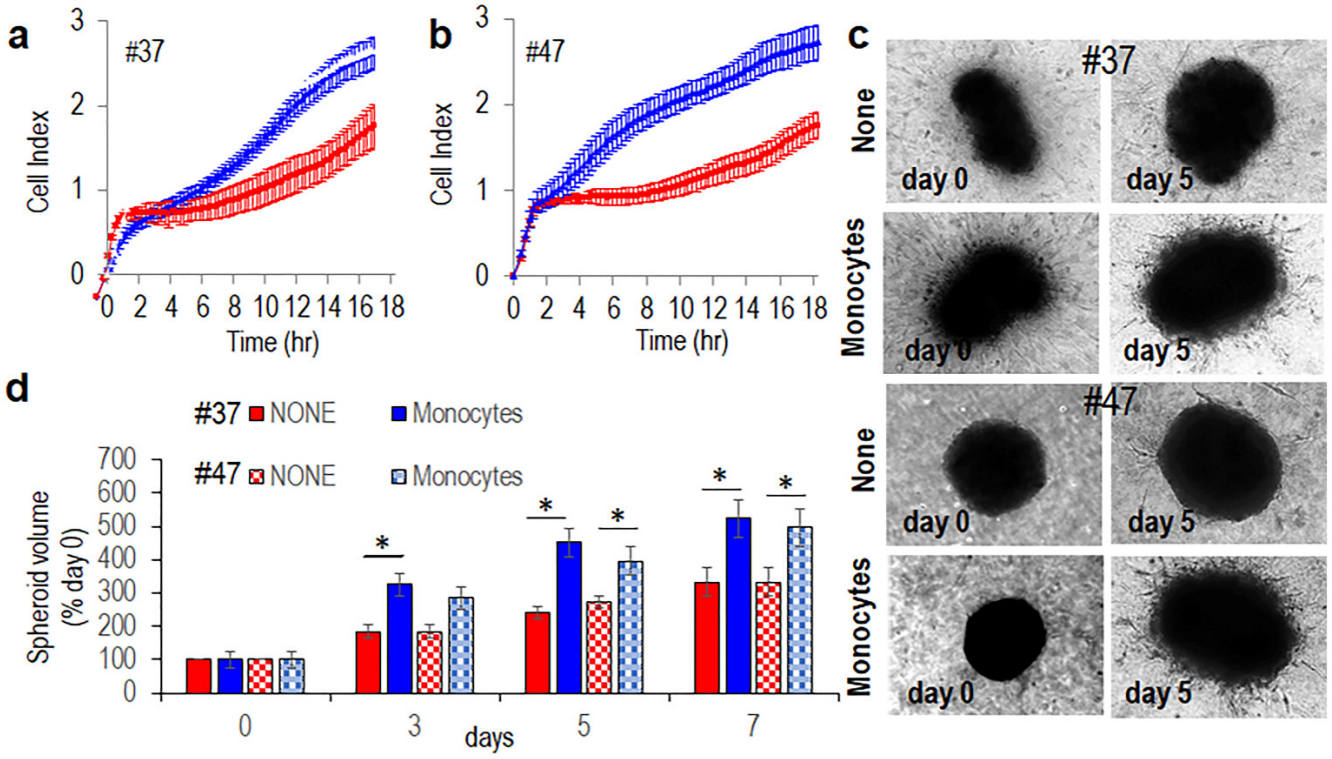

Figure 6. Monocytes pre-exposed to MPLS cells increases spreading of primary MLPS cells into matrices. (**a**,**b**). Primary #37 (**a**) and #47 (**b**) MLPS cells were suspended in CM from human monocytes pre-co-cultured with #37 and #47 (MLPS cells respectively (blue curves), or control monocytes (CTRL CM, red curves) and seeded onto matrigel-coated E-plates with serum added to a 10% final concentration. Matrigel invasion was monitored for 18 h by the RTCA xCELLigence technology. Data represent mean ± SD from a quadruplicate experiment representative of 2 replicates. (**c**,**d**). Spheroids containing primary #37 (**c**) or #47 (**d**) MLPS cells were embedded in the collagen/fibroblast mixture without (None), or with human monocytes. At the indicated times, images (**c**) were acquired at 50x magnification. (**d**) Time-dependent increase of spheroid size assessed by using the formula: $V = D(d)^2/2$, where D and d are the major and the minor spheroid diameter, respectively. Data expressed as percentage of volumes assessed at time zero are the mean ± SD of two independent experiments, performed in duplicate. Statistical significance with * $p < 0.0001$.

3.4. Monocytes Increase Transendothelial Migration of MLPS Cells

Beside invading the extracellular matrix, tumor aggressiveness depends on tumor cell ability to entering the bloodstream. To analyze the ability of alternatively activated M2 macrophages to modify MLPS cell ability to cross endothelial monolayers, endothelial cells were allowed to grow in E-plates for about 25 h until they formed a monolayer, prior to seeding primary #37 or #47 MLPS cells suspended in complete medium, plus CM from monocytes pre-cultured with MLPS cells or CM from control monocytes, both supplemented with 10% serum. At this time, reduction of impedance values, due to invading cells that interrupt endothelial monolayers, was monitored for a further 5 h. According to invasion data, both #37 or #47 MLPS cells were able to disrupt the endothelial monolayer

although to a different extent. In both cases, the presence of CM from monocytes pre-cultured with MLPS cells interrupted endothelial monolayers much more efficiently than in the presence of Control CM. Figure 7a,b).

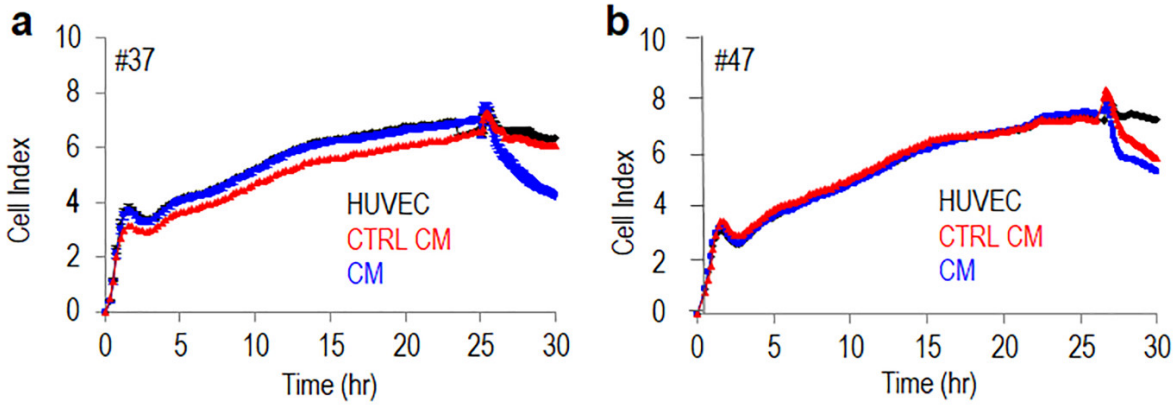

Figure 7. Monocytes pre-exposed to MPLS cells increases trans-endothelial migration of primary MLPS cells. HUVECs (1 × 10^4 cells/well) suspended in growth medium were seeded onto E-plates and allow to grow for 25 h until they form a confluent monolayer. Then, primary #37 (**a**) and #47 (**b**) MLPS (2 × 10^3 cells/well) suspended in CM from human monocytes pre-co-cultured with of MLPS cells, or control monocytes (CTRL CM) were seeded onto endothelial monolayers with serum added to a 10% final concentration. Cell index changes due to crossing of the endothelial monolayer were monitored in real-time for 5 h. The experiments were performed twice in quadruplicate.

Although the identification of soluble factors secreted by MLPS cells in the microenvironment milieu and responsible for M2-like polarization deserves further investigation, our findings indicate that MLPS cells really induce macrophage polarization in the direction of an M2-like pro-tumor phenotype and that once polarized, TAMs increase MLPS cell ability to spread and infiltrate surrounding tissues and ultimately entry of metastatic cells into the blood vessels.

4. Discussion

Although MLPS is relatively more sensitive to chemotherapy, compared with other soft tissue sarcomas, little advances have been made in the treatment of MLPS in the last three decades, and there is a strong request from patients of developing less toxic therapeutics that may improve patients' outcome. It is largely documented that complex interactions between tumor cells and host immune responses in the TME may influence tumor evolution [21,22]. Thus, characterizing the MLPS immune microenvironment may provide prognostic and predictive biomarkers to enable the development of new therapeutic targets and strategies.

In this study, a quantitative evaluation of cellular components of the tumor immune infiltrate was conducted on fifty MLPS tissues in order to investigate the existence of any association of T-cell subtypes and tumor associated macrophages with the histologic grade and PFS. As the results presented here show, high grade MLPS tissues exhibited a CD3+, CD4+, and CD8+ T lymphocyte-poor phenotype whereas a discrete amount of CD3+, CD4+, and CD8+ lymphocytes was found to infiltrate low grade MLPS tissues. Dancsok and co-workers reported that single infiltration of CD8+ T cells in MLPS tissues correlates with better overall survival than simultaneous infiltration of CD8+ and FOXP3+ T cells [41]. Accordingly, we found that infiltration of CD8+ T cells associated to a better PFS, although very few T-reg cells were found to infiltrate both low and high grade MLPS tissues. It has been reported that trials with immune checkpoint inhibitors are delivered contradictory results since TME of MLPS is not much responsive to anti-PD-1 monotherapy [30]. In this regard, we may speculate that forcing T-cell recruitment into high grade MLPS tissues could ameliorate the response of MLPS patients to checkpoint inhibitors.

For instance, immunotherapy targeting the cancer-testis antigen (NY-ESO-1) which is aberrantly expressed in MLPS [42] and has been reported to elicit both humoral and specific CD8+ cytotoxic T-cell immune responses [43,44] could improve the survival of patients affected by high grade MLPS. Furthermore, it has to be taken into account that most studies lump together different sarcoma subtypes that might exhibit immunological differences [45] and were carried out on different tissue areas, including tissue microarrays that may poorly represent the heterogeneity of histological pictures, compared to larger tumor sections.

In the TME, TAMs have been documented to promote tumor progression exerting immunosuppressive activities [38,46–49]. With regard to MLPS, the occurrence of a correlation between the infiltration of M2-like TAMs and poor prognosis was described for the first time by Nabeshima and co-workers on 78 MLPS samples [50]. Using immunohistochemistry for CD68 and CD163, they found that a high infiltration of either $CD68^+$ macrophages and $CD163^+$ M2-like TAMs associates with decreased overall survival and that conditioned medium from macrophages stimulates MLPS cell migration and invasion by activating the epidermal growth factor receptor (EGFR) [50]. We carried out a quantitative analysis of macrophages infiltrating 50 MLPS tissues by using CD68 as a macrophage marker and CD163 as a marker of alternatively activated M2 macrophages. According to Nabeshima and co-workers, we found that CD163+ alternatively activated M2 macrophages massively infiltrated high grade MLPS tissues, and their average counts positively correlated with patient age, but negatively with CD3+, CD4+, and CD8+ lymphocyte counts. Of note, patients whose tissues were heavily infiltrated by CD163+ macrophages showed a significant shorter PFS, compared with patients whose tissues were slightly infiltrated by macrophages, supporting the notion that TAMs negatively affect the prognosis of MLPS patients.

It is documented that TAMs originate from circulating monocytes that infiltrate tumor tissues differentiating into macrophages [51]. After monocyte recruitment in the solid tumors, a variety of signaling molecules, transcription factors, epigenetic mechanisms, and post-transcriptional regulators promote differentiation of the infiltrating monocytes, leading to "tumor-educated" macrophages which may exert immune-suppressive and pro-tumoral effects [52–54]. TAMs constitute a large portion of the tumor mass and regulate multiple aspects of cancer progression including matrix remodeling, tumor-associated angiogenesis, and immune surveillance [55,56].

Here, by non-contact co-cultures and 3D organotypic co-cultures, the last reproducing TME in a 3D-environment, we document the existence of a crosstalk occurring between primary MLPS cells and monocytes as MLPS cells trigger the differentiation of monocytes toward an M2-like anti-inflammatory phenotype, and M2-like macrophages increase spreading and invasiveness of MLPS cells into the matrices. Considering that TAM infiltration sustains tumor progression, many efforts have been made to prevent the recruitment of monocytes into tumor tissues, or to counteract their M2-like polarization, or, alternatively, to force their phenotype toward a M1 pro-inflammatory phenotype [57,58]. This is the case of the CCL2/CCR2 axis, which plays a role in the recruitment of monocytes in tumors: the CCR2 antagonist (PF-04136309) enhanced anti-tumor immunity, decreased tumor growth, and reduced metastasis in an orthotropic model of pancreatic cancer [59]. Trabectedin, approved for the treatment of MLPS, has been reported to reduce TAM density and decrease angiogenesis in mouse tumor models and in MLPS specimens [20]. Also, *all-trans* retinoic acid has been reported to reduce the number of pulmonary metastatic nodes of osteosarcoma cells in mice by inhibiting the M2 polarization of TAMs [60]. In the past years, we developed the retro-inverso peptide Ac-(D)-Tyr-(D)-Arg-Aib-(D)-Arg-NH2, named RI-3 that behaves, in vitro and in vivo, as a strong inhibitor of cell migration [35,61]. We have recently shown that following subcutaneous injection of primary chondrosarcoma cells in nude mice, a daily treatment with 6 mg/Kg RI-3 significantly reduced recruitment and infiltration of monocytes into tumors as compared to ones from untreated animals [29]. We are planning to investigate whether RI-3 exert similar effects on the monocyte recruitment into MLPS tissues in murine models.

Many pieces are still missing to clarify the complicated puzzle of the neoplastic strategy of sarcomas. This study has been developed retrospectively and over a period of approximately 20 years. We hope that our findings could help to understand the interplay between microenvironment, immune response, and MLPS cells. In this regard, we foresee that the identification of soluble factors secreted by MLPS cells in the microenvironment milieu, and responsible for M2-like polarization, could lay down the bases for development of new-targeted therapies aimed to counteract TAM pro-tumor functions.

5. Conclusions

This study was aimed to quantify and functionally characterize the cellular composition of the tumor immune infiltrate in a large cohort of MLPS tissues and to explore the contribution of macrophages in promoting invasiveness of MLPS cells. Our data show that high grade MLPS tissues exhibit T lymphocyte-poor and M2-like macrophage-rich phenotypes and that a high M2-like macrophage infiltration associates to a shorter PFS. We also found that, when co-cultured with MLPS cells, macrophages exhibit predominantly a M2-like pro-tumor phenotype which sustains invasion capability of MLPS cells. Although soft tissue sarcomas have long been considered "immune cold" tumors, recent reports have shown a high degree of heterogeneity of the immunogenic features of these tumors, including MLPS. We are confident that our findings could help to understand the interplay between microenvironment, immune response, and MLPS cells. In this regard, the identification of soluble factors secreted by MLPS cells in the microenvironment milieu, and responsible for M2-like polarization, could allow the development of new-targeted therapies aimed to ameliorate the survival of patients affected by high grade MLPS.

Supplementary Materials: The following are available online at www.mdpi.com/xxx/s1. Table S1: Clinicopathological findings of enrolled MLPS patients. Table S2: Immunophenotypic characteristics of immune infiltrate in MLPS tissues. Table S3: Pearson correlation coefficients referred to the correlation between patients age; max tumor size; averages of CD3, CD4, CD8, CD68, and CD163 positive cells in tumor tissues from MLPS patients. Figure S1. Contribution of primary MLPS cells in promoting M2-like polarization of human monocytes in non-contact co-cultures. Figure S2. Conditioned media from human monocytes co-cultured with primary MPLS cells do not modify proliferation rate of MPLS cells.

Author Contributions: M.V.C. and A.D.C. conceived and wrote the manuscript. M.V.C., M.M., and S.S. designed experiments. M.M., S.S., and G.S. performed the experiments. M.M. and S.S analyzed data. F.F., M.G., L.C., S.T, and G.A. provided human tissues and analyzed clinical data. R.A. provided buffy coats. M.V.C., A.D.C., S.T., B.D.A., E.T., C.G., Y.P., L.M., T.I., R.F., B.V., R.M. and K.S. supervised and finalized the project. All authors read and agreed to the published version of the manuscript.

Funding: This work was funded by the Italian Ministry of Health, "Ricerca Corrente" project #2611752, and by Alleanza Contro il Cancro Italian Network-Working Group Sarcomas.

Institutional Review Board Statement: The study was conducted according to the guidelines of the Declaration of Helsinki. All experimental protocols were performed in accordance with guidelines of the Istituto Nazionale Tumori "Fondazione G. Pascale"-IRCCS (Quality System n. LRC 6019486/QMS/U/IT-2015 certificated in conformity with UNI EN ISO 9001:2008). All patients had provided written informed consent for the use of tissue samples according to the institutional regulations. The research work with primary cell lines blood samples from healthy donors as well as MLPS tissues was approved by the Institutional Ethical Committee of the Istituto Nazionale Tumori IRCCS 'Fondazione G. Pascale, Naples, Italy (protocol 258/18, December 2018).

Informed Consent Statement: Informed consent was obtained from all subjects involved in the study. Written informed consent for publication were also obtained from each participating patient.

Data Availability Statement: All data generated during this study are available within the article and its supporting information. Further details are available from the corresponding author on reasonable request.

Acknowledgments: The authors are grateful for her technical assistance in in vitro experiments to Gioconda Di Carluccio working at the Istituto Nazionale Tumori IRCCS 'Fondazione G. Pascale', in the Neoplastic Progression Unit, Naples, Italy.

Conflicts of Interest: The authors declare no conflict of interest.

References

1. Fletcher, C.; Bridge, J.; Hogendoorn, P.; Mertens, F. *WHO Classification of Tumours of Soft Tissue and Bone*; WHO: Geneva, Switzerland, 2013; ISBN 978-92-832-2434-1.
2. Thway, K.; Nielsen, T. *WHO Classification of Tumours of Soft Tissue and Bone*, 5th ed.; International Agency for Research on Cancer (IARC): Lyon, France, 2020; ISBN 978-92-832-4502-5.
3. Kallen, M.E.; Hornick, J.L. The 2020 WHO Classification: What's New in Soft Tissue Tumor Pathology? *Am. J. Surg. Pathol.* **2021**, *45*, e1–e23, doi:10.1097/PAS.0000000000001552.
4. Antonescu, C.R.; Tschernyavsky, S.J.; Decuseara, R.; Leung, D.H.; Woodruff, J.M.; Brennan, M.F.; Bridge, J.A.; Neff, J.R.; Goldblum, J.R.; Ladanyi, M. Prognostic Impact of P53 Status, TLS-CHOP Fusion Transcript Structure, and Histological Grade in Myxoid Liposarcoma: A Molecular and Clinicopathologic Study of 82 Cases. *Clin. Cancer Res.* **2001**, *7*, 3977–3987.
5. Fiore, M.; Grosso, F.; Lo Vullo, S.; Pennacchioli, E.; Stacchiotti, S.; Ferrari, A.; Collini, P.; Lozza, L.; Mariani, L.; Casali, P.G.; et al. Myxoid/Round Cell and Pleomorphic Liposarcomas: Prognostic Factors and Survival in a Series of Patients Treated at a Single Institution. *Cancer* **2007**, *109*, 2522–2531, doi:10.1002/cncr.22720.
6. Lemeur, M.; Mattei, J.-C.; Souteyrand, P.; Chagnaud, C.; Curvale, G.; Rochwerger, A. Prognostic Factors for the Recurrence of Myxoid Liposarcoma: 20 Cases with up to 8 Years Follow-Up. *Orthop. Traumatol. Surg. Res.* **2015**, *101*, 103–107, doi:10.1016/j.otsr.2014.09.024.
7. Pérez-Losada, J.; Sánchez-Martín, M.; Rodríguez-García, M.A.; Pérez-Mancera, P.A.; Pintado, B.; Flores, T.; Battaner, E.; Sánchez-Garćia, I. Liposarcoma Initiated by FUS/TLS-CHOP: The FUS/TLS Domain Plays a Critical Role in the Pathogenesis of Liposarcoma. *Oncogene* **2000**, *19*, 6015–6022, doi:10.1038/sj.onc.1204018.
8. Racanelli, D.; Brenca, M.; Baldazzi, D.; Goeman, F.; Casini, B.; De Angelis, B.; Guercio, M.; Milano, G.M.; Tamborini, E.; Busico, A.; et al. Next-Generation Sequencing Approaches for the Identification of Pathognomonic Fusion Transcripts in Sarcomas: The Experience of the Italian ACC Sarcoma Working Group. *Front. Oncol.* **2020**, *10*, 489, doi:10.3389/fonc.2020.00489.
9. Koelsche, C.; Renner, M.; Hartmann, W.; Brandt, R.; Lehner, B.; Waldburger, N.; Alldinger, I.; Schmitt, T.; Egerer, G.; Penzel, R.; et al. TERT Promoter Hotspot Mutations Are Recurrent in Myxoid Liposarcomas but Rare in Other Soft Tissue Sarcoma Entities. *J. Exp. Clin. Cancer Res.* **2014**, *33*, 1–8, doi:10.1186/1756-9966-33-33.
10. Sanfilippo, R.; Dei Tos, A.P.; Casali, P.G. Myxoid Liposarcoma and the Mammalian Target of Rapamycin Pathway. *Curr. Opin. Oncol.* **2013**, *25*, 379–383, doi:10.1097/CCO.0b013e32836227ac.
11. Trautmann, M.; Cyra, M.; Isfort, I.; Jeiler, B.; Krüger, A.; Grünewald, I.; Steinestel, K.; Altvater, B.; Rossig, C.; Hafner, S.; et al. Phosphatidylinositol-3-Kinase (PI3K)/Akt Signaling Is Functionally Essential in Myxoid Liposarcoma. *Mol. Cancer Ther.* **2019**, *18*, 834–844, doi:10.1158/1535-7163.MCT-18-0763.
12. Negri, T.; Virdis, E.; Brich, S.; Bozzi, F.; Tamborini, E.; Tarantino, E.; Jocollè, G.; Cassinelli, G.; Grosso, F.; Sanfilippo, R.; et al. Functional Mapping of Receptor Tyrosine Kinases in Myxoid Liposarcoma. *Clin. Cancer Res.* **2010**, *16*, 3581–3593, doi:10.1158/1078-0432.CCR-09-2912.
13. Cheng, H.; Dodge, J.; Mehl, E.; Liu, S.; Poulin, N.; van de Rijn, M.; Nielsen, T.O. Validation of Immature Adipogenic Status and Identification of Prognostic Biomarkers in Myxoid Liposarcoma Using Tissue Microarrays. *Hum. Pathol.* **2009**, *40*, 1244–1251, doi:10.1016/j.humpath.2009.01.011.
14. Haniball, J.; Sumathi, V.P.; Kindblom, L.-G.; Abudu, A.; Carter, S.R.; Tillman, R.M.; Jeys, L.; Spooner, D.; Peake, D.; Grimer, R.J. Prognostic Factors and Metastatic Patterns in Primary Myxoid/Round-Cell Liposarcoma. *Sarcoma* **2011**, *2011*, 538085, doi:10.1155/2011/538085.
15. Schwab, J.H.; Boland, P.; Guo, T.; Brennan, M.F.; Singer, S.; Healey, J.H.; Antonescu, C.R. Skeletal Metastases in Myxoid Liposarcoma: An Unusual Pattern of Distant Spread. *Ann. Surg. Oncol.* **2007**, *14*, 1507–1514, doi:10.1245/s10434-006-9306-3.
16. Asano, N.; Susa, M.; Hosaka, S.; Nakayama, R.; Kobayashi, E.; Takeuchi, K.; Horiuchi, K.; Suzuki, Y.; Anazawa, U.; Mukai, M.; et al. Metastatic Patterns of Myxoid/Round Cell Liposarcoma: A Review of a 25-Year Experience. *Sarcoma* **2012**, *2012*, 345161, doi:10.1155/2012/345161.
17. Manji, G.A.; Schwartz, G.K. Managing Liposarcomas: Cutting Through the Fat. *J. Oncol. Pract.* **2016**, *12*, 221–227, doi:10.1200/JOP.2015.009860.
18. Martín-Broto, J.; Moura, D.S.; Van Tine, B.A. Facts and Hopes in Immunotherapy of Soft-Tissue Sarcomas. *Clin. Cancer Res.* **2020**, *26*, 5801–5808, doi:10.1158/1078-0432.CCR-19-3335.
19. Kirsanov, K.I.; Lesovaya, E.A.; Fetisov, T.I.; Bokhyan, B.Y.; Belitsky, G.A.; Yakubovskaya, M.G. Current Approaches for Personalized Therapy of Soft Tissue Sarcomas. *Sarcoma* **2020**, *2020*, 6716742, doi:10.1155/2020/6716742.
20. Germano, G.; Frapolli, R.; Simone, M.; Tavecchio, M.; Erba, E.; Pesce, S.; Pasqualini, F.; Grosso, F.; Sanfilippo, R.; Casali, P.G.; et al. Antitumor and Anti-Inflammatory Effects of Trabectedin on Human Myxoid Liposarcoma Cells. *Cancer Res.* **2010**, *70*, 2235–2244, doi:10.1158/0008-5472.CAN-09-2335.
21. Greaves, M.; Maley, C.C. Clonal Evolution in Cancer. *Nature* **2012**, *481*, 306–313, doi:10.1038/nature10762.

22. Hanahan, D.; Coussens, L.M. Accessories to the Crime: Functions of Cells Recruited to the Tumor Microenvironment. *Cancer Cell* **2012**, *21*, 309–322, doi:10.1016/j.ccr.2012.02.022.
23. Quail, D.F.; Joyce, J.A. Microenvironmental Regulation of Tumor Progression and Metastasis. *Nat. Med.* **2013**, *19*, 1423–1437, doi:10.1038/nm.3394.
24. Biswas, S.K.; Mantovani, A. Macrophage Plasticity and Interaction with Lymphocyte Subsets: Cancer as a Paradigm. *Nat. Immunol.* **2010**, *11*, 889–896, doi:10.1038/ni.1937.
25. Kitamura, T.; Qian, B.-Z.; Pollard, J.W. Immune Cell Promotion of Metastasis. *Nat. Rev. Immunol.* **2015**, *15*, 73–86, doi:10.1038/nri3789.
26. Zhang, Y.; Zhang, Z. The History and Advances in Cancer Immunotherapy: Understanding the Characteristics of Tumor-Infiltrating Immune Cells and Their Therapeutic Implications. *Cell Mol. Immunol.* **2020**, *17*, 807–821, doi:10.1038/s41423-020-0488-6.
27. Heymann, M.-F.; Schiavone, K.; Heymann, D. Bone Sarcomas in the Immunotherapy Era. *Br. J. Pharmacol.* **2020**, *178*, 1955–1972, doi:10.1111/bph.14999.
28. Simard, F.A.; Richert, I.; Vandermoeten, A.; Decouvelaere, A.-V.; Michot, J.-P.; Caux, C.; Blay, J.-Y.; Dutour, A. Description of the Immune Microenvironment of Chondrosarcoma and Contribution to Progression. *Oncoimmunology* **2017**, *6*, e1265716, doi:10.1080/2162402X.2016.1265716.
29. Minopoli, M.; Sarno, S.; Di Carluccio, G.; Azzaro, R.; Costantini, S.; Fazioli, F.; Gallo, M.; Apice, G.; Cannella, L.; Rea, D.; et al. Inhibiting Monocyte Recruitment to Prevent the Pro-Tumoral Activity of Tumor-Associated Macrophages in Chondrosarcoma. *Cells* **2020**, *9*, 1062, doi:10.3390/cells9041062.
30. Pollack, S.M.; He, Q.; Yearley, J.H.; Emerson, R.; Vignali, M.; Zhang, Y.; Redman, M.W.; Baker, K.K.; Cooper, S.; Donahue, B.; et al. T-Cell Infiltration and Clonality Correlate with Programmed Cell Death Protein 1 and Programmed Death-Ligand 1 Expression in Patients with Soft Tissue Sarcomas. *Cancer* **2017**, *123*, 3291–3304, doi:10.1002/cncr.30726.
31. Petitprez, F.; de Reyniès, A.; Keung, E.Z.; Chen, T.W.-W.; Sun, C.-M.; Calderaro, J.; Jeng, Y.-M.; Hsiao, L.-P.; Lacroix, L.; Bougoüin, A.; et al. B Cells Are Associated with Survival and Immunotherapy Response in Sarcoma. *Nature* **2020**, *577*, 556–560, doi:10.1038/s41586-019-1906-8.
32. Ayodele, O.; Razak, A.R.A. Immunotherapy in Soft-Tissue Sarcoma. *Curr. Oncol.* **2020**, *27*, 17–23, doi:10.3747/co.27.5407.
33. Pinto, M.L.; Rios, E.; Durães, C.; Ribeiro, R.; Machado, J.C.; Mantovani, A.; Barbosa, M.A.; Carneiro, F.; Oliveira, M.J. The Two Faces of Tumor-Associated Macrophages and Their Clinical Significance in Colorectal Cancer. *Front. Immunol.* **2019**, *10*, 1875, doi:10.3389/fimmu.2019.01875.
34. Bifulco, K.; Longanesi-Cattani, I.; Masucci, M.T.; De Chiara, A.; Fazioli, F.; Di Carluccio, G.; Pirozzi, G.; Gallo, M.; La Rocca, A.; Apice, G.; et al. Involvement of the Soluble Urokinase Receptor in Chondrosarcoma Cell Mobilization. *Sarcoma* **2011**, *2011*, 842842, doi:10.1155/2011/842842.
35. Carriero, M.V.; Bifulco, K.; Ingangi, V.; Costantini, S.; Botti, G.; Ragone, C.; Minopoli, M.; Motti, M.L.; Rea, D.; Scognamiglio, G.; et al. Retro-Inverso Urokinase Receptor Antagonists for the Treatment of Metastatic Sarcomas. *Sci. Rep.* **2017**, *7*, 1312, doi:10.1038/s41598-017-01425-9.
36. Ragone, C.; Minopoli, M.; Ingangi, V.; Botti, G.; Fratangelo, F.; Pessi, A.; Stoppelli, M.P.; Ascierto, P.A.; Ciliberto, G.; Motti, M.L.; et al. Targeting the Cross-Talk between Urokinase Receptor and Formyl Peptide Receptor Type 1 to Prevent Invasion and Trans-Endothelial Migration of Melanoma Cells. *J. Exp. Clin. Cancer Res.* **2017**, *36*, 180, doi:10.1186/s13046-017-0650-x.
37. Pollard, J.W. Tumour-Educated Macrophages Promote Tumour Progression and Metastasis. *Nat. Rev. Cancer* **2004**, *4*, 71–78, doi:10.1038/nrc1256.
38. Allavena, P.; Sica, A.; Garlanda, C.; Mantovani, A. The Yin-Yang of Tumor-Associated Macrophages in Neoplastic Progression and Immune Surveillance. *Immunol. Rev.* **2008**, *222*, 155–161, doi:10.1111/j.1600-065X.2008.00607.x.
39. Italiani, P.; Boraschi, D. From Monocytes to M1/M2 Macrophages: Phenotypical vs. Functional Differentiation. *Front. Immunol.* **2014**, *5*, 514, doi:10.3389/fimmu.2014.00514.
40. Mantovani, A.; Marchesi, F.; Malesci, A.; Laghi, L.; Allavena, P. Tumour-Associated Macrophages as Treatment Targets in Oncology. *Nat. Rev. Clin. Oncol.* **2017**, *14*, 399–416, doi:10.1038/nrclinonc.2016.217.
41. Dancsok, A.R.; Setsu, N.; Gao, D.; Blay, J.-Y.; Thomas, D.; Maki, R.G.; Nielsen, T.O.; Demicco, E.G. Expression of Lymphocyte Immunoregulatory Biomarkers in Bone and Soft-Tissue Sarcomas. *Mod. Pathol.* **2019**, *32*, 1772–1785, doi:10.1038/s41379-019-0312-y.
42. Hemminger, J.A.; Ewart Toland, A.; Scharschmidt, T.J.; Mayerson, J.L.; Kraybill, W.G.; Guttridge, D.C.; Iwenofu, O.H. The Cancer-Testis Antigen NY-ESO-1 Is Highly Expressed in Myxoid and Round Cell Subset of Liposarcomas. *Mod. Pathol.* **2013**, *26*, 282–288, doi:10.1038/modpathol.2012.133.
43. Pollack, S.; Jungbluth, A.; Cassian Yee, M.; Hoch, B.L. NY-ESO-1 Is a Ubiquitous Immunotherapeutic Target Antigen for Patients with Myxoid/Round Cell Liposarcoma. *Cancer* **2012**, *118*, 4564–4570, doi:10.1002/cncr.27446.
44. Jäger, E.; Nagata, Y.; Gnjatic, S.; Wada, H.; Stockert, E.; Karbach, J.; Dunbar, P.R.; Lee, S.Y.; Jungbluth, A.; Jäger, D.; et al. Monitoring CD8 T Cell Responses to NY-ESO-1: Correlation of Humoral and Cellular Immune Responses. *Proc. Natl. Acad. Sci. USA* **2000**, *97*, 4760–4765, doi:10.1073/pnas.97.9.4760.
45. Klaver, Y.; Rijnders, M.; Oostvogels, A.; Wijers, R.; Smid, M.; Grünhagen, D.; Verhoef, C.; Sleijfer, S.; Lamers, C.; Debets, R. Differential Quantities of Immune Checkpoint-Expressing CD8 T Cells in Soft Tissue Sarcoma Subtypes. *J. Immunother. Cancer* **2020**, *8*, e000271, doi:10.1136/jitc-2019-000271.
46. Mantovani, A.; Allavena, P.; Sica, A.; Balkwill, F. Cancer-Related Inflammation. *Nature* **2008**, *454*, 436–444, doi:10.1038/nature07205.

47. Du, M.; Roy, K.M.; Zhong, L.; Shen, Z.; Meyers, H.E.; Nichols, R.C. VEGF Gene Expression Is Regulated Post-Transcriptionally in Macrophages. *FEBS J.* **2006**, *273*, 732–745, doi:10.1111/j.1742-4658.2006.05106.x.
48. Lamagna, C.; Aurrand-Lions, M.; Imhof, B.A. Dual Role of Macrophages in Tumor Growth and Angiogenesis. *J. Leukoc. Biol.* **2006**, *80*, 705–713, doi:10.1189/jlb.1105656.
49. Mantovani, A.; Schioppa, T.; Porta, C.; Allavena, P.; Sica, A. Role of Tumor-Associated Macrophages in Tumor Progression and Invasion. *Cancer Metastasis Rev.* **2006**, *25*, 315–322, doi:10.1007/s10555-006-9001-7.
50. Nabeshima, A.; Matsumoto, Y.; Fukushi, J.; Iura, K.; Matsunobu, T.; Endo, M.; Fujiwara, T.; Iida, K.; Fujiwara, Y.; Hatano, M.; et al. Tumour-Associated Macrophages Correlate with Poor Prognosis in Myxoid Liposarcoma and Promote Cell Motility and Invasion via the HB-EGF-EGFR-PI3K/Akt Pathways. *Br. J. Cancer* **2015**, *112*, 547–555, doi:10.1038/bjc.2014.637.
51. Cortez-Retamozo, V.; Etzrodt, M.; Newton, A.; Rauch, P.J.; Chudnovskiy, A.; Berger, C.; Ryan, R.J.H.; Iwamoto, Y.; Marinelli, B.; Gorbatov, R.; et al. Origins of Tumor-Associated Macrophages and Neutrophils. *Proc. Natl. Acad. Sci. USA* **2012**, *109*, 2491–2496, doi:10.1073/pnas.1113744109.
52. Clark, C.E.; Hingorani, S.R.; Mick, R.; Combs, C.; Tuveson, D.A.; Vonderheide, R.H. Dynamics of the Immune Reaction to Pancreatic Cancer from Inception to Invasion. *Cancer Res.* **2007**, *67*, 9518–9527, doi:10.1158/0008-5472.CAN-07-0175.
53. Sica, A.; Mantovani, A. Macrophage Plasticity and Polarization: In Vivo Veritas. *J. Clin. Investig.* **2012**, *122*, 787–795, doi:10.1172/JCI59643.
54. Harper, K.L.; Sosa, M.S.; Entenberg, D.; Hosseini, H.; Cheung, J.F.; Nobre, R.; Avivar-Valderas, A.; Nagi, C.; Girnius, N.; Davis, R.J.; et al. Mechanism of Early Dissemination and Metastasis in Her2+ Mammary Cancer. *Nature* **2016**, *540*, 588–592, doi:10.1038/nature20609.
55. Van Overmeire, E.; Laoui, D.; Keirsse, J.; Van Ginderachter, J.A.; Sarukhan, A. Mechanisms Driving Macrophage Diversity and Specialization in Distinct Tumor Microenvironments and Parallelisms with Other Tissues. *Front. Immunol.* **2014**, *5*, 127, doi:10.3389/fimmu.2014.00127.
56. Martinez, F.O.; Sica, A.; Mantovani, A.; Locati, M. Macrophage Activation and Polarization. *Front. Biosci.* **2008**, *13*, 453–461, doi:10.2741/2692.
57. Zhou, J.; Tang, Z.; Gao, S.; Li, C.; Feng, Y.; Zhou, X. Tumor-Associated Macrophages: Recent Insights and Therapies. *Front. Oncol.* **2020**, *10*, 188, doi:10.3389/fonc.2020.00188.
58. Fujiwara, T.; Healey, J.; Ogura, K.; Yoshida, A.; Kondo, H.; Hata, T.; Kure, M.; Tazawa, H.; Nakata, E.; Kunisada, T.; et al. Role of Tumor-Associated Macrophages in Sarcomas. *Cancers* **2021**, *13*, 1086, doi:10.3390/cancers13051086.
59. Sanford, D.E.; Belt, B.A.; Panni, R.Z.; Mayer, A.; Deshpande, A.D.; Carpenter, D.; Mitchem, J.B.; Plambeck-Suess, S.M.; Worley, L.A.; Goetz, B.D.; et al. Inflammatory Monocyte Mobilization Decreases Patient Survival in Pancreatic Cancer: A Role for Targeting the CCL2/CCR2 Axis. *Clin. Cancer Res.* **2013**, *19*, 3404–3415, doi:10.1158/1078-0432.CCR-13-0525.
60. Zhou, Q.; Xian, M.; Xiang, S.; Xiang, D.; Shao, X.; Wang, J.; Cao, J.; Yang, X.; Yang, B.; Ying, M.; et al. All-Trans Retinoic Acid Prevents Osteosarcoma Metastasis by Inhibiting M2 Polarization of Tumor-Associated Macrophages. *Cancer Immunol. Res.* **2017**, *5*, 547–559, doi:10.1158/2326-6066.CIR-16-0259.
61. Minopoli, M.; Polo, A.; Ragone, C.; Ingangi, V.; Ciliberto, G.; Pessi, A.; Sarno, S.; Budillon, A.; Costantini, S.; Carriero, M.V. Structure-Function Relationship of an Urokinase Receptor-Derived Peptide Which Inhibits the Formyl Peptide Receptor Type 1 Activity. *Sci. Rep.* **2019**, *9*, 12169, doi:10.1038/s41598-019-47900-3.